1246

Université de Neuchâtel

Institut de Microtechnique

PHASE-MATCHED OPTICAL FRESNEL ELEMENTS

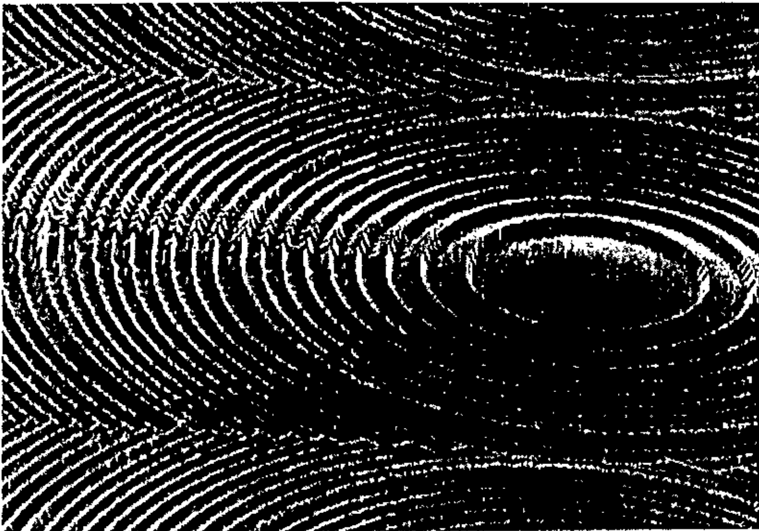

Thèse

Présentée à la Faculté des sciences
pour obtenir le grade de docteur ès sciences

par

Markus Rossi

Neuchâtel, janvier 1995

Université de Neuchâtel

Institut de Microtechnique

PHASE-MATCHED OPTICAL FRESNEL ELEMENTS

Thèse

Présentée à la Faculté des sciences
pour obtenir le grade de docteur ès sciences

par

Markus Rossi

Neuchâtel, janvier 1995

IMPRIMATUR POUR LA THÈSE

Phase-matched Optical Fresnel Elements

de M. Markus Rossi

UNIVERSITÉ DE NEUCHÂTEL

FACULTÉ DES SCIENCES

La Faculté des sciences de l'Université de Neuchâtel sur le rapport des membres du jury,

Messieurs R. Dändliker, N.F. de Rooij, H. Buczek (Marin), R.E. Kunz (PSI Zurich) et M. Hutley (Teddington, UK)

autorise l'impression de la présente thèse.

Neuchâtel, le 5 janvier 1995

Le doyen:

H.-H. Nägeli

ABSTRACT

A novel design method for planar optical elements in the form of segmented microstructures, combining the advantages of geometrical and diffractive optical components, is developed. Optimizing the microstructure with respect to *both* the requirements of the application and the constraints imposed by fabrication is an important integral part of the design process. The refractive and diffractive properties of these planar microoptical elements are theoretically investigated by numerical simulations of fabrication inaccuracies and wavelength deviations. Phase-matched Fresnel elements are well suited for fabrication by direct laser writing in photoresist and subsequent low-cost mass production by replication. A wide range of applications, including high numerical aperture lenses and focusing fan-out elements, has been demonstrated.

PREFACE

I wish to thank Prof. R. Dändliker, director of this thesis, for the helpful discussions concerning the subject.

Very special thanks go to Dr. R.E. Kunz who was the supervisor of my thesis at the Paul Scherrer Institute Zurich. I thank him for introducing me into the field of diffractive optics. His extensive knowledge, large experience and his great enthusiasm were an invaluable motivation for my work.

To M.T. Gale I am indebted for creating and maintaining a pleasant and challenging atmosphere within his group. I owe thanks to H. Schütz, J. Pedersen, R. Stutz, Dr. J. Söchtig, G.K. Lang, C. Appassito, H. Siegwart, and J.M. Raynor for their very important assistance in the various fabrication steps and in the software development. I would like to thank the other PhD students and many of the scientists and technicians at PSIZ for their support and friendship in the last years. Special thanks to Dr. K. Knop, director of the department F3B of PSI, for giving me the opportunity to work at PSIZ.

My best thanks go to Dr. H.P. Herzig, P. Ehbets and the Diffractive Optics Group at the IMT Neuchâtel for the interesting discussions and their friendly contacts. I am very grateful to Dr. G.L. Bona (IBM Rüschlikon), Dr. K. Engelhardt (PSI Zurich) and many other scientists from various institutes and companies for their fruitful collaboration.

I would like to thank Dr. M.C. Hutley, Dr. H. Buczek, Dr. R.E. Kunz and Prof. N. de Rooij for their interest in my thesis as members of the jury.

Finally, my family and my friends deserve an acknowledgment for their patience and encouragement.

Zurich, January 1995
Markus Rossi

LIST OF PUBLICATIONS

This thesis is an overview of the author's work in the field of planar microoptical elements. It consists of an overview and the following selection of the author's publications in this field.

I R.E. Kunz and M. Rossi, "Phase-matched Fresnel elements," Opt. Comm. **97**, 6-10 (1993).

II M.T. Gale, M. Rossi, J. Pedersen, and H. Schütz, "Fabrication of continuous-relief microoptical elements by direct laser writing in photoresist," Opt. Eng. **33**, 3556-3566 (1994).

III M. Rossi, R.E. Kunz and H.P. Herzig, "Refractive and diffractive properties of planar microoptical elements," submitted for publication in Appl. Opt. (Dec. 1994).

IV M. Rossi, G.L. Bona and R.E. Kunz, "Arrays of anamorphic phase-matched Fresnel elements for diode-to-fiber coupling," accepted for publication in Appl. Opt. (1994).

V M. Rossi and R.E. Kunz, "Focusing fan-out elements based on phase-matched Fresnel lenses," Opt. Comm. **112**, 258 - 264 (1994).

Throughout the overview, these papers will be referred to by Roman numerals.

CONTENTS

1. Introduction 1

2. Design and Fabrication of PMFEs 4
  2.1 Design Principle 4
  2.2 Fabrication of Planar Microoptical Elements 10
    2.2.1 Overview of different fabrication methods 10
    2.2.2 Direct laser beam writing in photoresist 11
    2.2.3 Replication 13
    2.2.4 Consequences for PMFE design 13

3. Theoretical Description: Refractive & Diffractive Properties 16

4. Experimental Characterization 20
  4.1 Characterization by Atomic Force Microscope and SEM 20
  4.2 Optical Characterization 21

5. Focusing Fan-out Elements 25
  5.1 Concept and Design 25
  5.2 Experimental Results 27
  5.3 Comparison with related fan-out approaches 28

6. Applications 30
  6.1 PMFE Arrays for Confocal Microscopy 30
  6.2 Application in a Telecentric Optical Metrology System 32
  6.3 Laser Diode-to-Fiber Coupling / Anamorphic Elements 34
  6.4 Reflective PMFEs in Optical Sensor Systems 37

7. Conclusions 39

References 40

Abstracts of Publications I - V 43

1. INTRODUCTION

This dissertation is concerned with studies on planar microoptical elements. It includes the development of a novel design concept, numerical simulations on the optical properties of the resulting elements, their fabrication and experimental characterization, and a summary of the most important applications in the visible and NIR spectral range.

In most modern research and industrial optical applications, such as imaging, detection and interconnection systems, optical elements with focusing, beam splitting and beam shaping properties are of significant interest. These elements can either be designed as classical optical lenses or mirrors, or as diffractive optical elements. Refractive elements, designed by using the laws of refraction and reflection of geometrical light rays, show only low chromatic aberrations and can be fabricated by standard industrial fabrication processes, which guarantee a good optical performance. However, the flexibility in the optical functions and the possibility for integration in optical and electronical microsystems are limited for these types of elements.

In contrast, diffractive optical elements (DOEs) offer many of the attributes needed for integration schemes of optical interconnections [1],[2]. They can be realized as planar optical elements, which have the advantages of being small, lightweight and suitable for low-cost mass production by replication techniques. Since these computer-generated elements are designed by taking into account the wave nature of light, they can transform the optical wave fronts with much more flexibility than classical optical elements. Therefore, very complex optical functions can be performed by one single planar element. However, the design and optimization routines often need the evaluation of complicated integrals describing the wave propagation, thus require much more computational power than geometrical optics. In addition, the forming of a master surface relief structure is a major challenge in the fabrication process, since typical feature sizes of DOEs can be in the order of the wavelength of light.

In order to profit of the advantages of refractive and diffractive elements, we have developed a novel kind of planar microoptical element, the phase-matched Fresnel element (PMFE). The PMFE is a surface microrelief structure consisting of individual segments whose lateral feature sizes are in the range of a few micrometers to several hundred micrometers. The design concept uses the laws of both wave and geometrical optics. Wave optics is used in order to get constructive interference between the waves emanating from different segments, whereas the surface relief shapes of the individual segments are optimized by the much faster procedures of geometrical optics. As an important feature, the PMFE design inherently takes into account the constraints of all fabrication processes involved and locally optimizes the surface relief structure. As a consequence, the realization of PMFEs as planar

1. INTRODUCTION

microoptical elements is made possible also with technologies that do not provide submicron resolution. The design of PMFEs and their realization by laser beam writing - as one possible fabrication technology - are outlined in Section 2 of this overview.

The PMFE concept not only uses the advantages of refractive and diffractive elements in the design procedure, it also enables the creation of elements which show a purely refractive or diffractive behavior. Due to the degrees of freedom in the design procedure, namely the phase difference between neighboring segments, these two extreme types of elements *and* the transition region between them are covered by the PMFE concept. The optical properties of a PMFE consisting of one single segment correspond to those of a refractive lens, i.e. the chromatic aberrations are determined by the material dispersion and the focus position is directly related to the shape of the surface relief profile. In contrast, a diffractive lens with a high number of segments shows large chromatic aberrations, whereas the exact shape of the surface relief profile primary influences the efficiency of a focal point and not its position. The theoretical description and the numerical simulations of the transition from refractive to diffractive optical properties are the main topics of Section 3.

Section 4 is devoted to the experimental characterization of fabricated elements. Besides irregularities in the practical use of the microoptical elements, such as wavelength deviations or alignment errors, the fabrication accuracy mainly determines their optical performance. In this Section we will concentrate on elements fabricated by direct laser beam writing in photoresist. The most important sources of fabrication inaccuracies are the effects originating from the raster scan with a Gaussian beam and errors in the absolute profile depth due to irregularities in the photoresist processing. With measurements by an Atomic Force Microscope (AFM), the deviations of a PMFE profile fabricated by direct laser beam writing from the calculated profile can be revealed. The effects of depth errors are also theoretically simulated in Section 3 and will be compared with experimental results obtained by measuring the diffraction patterns in the image space.

A very attractive and important application of PMFEs are focusing fan-out elements. In Section 5, we present a novel approach for these key elements in optical computing and interconnection schemes which is based on a spatially interlaced arrangement of different types of PMFEs. Due to the low number of parameters, the optimization procedures are simple and very fast. The fabricated elements showed a very good uniformity of the focused spot array and a remarkable tolerance with respect to fabrication errors.

1. INTRODUCTION

PMFEs already have been applied successfully in many different optical prototype systems. Besides good optical performance, the suitability of the resulting elements for low-cost mass-production by replication is of major concern in any industrial project. The flexibility of the PMFE design allows an adaptation to these various demands. This interaction between external requirements and the design procedure will be demonstrated for some selected examples in Section 6. This includes transmissive and reflective planar microlenses with numerical apertures ranging from 0.01 to 0.5, anamorphic elements, and PMFEs used in imaging systems with broad-band illumination. A comparison of the optical behavior of replicated PMFEs ranging from a first laboratory sample to an industrially fabricated element is also given.

2. DESIGN AND FABRICATION OF PMFEs

2.1 DESIGN PRINCIPLE

Design algorithms for planar microoptical elements aim at the optimization of a surface relief structure of a thin layer in order to get a desired light distribution in a given plane. The basis of all optical design algorithms are the propagation equations of light through different types of media. The derivation of the scalar diffraction formulas starting from Maxwell's equations, via the Helmholtz equation, Green's theorem to the integral theorem of Helmholtz and Kirchhoff is widely covered in text books [3], [4], [5]. Depending on the relative dimensions of the elements in an optical setup, additional approximations can be made. The Rayleigh-Sommerfeld, the Fresnel and the Fraunhofer approximation are the most often used formulas for the calculation of scalar optical fields [6]. These diffraction formulas may all be regarded as mathematical refinements of Huygens-Fresnel principle, according to which the field at some observation point is given as a sum of an infinite number of secondary waves, one from each point in the aperture. The evaluation of this sum often represents a serious problem, because the integrands in the diffraction integrals vary rapidly over the integration domain. Numerical evaluations of diffraction integrals therefore can be very time-consuming. Consequently, they are not well suited for the optimization of planar, aperiodic surface relief structures over large apertures, especially when special application requirements and fabrication limitations locally shall be taken into account.

A good approximation of the propagation laws may be expected in the limiting case where the finiteness of the optical wavelength is neglected. This branch of optics is known as *geometrical optics*, since in this approximation the optical laws are formulated in the language of geometry. In the limit where the wavelength tends to zero, the electromagnetic wave equations reduce to the eikonal equation

$$(\operatorname{grad} S)^2 = n^2(x,y,z), \tag{2.1}$$

which is the basis for geometrical optics. The real-valued function $S(\mathbf{x})$ is called the eikonal [3], $n(x,y,z)$ denotes the refractive index of the medium which depends on the spatial coordinates $\mathbf{x} = (x,y,z)$. The surfaces S_j where $S(\mathbf{x})$ is constant are called *geometrical wave-fronts* and are characterized by a constant optical path

$$W(S_j) = \int_O^{S_j} n \cdot ds \tag{2.2}$$

from the object point O to any point on the surface S_j along a ray $r(s)$. The geometrical light rays r are defined as the orthogonal trajectories to the geometrical wave-fronts by

$$n\frac{dr}{ds} = \operatorname{grad} S. \tag{2.3}$$

To an adequate approximation, rays can be regarded as the paths along which the radiation energy travels. Except in regions, where the geometrical description of light is not valid, e.g. near focal points and discontinuities of the transmission function in the element aperture, geometrical wavefronts and physical optical phasefronts can be taken to coincide. In [7] a historical link between the concept of geometrical wavefronts and the wave diffraction theories is given.

The aim of the PMFE concept is the elaboration of a general approach which allows a local and fast optimization of a surface microrelief profile in order to fulfill the demands of the application within the limitations of the fabrication technology. Based on the above considerations, this calls for geometrical ray tracing procedures combined with calculations of the optical phasefronts.

A phase-matched Fresnel element [8] is defined as a *segmented surface microrelief structure*, i.e. the active surface of the planar element is divided into individual segments σ_j. An incident wave u is split into secondary wavelets u_j by the segments σ_j (cf. Fig. 1), where each segment is characterized by its surface relief profile and its segment boundary. The surface relief structure is designed in a way that the desired optical function is performed by each segment σ_j individually. Therefore, the laws of geometrical optics can be used for their calculation. The concept of geometrical wavefronts imposes a constant optical path length of each ray r_j from the object point O to the image point P via any point on the segment σ_j (cf. Fig. 2). In consequence, each secondary wavelet u_j is characterized by geometrical

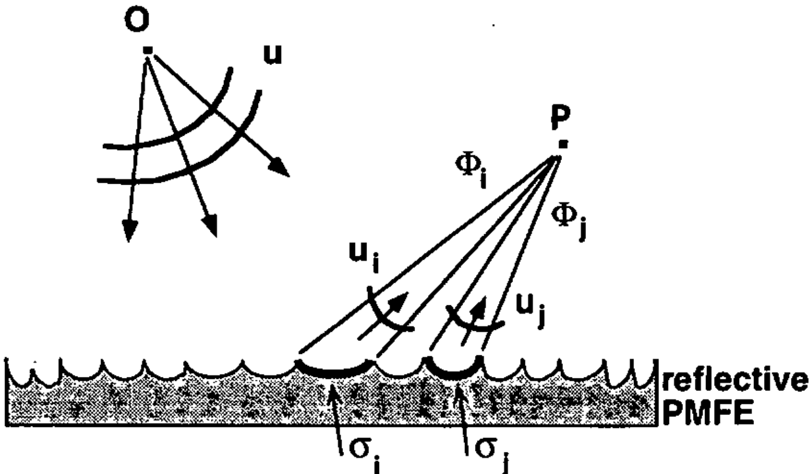

Fig. 1. Schematic drawing of PMFE concept.

wavefronts which have the correct form corresponding to the desired optical function, e.g. spherical waves converging in P. The exact form of the secondary wavelets u_j is not calculated in this model. For small segment sizes, diffraction effects become important; in the case of deep and small structures even rigorous diffraction analysis would be necessary.

The amplitude of the optical field in the far field is given by the superposition of all secondary wavelets u_j. This close relation to the Huygens-Fresnel principle was the reason for using *"Fresnel"* in the term *"phase-matched Fresnel elements"*. In order to take advantage of interference effects (be it constructive or destructive) of the secondary wavelets, a controlled phase relation between them has to be established. This is achieved by choosing the segment boundaries, described by a radius vector of length r_j, in a manner that the optical phase difference in P of two rays r_j and r_{j+1}, crossing neighboring segments σ_j and σ_{j+1} is an integer multiple M_j of 2π (cf. Fig. 2). The integer M_j is called the *phase-matching number*.

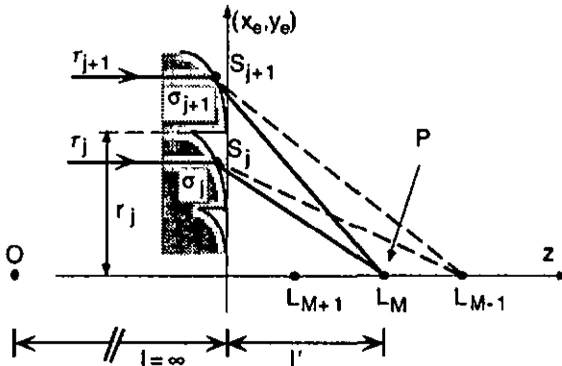

Fig. 2. Definition of PMFE segments and focal points of different diffraction orders.

The most important consequences of this general approach are the various degrees of freedom in the design procedure. They can be used to inherently take into account constraints of the fabrication technology and to adjust the optical behavior of the elements in the sense of refractive and diffractive properties. The most important parameter is the phase-matching number M_j, which can be changed from one segment to another. The value of M_j basically determines the segment width w_j and depth h_j [8]. This is illustrated in Fig. 3, where these two values are plotted as a function of the numerical aperture NA of the PMFE and of the phase-matching number M_j. The phase-matching condition does not completely determine the spatial position of the segment boundaries, only the value of the optical phase step is of importance. As two examples, the segment boundaries can for instance be aligned relative to the top or to the bottom of the relief step. This design aspect, which gets only relevant when the segment depth shows large variations over the element aperture (cf. Fig. 3b), is illustrated by two differently calculated surface relief profiles in Fig. 4. More examples for different design strategies are given in Section 5.

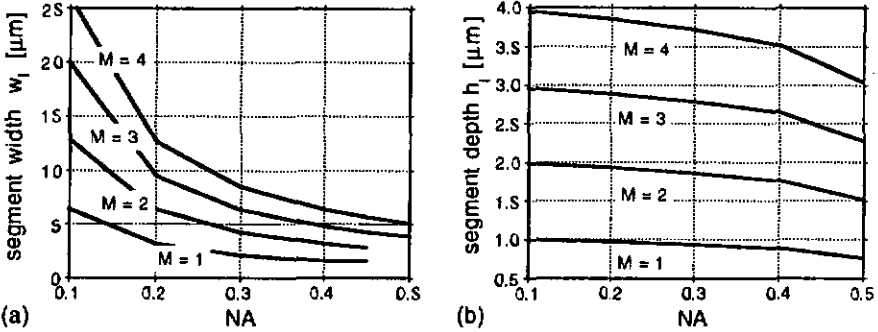

Fig. 3. Segment width (a) and depth (b) of a PMFE in photoresist designed for focusing a collimated HeNe laser beam as a function of the numerical aperture NA and the phase matching number M.

The result of the PMFE design procedure can be described as a microstructure with continuous surface relief segments whose width and depth is locally varying. No other assumptions than the validity of the scalar theory (cf. Sec. 6.3) have been made, i.e. also in the nonparaxial domain good results are obtained. In contrast to other design methods which determine a phase shift distribution in a plane and convert it into a surface relief profile with complicated corrections [9], we directly obtain the desired profile. The concept of a variable phase difference between neighboring segments was also developed by Futhey [10] in the design of "superzone diffractive lenses" and by Marron et al. [11] for their "higher order kinoforms". However, they were derived as special cases of Fresnel lenses, whereas the PMFE concept offers a more general and flexible approach. The basic concept of subdividing the active area into segments with a controlled phase relation between them has its counterpart in the "phased arrays" [12], well established in microwave technology. The combination of multiple apertures to *optical* phased telescopes or antenna arrays has been described in [13] and [14]. In these systems, the far fields of

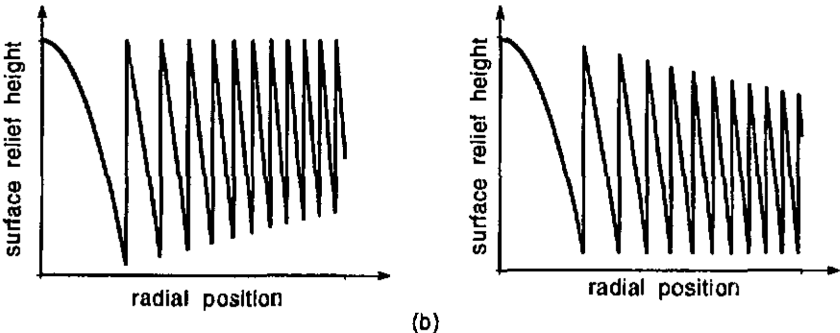

Fig. 4. Schematic design examples for top-aligned (a) and bottom-aligned (b) PMFE microstructure.

a low number of subapertures (typically less than 10) interfere and by phase shifting of the subaperture output beams, the main lobe of the interference pattern can be moved.

For the numerical design of PMFEs, two different computer programs have been developed. The first allows the calculation of a reflective structure which images an object point O on an image point P. In this special configuration, the segment boundaries can be calculated in an analytic form. They consist of ellipses whose centers are shifted relative to the vertex V as a function of the segment number j (cf. Fig. 5). Geometric optical calculations lead to surface relief segments which consist of continuous portions of rotational ellipsoids with focal points in O and P. Fig. 5 shows one typical design strategy where the phase-matching number is increased as soon as the segment width w_j falls short of a minimal value w_{min}. In contrast to this analytical calculation, a second design program was developed which allows the optimization for more general cases. These algorithms are capable of handling transmissive arrangements with an arbitrary number of different media on both sides of the microoptical surface. Although in most cases planar substrate or cover layers make up the media involved in the design, also arbitrary curved surfaces can be a part of the optical system. The design procedures optimize a surface microrelief structure along a given direction in the (x_e, y_e) element plane by phase-sensitive ray tracing algorithms [15], [16], where special iterations determine the exact positions of the segment boundaries. Depending on the spatial symmetries of the optical setup, these sets of profile data points are further processed before or during the fabrication process. For on-axis elements, one data set contains all the information necessary for

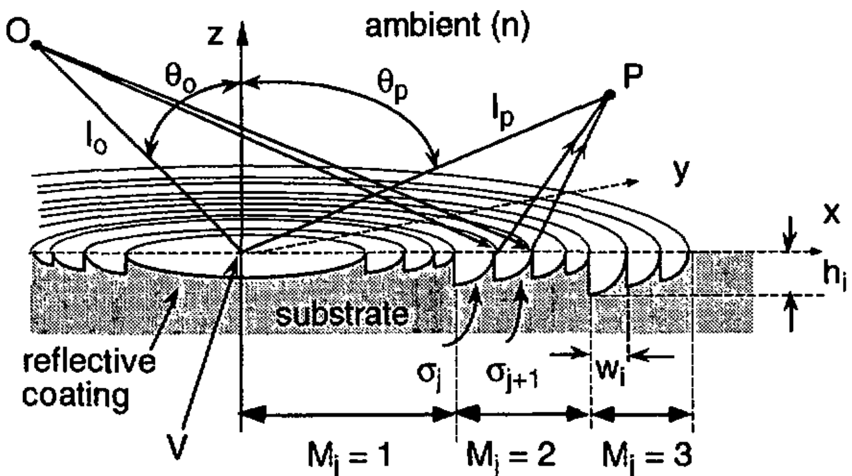

Fig. 5. Schematic drawing of a reflective PMFE structure showing regions with different phase-matching number M_j.

the fabrication; off-axis or anamorphic elements require the calculation of several sets along different directions in the (x_e, y_e) plane.

A more detailed description of the PMFE design procedure is given in papers *I* and *III*. Paper *I* describes the basics of the PMFE concept, whereas in paper *III* the interpretation of the PMFE structure in terms of wave optics and the transition between refractive and diffractive elements are discussed.

2.2 FABRICATION OF PLANAR MICROOPTICAL ELEMENTS

In this Section, an overview over different fabrication methods for planar microoptical elements is given in the first part. The laser beam writing system installed at the Paul Scherrer Institute Zurich (PSIZ) will be described in detail and finally, the consequences of the features of this system on the PMFE design procedure are derived.

2.2.1 Overview of different fabrication methods

For the fabrication of refractive microlenses, i.e. lenses consisting of one single segment, many methods yielding excellent results have been demonstrated. For optical systems where the planarity of the elements is not crucial, lenses can be formed by curing droplets in a defined geometrical shape. As an example, lenses are industrially fabricated on a pedestal in the vertical position with a pendant monomer droplet suspended downward [17]. By an appropriate choice of the pedestal, the droplet volume and consistence, aspheric and even anamorphic lenses can be obtained. Additional refractive index gradients are formed by special mixture procedures of the droplets. The resulting elements have geometrical dimensions and focal lengths in the order of a few millimeters. This technique is suitable for lenses with f-numbers in the range from f/1 to f/2. A method which offers a monolithic fabrication of microlenses and microlens arrays on integrated semiconductor circuits, is the thermal reflow of cylindrical islands of photoresist [18], [19]. After melting of the cylinders, which are fabricated by standard photolithographic techniques, they are forming into small hemispheres due to surface tension forces. Since the molten resin has the tendency to spread out, so that the lens size and shape are difficult to control, the lenses are usually formed on top of a pedestal. As in the method described at the beginning, the geometrical dimensions of the pedestal determine the optical function of the lens. Typical lens parameters for thermal reflow techniques are diameters in the order of 20 μm and f-numbers between f/1 and f/3. A similar method is the fabrication of microlenses using photothermal techniques [20], where a surface relief pattern is achieved by a chemical reaction and physical relaxations of a special glass material. First, a photosensitive glass material is exposed with an appropriate pattern. The exposed regions are densifying during a thermal cycle and are squeezing the unexposed cylindrical regions beyond the surface to form a lenslet. These three selected methods for the fabrication of refractive microlenses have in common, that the composition of the materials, their chemistry and surface physics, as well as an accurate control of the process parameters are of great importance for a good and reproducible quality of the microoptical elements. In the ideal case, such lenses have very smooth surfaces and show diffraction limited imaging quality. However, these techniques do not enable the fabrication of planar elements performing a large variety of optical functions and having complex surface relief structures.

In order to generate surface micro-relief structures of arbitrary shapes, methods with higher resolutions and more flexibility were developed. Diamond turning of metal (copper or aluminum) or plastic surfaces is a high precision fabrication method for circular elements with smooth and slowly varying relief structures. Under these conditions, circular tools of relatively large radii can be used to accurately cut blazed profiles with a good surface finish (< 1 nm rms surface roughness). However, if the minimum feature sizes are below a typical value of 50 µm, severe defects occur due to the geometrical dimensions of the cutting tools [21], [22]. In addition, for small feature sizes the shapes, of the surface relief structures are limited to linear depth profiles. Therefore, fabrication by diamond turning is currently of high interest primarily for infrared and microwave systems, where the requirements for small segment sizes are less stringent.

The highest resolution for the fabrication of continuous relief microoptical elements is achieved by direct writing techniques such as laser or e-beam exposure of a radiation sensitive resist film using a computer-controlled scanning system. Electron-beam writing [23], [24], [25] requires exposure under vacuum and a conducting film under the resist layer to avoid charging effects. Whereas the electron-beam can be focused to spot sizes to 50 - 100 nm, the lateral resolution and minimum feature size for e-beam writing is limited by the "proximity effect", i.e. the scattering of the electrons in the resist layer. This effect can be reduced by using higher electron energies and by a mathematical compensation of the e-beam point spread function in the exposure pattern [26]. By these methods, the optimum lateral resolution for structures with a depth of up to 2.5 µm is in the range of 1 µm. Most of the e-beam writing systems have scan field sizes in the order of a few hundred micrometers. Elements with larger areas have therefore to be combined of different scan fields, introducing stitching errors of adjacent fields and long writing times. New e-beam writing systems overcome this drawback by sample movements over long distances and a simultaneous e-beam deflection for correction of positioning errors [27].

Related fabrication methods such as binary optics [28] or halftone mask techniques [29], [30] make use of similar equipment for exposure of binary or grey-scale masks. Since for binary structures on thin films the proximity effect is negligible, the lateral resolution of the mask can be in the range of 50 nm. However, the resolution of these techniques is limited by the optical imaging system and the spatial filtering for halftone masks and by the precision of the mask alignment for binary optics.

2.2.2 Direct laser beam writing in photoresist

An alternative fabrication technique for microoptical surface relief structures which has shown good results is direct laser beam writing [31], [32]. In this method, a photoresist-coated sample is scanned under a focused laser beam whose intensity is synchronously modulated to write a continuous exposure in the resist film. This

allows the exposure of the gray scale pattern in one fabrication step. In order to obtain the desired surface relief profile with a high precision, an accurate control of the sample movements, of the modulated laser intensity and of the resist development process are required. A further attraction of direct laser beam writing is the use of less complicated and therefore less expensive equipment compared to e-beam based methods.

The laser beam writing system installed at the Paul Scherrer Institute and the process steps involved with the fabrication of continuous-relief microoptical elements are described in detail in paper *II*. The system parameters can be summarized as follows (cf. Fig. 6): A photoresist-coated substrate is exposed by *xy*-raster scanning under a focused HeCd beam (wavelength $\lambda = 442$ nm). The *xy*-translation stage is an air-bearing table driven by linear motors with HeNe-interferometer position measurement (resolution $\lambda/32 \approx 20$ nm). During a scan along the *x*-axis, deviations of the *y*-position of about $\pm$ 150 nm are detected. This dynamic positioning accuracy is limited by the control system and vibrations of the whole writing system. An acousto-optic modulator controls the laser beam intensity with 256 discrete levels. Therefore, the surface relief data points need to be given in a two-dimensional bitmap format of exposure intensities. For this, an adaptation of the data points to the writing raster and a conversion from depth to intensity data have to be performed. The latter step requires an accurate and periodic characterization of the photoresist layers. Given this conversion information, the calculation of the intensity values for one scan line can either be done in advance or - especially for large amounts of data - during the writing process on a separate computer with high computational power (e.g. Sun SparcStations). The 8-bit pixel intensity data are then loaded line by line into the buffer and clocked out by the interferometer pulses during each line scan. This ensures a good synchronization of the laser intensity with the stage position and is relatively insensitive to the constancy of the scan velocity. An autofocus system automatically holds focus over the scan area during the writing procedure.

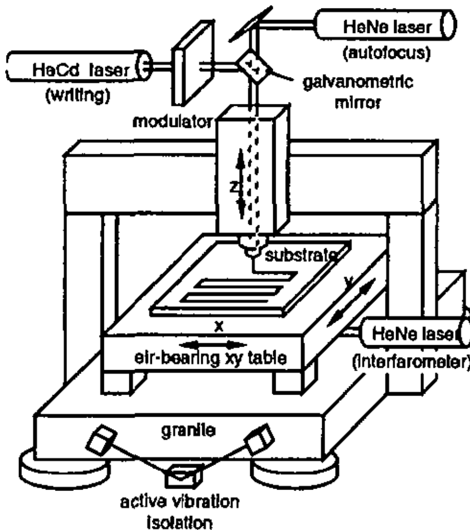

Fig. 6. PSIZ laser writing system.

Typical writing parameters for the fabrication of microoptical elements are an interline spacing of $s = 1$ µm, a focused spot diameter of $D = 1.5$ µm (at 1/e intensity points, determined by knife-edge measurements) and a writing speed of 10 mm/sec. In theory, the

overlap of lines with a Gaussian irradiance distribution of width D at a distance s should lead to a surface modulation of less than 1% of the relief height, if the condition $D > 1.44s$ is fulfilled [31]. In practice, surface modulations in the order of about 100 nm rms are measured, mainly caused by the relatively high errors in the dynamic positioning accuracy of the current system. In order to minimize these effects of vibrations and positioning errors, the writing spot size D is chosen as large as possible for a given structure and may vary from 1.5 µm up to about 8 µm. A larger spot leads to smoother surface profiles (≈ 25 nm rms for an 8 µm writing spot), but results in a loss in feature resolution. Writing times using such an *xy*-scanning system can be relatively high - typically up to 12 hours for a microstructure of 10x10 mm^2 area. But since the photoresist recording is generally converted to a replication mould for producing replicas for use in microoptical systems (cf. paper *II*), this is in practice not of great significance.

The photoresist processing is of major importance in the whole fabrication by direct laser beam writing. Details about preparation, development, characterization and long term stability of an exposure are also given in paper *II*. Good experimental reproducibility of the development characteristic requires careful control over the coating and development procedures. In practice, an accuracy and a reproducibility of about ± 5 % in average relief height is relatively straightforward, a tolerance of ± 2 % requires considerable effort. The effects of depth errors on the PMFE behavior are theoretically investigated in the next Section.

2.2.3 Replication

A major attraction of planar microoptical elements lies in the potential of mass-production. The individual production steps and their influence on the profile fidelity are outlined in paper II. The most important results are, that replication by hot embossing or casting techniques has demonstrated good results for PMFE structures with a maximum depth $h_{max} \approx 5$ µm and a minimum segment width $w_{min} \approx 5$ µm. The additional surface roughness introduced by the different replication steps are in the order of a few nanometers and therefore negligible to the roughness of the original resist profile.

2.2.4 Consequences for PMFE design

The parameters of the laser beam writing system described above impose several constraints for the design and the data preparation of PMFE microstructures. The typical width $D \approx 1.5$ µm of the focused laser writing beam limits the minimum width of a continuous relief segment. This value is normally set to w_{min} = 5 µm for two reasons:

1. The formation of typical PMFE structures with a depth of 3 µm and more by Gaussian beams gets inaccurate for widths $w < 5$ µm. The aim of the design is to

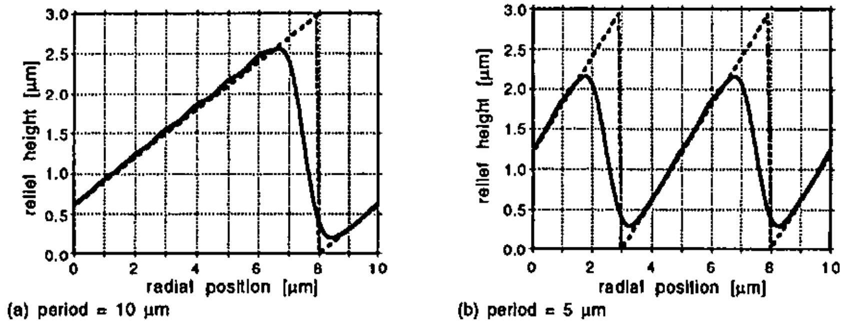

Fig. 7. Numerical simulation of the generation of microprisms with periods 10 µm (a) and 5 µm (b) by overlap of Gaussian beams (1/e-diameter D = 1.5 µm). The broken lines show the desired surface relief, the solid lines are the result of the overlap of Gaussian beams separated by s = 1 µm.

have a segment width of at least 3 µm showing only small deviations from the calculated profile. A numerical simulation on the generation of microprisms with different widths by Gaussian beams is given in Fig. 7. For the calculation of the surface relief profile, the convolution with Gaussian beams was not yet taken into account.

2. For circular and elliptical forms of the segment boundaries, the realization by a bitmap format with quadratic pixels of size $p = 1$ µm introduces rough structures in the regions of segment boundaries. The pixelated segment boundary follows the calculated line with a maximum deviation of $\pm p / \sqrt{2}$. The value of $w_{min} = 5p$ keeps these aliasing errors small compared to the segment width. A possibility for reducing these rough segment boundaries is writing with a smaller pixel size, which in contrast leads to a multiplication of the writing time.

The maximum profile depth is restricted by the depth of focus b of the laser beam and by the limits of the low-cost replication techniques, such as embossing or casting. The depth of focus of a Gaussian beam with $^1/_e$-diameter D in a medium of refractive index n is given by [33]:

$$b = \frac{2\pi n D^2}{4\lambda} \approx 13 \mu m \qquad (2.4)$$

Since the autofocus is normally adjusted to keep the Gaussian beam waist at the photoresist surface, the beam spot size increases by a factor $\sqrt{2}$ at a photoresist depth of $b / 2$. Therefore, the depth of the structures should not exceed this value.

A maximum profile depth of the same order is also imposed by replication experiments. Typical results show a good and reproducible profile fidelity for the

replication of segments with a width of $w_{min} = 5\ \mu m$ up to a maximum depth of $h_{max} \approx 5\ \mu m$. These values are guidelines for replication by hot embossing and may be improved by other techniques, such as injection moulding.

Based on these two empirical limits of w_{min} and h_{max} two simple restrictions for the choice of the phase-matching number M in the PMFE design imposed by the fabrication process can be identified:

1. M has to be increased, as soon as the minimal segment width w_{min} is achieved (cf. Fig. 2a).
2. The maximum value of the phase-matching number M is restricted by h_{max} (cf. Fig. 2b).

This demonstrates that the design parameter M_j is of great importance for the design and fabrication of planar elements which would not be accessible for a given fabrication technology if standard design procedures would be used. In this way, PMFEs with numerical apertures NA as high as 0.5 have been successfully fabricated by direct laser writing [34]. Without the change to higher values of M_j, a fabrication technology with a three times better resolution would be required for similar elements. One limit of this design method is reached when the demand for a higher M by rule *1* is prohibited by rule 2.

In the cases not concerned by the above restrictions, the choice of M_j can be the object of additional design rules. In the next Section, the optical behavior of elements based on different design strategies are compared.

3. THEORETICAL DESCRIPTION, MODELLING

In this Section, the consequences of different PMFE designs on the optical behavior are investigated. In particular, the transition between refractive and diffractive optical elements is described.

For the case where the phase-matching number M_j has a constant value of 1 over the whole area of a planar microlens, the resulting PMFE is identical to a phase-Fresnel lens as described in [35]. This will be referred to as the purely diffractive case. For increasing phase-matching numbers, the number of segments decreases while their widths become larger. The limiting case where the element consists of one segment is a purely refractive lens. Therefore, the PMFE concept offers the possibility to vary the optical properties of a planar microoptical element from a purely diffractive to a purely refractive behavior. A theoretical description of PMFE structures and numerical simulations on their refractive and diffractive properties are given in paper *III*. The results are summarized in the following paragraphs.

In a first step, a theoretical model for diffractive microlenses in the paraxial domain is developed. Such a lens is characterized by a set of segments, where the distances of their boundaries from the origin are given by

$$r_j^2 = 2jM_j\lambda_0 l'. \tag{3.1}$$

j is the segment number, l' the back focal length of the lens, λ_0 the design wavelength and M_j the phase-matching number. The phase-shift introduced by each surface relief segment is approximated by a quadratic function

$$\Phi(r) = 2\pi M_j\left(j - \frac{r^2}{2M_j\lambda_0 l'}\right), \text{ for } r_j \le r < r_{j+1}. \tag{3.2}$$

Two multiplicative factors α and ν are introduced in Eq. (3.2) in order to describe the influences of wavelength deviations and linear surface relief errors, respectively, on the phase function [36]. The transmission function $t(r) = \exp[i\Phi(r)]$ of a paraxial Fresnel lens with a constant phase-matching number $M_j = M$, obtained by periodic extension of the segment transmission function, can be approximated by a Fourier series

$$t(r) = \sum_{N=-\infty}^{\infty} \exp\left[-i\pi\left(\alpha\nu M - N\right)\right]\cdot \operatorname{sinc}\left(\alpha\nu M - N\right)\cdot \exp\left[-\frac{i\pi N r^2}{M\,\lambda_0 l'}\right], \tag{3.3}$$

where the *sinc*-function is defined as:

$$\mathrm{sinc}(x) = \frac{\sin(\pi x)}{\pi x}. \tag{3.4}$$

The expansion (3.3), which is an accurate approximation for the transmission function when a large number of segments are present, is then compared with the transmission function of a refractive lens consisting of one single segment [4]:

$$t(r) = \exp\left[-\frac{i\pi r^2}{\lambda_1 f}\right] \tag{3.5}$$

A focal length f and an illumination wavelength λ_1 were assumed. A comparison of the last term in (3.3) with (3.5) suggests that the transmission function of a paraxial PMFE can be interpreted as a sum over different refractive lenses with focal lengths

$$l_N = \frac{M\,l'}{N} \cdot \frac{\lambda_0}{\lambda_1}. \tag{3.6}$$

The normalized energy in these focal points is proportional to the squared modulus of the Fourier coefficient

$$\eta_N = \mathrm{sinc}^2\left(\alpha v M - N\right). \tag{3.7}$$

Equations (3.6) and (3.7) reveal the most important differences between lenses with refractive and diffractive behavior. Whereas a refractive lens (or a PMFE consisting of one single segment) shows one single focal point, a diffractive lens (a PMFE with a large number of segments) has potentially an infinite number of foci. Deviations in the surface relief profile depth of a refractive lens lead primarily to a shift in the focal position. According to Eq. (3.6), the focal positions of a diffractive lens are not affected by surface relief errors (expressed by a factor $v \neq 1.0$). However, the energy distribution among the foci is altered (cf. Eq. 3.7). Deviations of the illuminating wavelength $\lambda_1 = \alpha \cdot \lambda_0$ from the design wavelength λ_0 are described by a factor $\alpha \neq 1.0$. The chromatic aberrations of a refractive lens are determined by the material dispersion $n(\lambda)$ and are in general much smaller than for a diffractive lens, for which a shift of the possible focal points and a different energy distribution are resulting.

According to the above description of PMFEs in the paraxial region, the segment boundary pattern of a PMFE with a constant phase-matching number M can be interpreted as a focusing diffraction grating having the *Mth* order focus at the desired image point P. The positions of constructive interference of light diffracted at the segment boundary pattern are given by (3.6) and are referred to as higher ($N > M_j$) and lower ($N < M_j$) order focal points L_N (cf. Fig. 2). The segment relief shape determines the energy distribution among these focal points, expressed by Eq. (3.7) and is optimized for the geometrical refraction of light rays into the point P.

3. THEORETICAL DESCRIPTION, MODELLING

In the next step, the behavior of PMFEs with different phase-matching numbers is compared. The factors α and ν, which describe linear surface relief errors and wavelength deviations, respectively, shall be taken to be constant for all different phase-matching numbers. According to Eq. 3.6, the axial density of higher and lower order focal points is in first order a linear function of M. Additional focal points are therefore located the nearer to the original focus, the higher the value of M is. Equation 3.7 reveals that the efficiencies in the normally unwanted higher and lower diffraction orders are increasing for elements with a high phase-matching number M. Therefore, elements designed with a high M need to be fabricated with a better relative depth accuracy in order to show the same performance as elements with low phase-matching numbers. A characteristic of the axial energy distribution described by Eq. 3.7 is that not more than 2 focal points simultaneously can have an efficiency of more than 5%, since not more than 2 integer values N are under the central $sinc^2$-lobe. Numerical simulations in the different image planes demonstrated that the diameters of the focal spots are in a first approximation not affected by the modelled effects. For surface relief errors exceeding ±10%, the optical performance may be severely reduced.

In most applications, the existence of higher and lower order focal points is an unwanted effect and should be avoided by means of design considerations and fabrication improvements. However, by an appropriate choice of λ_1 and N in Eq. 3.6, the *Nth* diffraction order at wavelength λ_1 can be brought to coincidence with the original focal length l' at the design wavelength λ_0. These types of element show an achromatic behavior for a set of discrete wavelengths and were proposed under the name "multiple order diffractive lenses" in [37].

All the above results are obtained by interpretation of the paraxial transmission function of a PMFE with a large number of segments. However, for design variants with high phase-matching numbers and consequently a low number of segments, the assumptions for the expansion (3.3) are no longer fulfilled. In order to investigate the optical behavior of PMFEs as a function of the number of segments, their diffraction patterns were numerically evaluated. Since elements with high numerical apertures NA are also of interest, the Rayleigh-Sommerfeld approximation [6] is used instead of the paraxial or Fresnel approximation. The numerical simulations were done for the example of 8 different PMFEs, all having the same numerical aperture of NA = 0.05 and focal length l' = 4.0 mm, but consisting of 1 to 8 segments with depths ranging from 8 to 1 μm.

The aim of the numerical simulations with the Rayleigh-Sommerfeld diffraction formula was the investigation of the behavior of these elements in the presence of surface relief errors and wavelength deviations. The detailed results of these calculations, including the investigations on higher and lower diffraction orders of these elements, are given in paper *III*. As a typical result, the longitudinal chromatic aberrations, originating from $\lambda_1 \neq \lambda_0$, are plotted in Fig. 8. It can be seen that the transition from the refractive (M = 8) to the diffractive behavior (M = 1) occurs between the elements with one and four segments. The element with $M_j = 2$,

consisting of $Q = 4$ segments, shows longitudinal chromatic aberrations already very close to those for of a diffractive lens, calculated by Eq. (3.6) and expressed by the broken line in Fig. 8. Similar calculations have been performed for the behavior under surface relief distortions. All resulted in the statement, that the diffractive behavior of a planar microlens is dominant already when a small number of segments (typically 4) is illuminated. Analogous numerical simulations on elements with different aperture sizes proved that this qualitative change in the behavior is not dependent on the value of the phase-matching number.

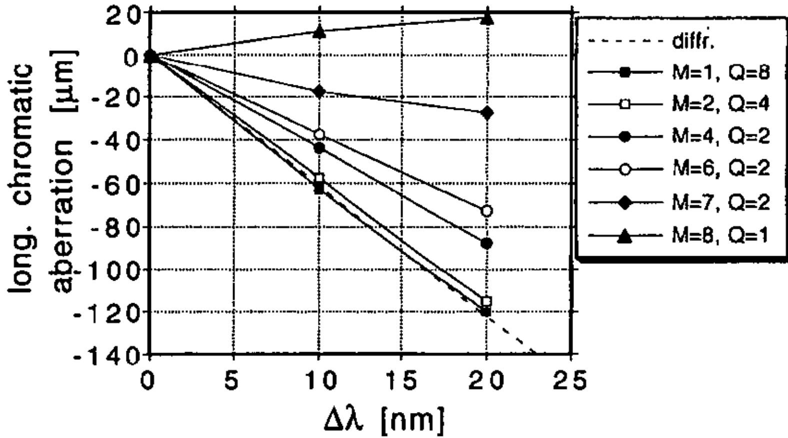

Fig. 8. Longitudinal chromatic aberration for PMFEs with varying phase-matching numbers M and numbers Q of illuminated segments. The broken line shows the values for a purely diffractive lens calculated with Eq. 3.6.

4. EXPERIMENTAL CHARACTERIZATION

The experimental characterization of the fabricated elements included inspections of the surface microrelief and optical characterizations such as efficiency and diffraction pattern measurements. In this Section, only a few typical characterizations of each type are presented. More experimental results are reported in Section 5 and in the papers *I-V*.

4.1 CHARACTERIZATION BY ATOMIC FORCE MICROSCOPE AND SEM

For the topography measurement of PMFEs, Atomic Force Microscopes (AFM) are well suited. They offer a subnanometer lateral and vertical resolution over scanfields with a maximum size of about 160 x 160 μm^2. The maximum slope that can be measured is limited by the tip vertex angle, which is in the order of 40-50° for commercially available AFM tips. In Fig. 9, the surface relief profiles of microprisms with a period of 10 µm and 5 µm, respectively, and a designed depth of 3 µm is shown. These profiles, which were obtained with a Nanoscope III (Digital Instruments), show a good coincidence to the theoretical data in Fig. 6. The accuracy of these measurements is in the range of ± 5%, provided that the microscope was calibrated previously. The results prove that continuous surface relief profiles with inclination angles of up to 60° can be fabricated by laser beam writing with an excellent accuracy. For the profile at the segment boundary, a slope of ≈ 75° is predicted by the numerical simulations in Section 2.2.4. Angles of this order are exceeding the limits of AFMs with commercial measuring tips. Therefore, the exact form of the profile near the depth step at a segment boundary can not be obtained by this method. Nevertheless, it can be observed that in an area of 2 µm width around the depth step, the profiles fabricated by laser beam writing show large deviations from the desired values. Therefore, these regions will not fulfill the designed optical function and will be the main contribution to reduced efficiency and stray light.

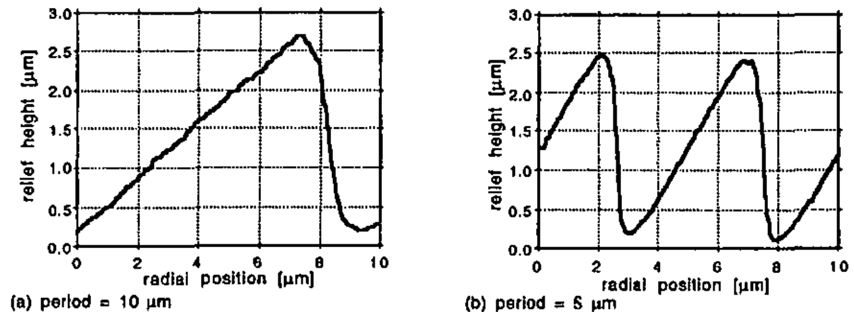

Fig. 9. Surface relief of microprisms with periods of (a) 10 µm and (b) 5 µm and a designed depth of 3.0 µm, measured by an Atomic Force Microscope (AFM).

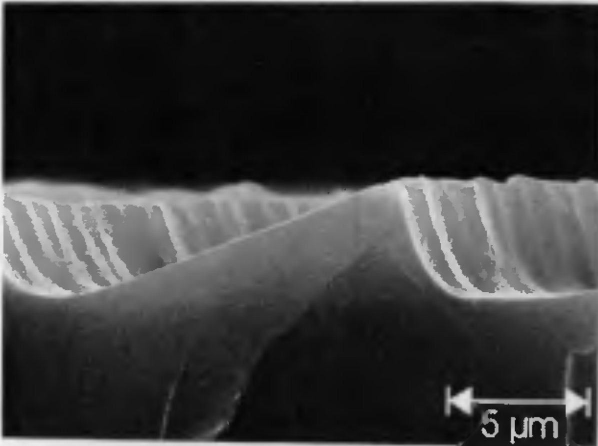

Fig. 10. SEM picture of a segment with a designed width of 15 µm and a depth of 4.5 µm. The element was replicated in epoxy.

An SEM micrograph of a single segment is shown in Fig. 10. In addition to the inaccuracies at the segment boundaries, the typical grating structure originating from the laser writer raster scan can be seen.

4.2 OPTICAL CHARACTERIZATION

The measurement setup for the optical characterization is shown in the photograph in Fig. 11. In the center, a sample holder for transmissive microoptical elements is shown. On its left, the optics for the laser beam collimation, attenuation and expansion are located. The diffraction pattern is analyzed either by a CCD camera or by a photodiode scanning in the *xy*- or *xz*-plane. Depending on the required resolution, the field in the image space was either imaged via a microscope objective as shown in Fig. 11 or measured directly without additional optics. For measurements at small distances behind the microoptical elements, a CCD camera was modified by moving the CCD sensor chip fully to the front and rearranging and recessing the electronics board. With slight modifications, the same setup was used also for elements working in reflection.

For first basic optical characterizations, a series of differently designed PMFEs was fabricated and replicated in polycarbonate foil. These elements with a diameter of 5 mm focused a collimated HeNe laser beam ($\lambda = 632.8$ nm) at a distance of $l' = 10$ mm. Typical diffraction efficiencies in the range of $\eta = 70$-80% were measured. By writing a linear array of each lens and scaling the depth profile of the individual elements by different linear factors ν, the effects of depth scaling errors

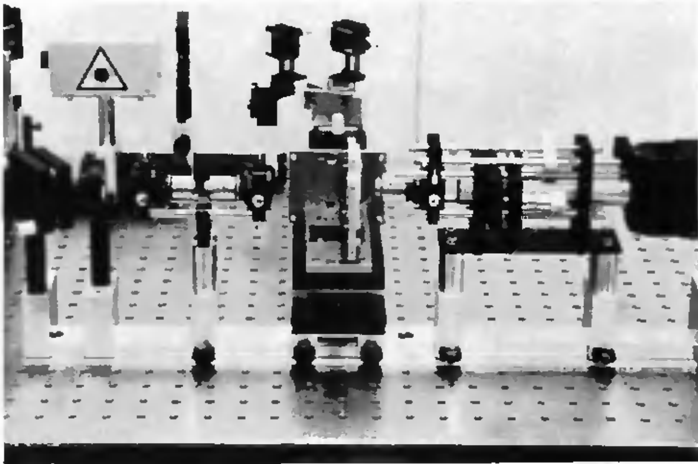

Fig. 11. Measurement setup for the optical characterization of PMFEs

described in Section 3 were investigated. The measured positions of the resulting additional axial focal points and their efficiencies showed a good coincidence with the values predicted by Eqs. 3.6 and 3.7.

A qualitative investigation of the stray light generated by laser written PMFEs shows a significant accumulation in a plane perpendicular to the scan direction of the laser writer and two bright spots in this plane. This is a consequence of a grating structure which is superposed to the PMFE surface relief, originating from the laser writer raster scan. By AFM measurements, a surface modulation with an rms value of typically 100 nm was observed for 3 µm deep structures. The two bright spots in the stray light pattern can be identified with the ±1st diffraction orders of this grating. For elements with segments having a depth of $w_{max} \approx 3$ µm, typically 1 - 1.5% of the energy in the main focal point is measured in each diffraction order. Elements with a shallower segment structures ($w_{max} \approx 1$ µm), showed also a lower energy ($\leq 0.5\%$) in the raster scan grating diffraction orders.

In order to demonstrate the potential of the PMFE design procedure and the fabrication by laser beam writing, the optical properties of laser written PMFEs with a numerical aperture NA = 0.45 (f-number = 1) at a focal length $l' = 2$ mm were characterized. According to Fig. 3, a maximum phase-matching number of $M = 4$ has to be used to achieve the required NA. In the design, M_j was set to one in the center and increased each time the minimum segment width $w_{min} = 5$ µm was achieved. The diffraction pattern of such an element is shown in Fig. 12. It was measured by scanning a photodiode masked with a slit of 2 µm width in the x- and z-direction. The irradiance distribution in the y-direction was integrated by the slit mask. Besides the designed focal point at $z = 2.0$ mm, two additional foci occur at $z = 3.0$ mm and

$z = 4.0$ mm. These foci can be attributed to lower diffraction orders of the PMFE regions with $M = 2$, 3 and 4. For the main focal point an efficiency $\eta \approx 70\%$ was measured. The irradiance distribution of the spot, which is shown in Fig. 13, had a width of 1.5 μm (FWHM). This experimental value corresponds well to the spot diameter of 1.0 μm obtained by calculations using the Rayleigh-Sommerfeld diffraction formula.

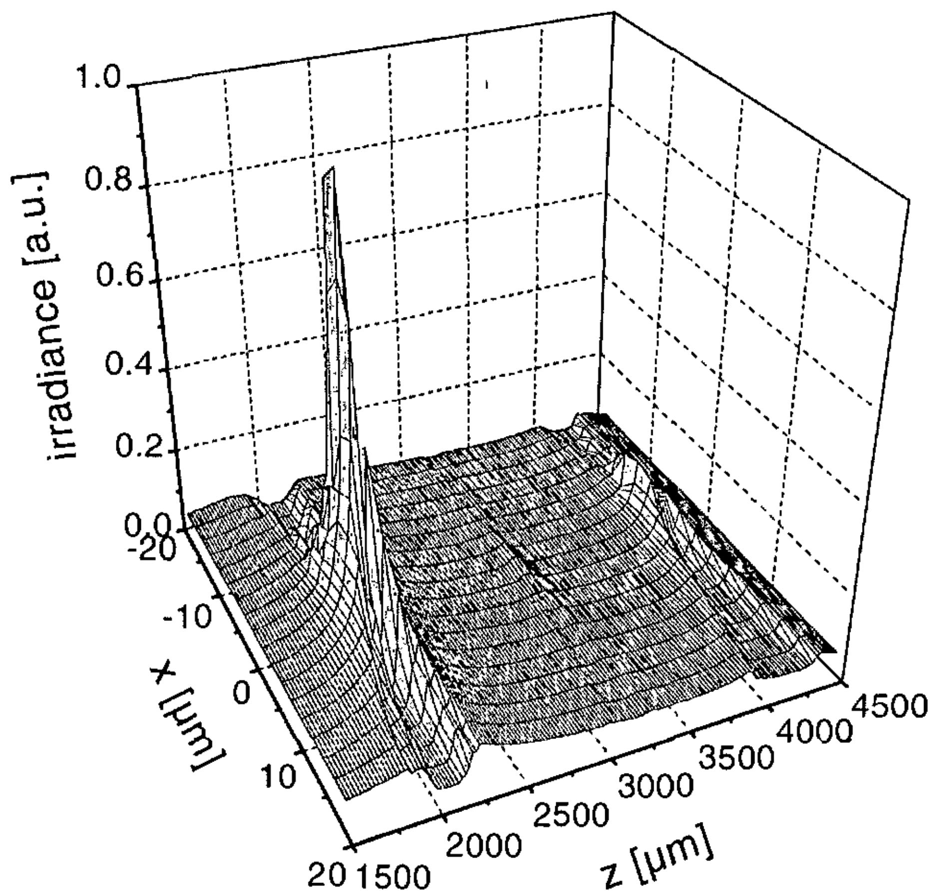

Fig. 12. Irradiance distribution in the image space of an f/1 lens measured by scanning a photodiode, masked with a slit of 2 μm width, along the z-coordinate.

An additional method for characterization of microoptical elements is presented in paper *IV*. By knife-edge measurements, the Gaussian beam parameters of an optical field before and after the microoptical element are determined. The comparison of the $\mathcal{M}^2$-factors [38], which is a measure for the optical quality of a beam, leads to statements about the aberrations introduced by the element.

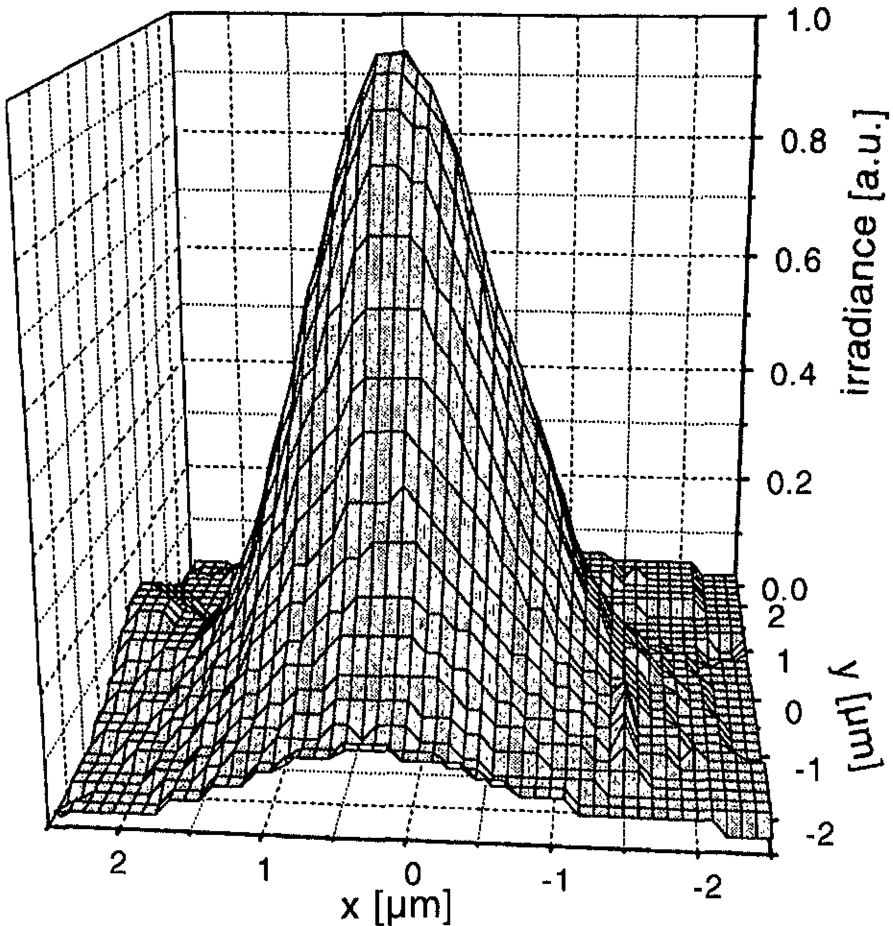

Fig. 13. Irradiance distribution in the focal plane of an f/1 lens. The measurement was performed by means of a 20x microscope objective imaging the focal plane of the PMFE onto a photodiode with a mask of 2x2 µm².

5. FOCUSING FAN-OUT ELEMENTS

Fan-out elements are important components for optical computing and interconnection applications. Many different algorithms have been developed for their design, leading to elements with a high efficiency and a good uniformity [39],[40]. The purpose of these elements is to split an incoming planar wave into an array of quasiparallel waves. Therefore, in a typical fan-out arrangement, these diffractive optical elements are combined with other optical elements, such as lenses, to produce multiple images of an input light source. Furthermore, their optical performance is strongly dependent on a very accurate realization of the theoretically calculated surface relief profile [32], [41].

In this Section, a concept is presented for combining the focusing and the splitting function into one single element and simultaneously reducing the dependence of their performance on fabrication tolerances. The following paragraphs will give an overview about the work on this subject published in paper *V* and in [42], [43].

5.1 CONCEPT AND DESIGN

A focusing fan-out element has to perform simultaneously two functions usually provided by different elements, namely that of focusing and beam splitting. In the approach presented here, the focusing part will be realized in the form of PMFEs. For each of the N interconnection channels, a specific PMFE is designed. One approach would be to arrange these different PMFEs as whole units to a microlens array. However such a fan-out element would require a highly uniform illumination in the aperture, and the imaging resolution would be limited by the aperture of each lenslet. In the concept presented here, each type of PMFE is divided into a subarray structure, which is distributed over the whole aperture. The complete PMFE fan-out structure is then obtained by interlacing the N different subarrays, denominated as $(\overline{C}, \overline{B}, A, B, C)$ in Fig. 14, which shows the AFM picture of a portion of an element fabricated in photoresist. This combination of a PMFE with a subarray structure leads to an array of focused diffraction orders centered around the former focal point of the unsplitted PMFE. In order to obtain a linear array of N image points, the period Λ of the different subarray structures is chosen so that the diffraction orders coincide with the desired image point array. This leads to the

$$\Lambda = l' \frac{\lambda}{\Delta x'} \tag{5.1}$$

condition for the subarray period Λ (cf. Fig. 14), where l' is the focal length of the focusing fan-out element, $\Delta x'$ the pitch of the image point array and λ the wavelength.

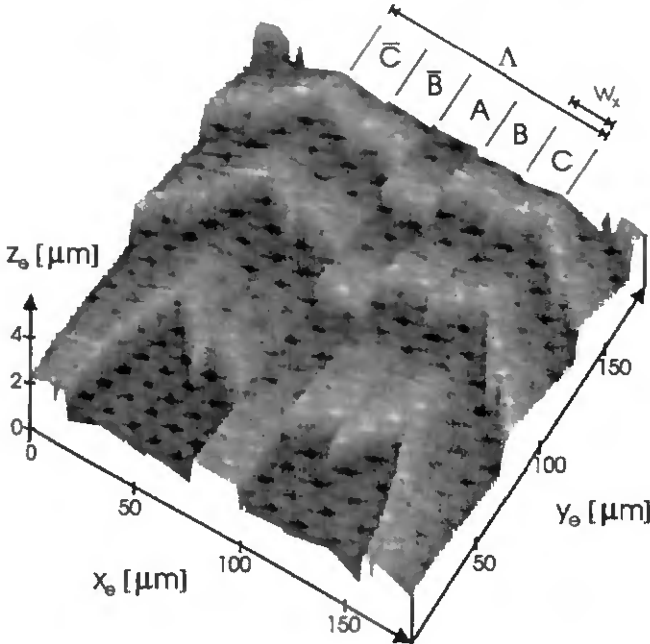

Fig. 14. AFM picture of the surface relief for one complete subarray period of a 5x1 fan-out element based on spatially interlaced PMFEs.

The optimization procedure for fan-out elements aims at achieving a high uniformity in the peak powers of the image points and a high overall efficiency. Uniformity error and efficiency are defined as

$$\sigma = \frac{P_{\max} - P_{\min}}{P_{\max} + P_{\min}}, \tag{5.2}$$

and

$$\eta = \frac{\sum_{j=1}^{N} P_j}{P_0}, \tag{5.3}$$

respectively, where P_j are the peak powers in the image points, P_{max} and P_{min} their maximum and minimum values, respectively, and P_0 the illuminating power incident on the total PMFE area. The peak powers P_j are obtained by coherent superposition of the diffraction patterns of the different subarray types (e.g. $(\overline{C}, \overline{B}, A, B, C)$). Most

important in the optimization are the arrangement of the different subarrays and the relative phases of their diffraction patterns. These can be calculated by Fourier optics, using a model that replaces the PMFEs by thin ideal lenses and describes the subarray structures as aperture functions. Symmetry conditions require symmetric spatial configurations of the different subarray types and also symmetric values for their relative phases. Based on these restrictions, the optimization of the relative phases of the subarray diffraction patterns for a given arrangement can be performed using fast converging algorithms, leading to focusing fan-out elements with a theoretically vanishing uniformity error and an efficiency in the range between 85% and 95%.

The design of *two-dimensional* focusing fan-outs based on spatially interlaced PMFEs is a straightforward extension of the above concept. The microrelief then consists of pads arranged in a two-dimensional checkerboard pattern instead of the one-dimensional subarray structure of Fig. 14. First *reflective* focusing fan-out elements designed by this concept were reported in [42] and [43]. Reflective beam splitting and focusing elements as described here and in Sec. 6.4 are important components in planar integration schemes of free-space optical interconnects [1], [2]. The optimization of reflective fan-outs has to take into account, that the angles of incidence on the subarray structure vary over the element area. Therefore the mutual coincidence between focal points and diffraction orders from different subarray types is no longer achieved by a periodic subarray structure. It was experimentally demonstrated, that this effect can be compensated by a local adjustment of the subarray period Λ.

5.2 EXPERIMENTAL RESULTS

For demonstrating the design and fabrication of a fan-out PMFE, the example of a transmissive element which focuses a collimated HeNe laser beam (wavelength $\lambda = 632.8$ nm) into a linear array of 5 image spots, equally spaced by 67 µm, is considered. The focal length was 10 mm, leading to a subarray period $\Lambda = 100$ µm.

In the previous Section, we dealt with the case of a *Nx1* fan-out realized by *N* different subarray structures. However, it is also viable to use a greater or smaller number *L* of different interlaced PMFEs. In this specific case, for $L = N = 5$ the theoretical uniformity error can be optimized to zero, the calculated efficiency of such an element is $\eta_{th} \approx 88\%$. If $L = 7$ different subarrays are used, the theoretical efficiency can be increased to 92%. However, the optimization process becomes more time consuming and the fabrication may come to a limit due to the smaller widths w_x of the subarray elements (cf. Fig. 14). A solution with a very fast optimization and a reduction in the fabrication requirements is the use of only 3 different subarrays for the generation of 5 image spots. Although, a vanishing uniformity error is no more possible by theory, the values of $\sigma = 1.5\%$ and $\eta = 87\%$ may still be good enough for many applications.

The fan-out PMFEs used for these investigations were fabricated by laser beam writing in photo resist layers on glass substrates [paper *II*]. A previously designed contiguous PMFE, fulfilling the task of focusing the laser beam into one image point, was the basis for realizing these elements. The data for the fan-out structure were calculated in *real-time* during the writing process on a Sun SparcStation and transmitted via DecNet to the control PC. The efficiencies η_r of the fan-out PMFEs were measured relative to the efficiency of a single, unsplitted PMFE, whose typical absolute values was $\eta_a \approx 70\%$. For $L = N = 5$ an experimental uniformity error of 1.6% at an efficiency close to the theoretical value of $\eta_r \approx 88\%$ was achieved. Figure 15 shows a scan through the irradiance distribution in the image plane of an element, measured by a CCD camera. A good agreement with the theoretical values was observed. These results, as well as the low calculation effort in the design procedure, compete favorably with results presented elsewhere [44], [45].

A major aspect of the PMFE fan-out approach is the large tolerance with respect to fabrication errors. In a series of experiments, where depth scaling errors over a range of ±20% have been introduced, PMFE fan-outs showed a uniformity error of < 3%. This is much superior to the performance of conventional surface relief fan-out elements for which a uniformity reduction by 10% typically results from a depth scaling error of only a few percent [32], [41].

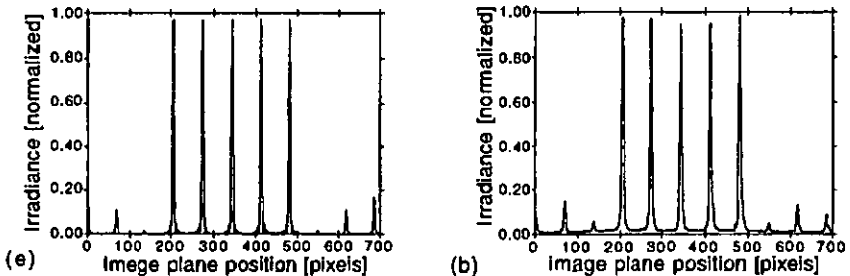

Fig. 15. Irradiance distribution scan through the central line in the image plane of a 5x1 fan-out showing theoretical (a) and experimental (b) results.

5.3 COMPARISON WITH RELATED FAN-OUT APPROACHES

This high tolerance of PMFE fan-outs with respect to depth errors can be understood by a closer look at their phase function. The overall phase variation of PMFE fan-outs is a combination of a focusing and a splitting function [44]. In a first approximation, the focusing phase function of the individually designed PMFEs for the different interconnection channels can be assumed to be identical. Therefore, the overall phase function is obtained by applying a series of splitting and shifting operations on the focusing phase function. Due to the basic Fourier transform

properties [4], the spatial shift of a phase function in the element plane is equivalent to the multiplication with a linear phase factor in the Fourier plane. Based on such considerations, the splitting function of a PMFE fan-out can be identified with a function of period Λ and function values which vary linearly within N discrete subintervalls. In contrast, other approaches calculate *continuous* phase functions [40] yielding efficiencies close to 100%. However, these splitting functions require the realization of a surface relief profile with very high fabrication accuracies for good optical performance. Our concept relies on a simpler form of the splitting function, but its realization in a focusing fan-out is achieved by lateral modifications of the focusing function. The lateral accuracy in typical fabrication technologies such as laser or e-beam writing is very high. Therefore, good uniformities can be obtained. Eventual depth errors in the surface relief profile do not affect the splitting function and the uniformity. They only reduce the efficiency of the elements.

6. APPLICATIONS

6.1 PMFE ARRAYS FOR CONFOCAL MICROSCOPY

Confocal microscopy [46], [47] is a widely used method for the inspection of surfaces and structures. In the basic arrangement of a reflection confocal microscope, a point light source at a pinhole P is imaged via an optical system on a diffraction-limited point P' on the sample. The reflected light at P' is collected by the same objective, focused on a pinhole, and imaged to the detector. In perfect autocollimation, the detector measures a maximum signal. The depth information of a sample is obtained by scanning a focused spot over the object and simultaneously adjusting the system for autocollimation by axially shifting the object. For good lateral and depth resolutions, high NA lenses have to be used, which in contrast reduces the object field. In order to have both a high resolution and a large object field, the application of microlens arrays was proposed [48]. In addition, the measuring time can be reduced by the parallel data sampling.

The requirements for the use of microlens arrays in confocal microscopy are high numerical aperture, low aberrations for diffraction-limited imaging [49], and good uniformity of the focal lengths l' over the microlens array.

A 256 x 256 array of quadratic PMFEs with a focal length $l' = 250\ \mu m$ and a size of 150 µm was designed for the wavelength $\lambda = 780$ nm. First estimations showed that for the resulting NA = 0.29 and the limitation for the segment width $w > w_{min} = 5\ \mu m$, a phase-matching number of $M = 3$ was required in the outer regions of the PMFE. The choice of M in the central PMFE region was determined by another fabrication constraint: The total array size of 38.4 x 38.4 mm^2 led to writing times on the laser beam writing system in the order of 60 hours. In paper *II*, measurements on the "latent image decay" are reported. Due to this effect, the depth of a structure is a function of the exposure dose as well as of the time between exposure and development. In principle, this latent image decay could be precompensated by higher exposure doses, but at the present time this option was not yet installed. According to the measurements presented in paper *II*, a depth gradient of up to ± 5% over a PMFE array of this size has to be expected.

The numerical simulations of the behavior PMFEs under small depth errors presented in Section 3 were applied to the elements under consideration in this application. For a PMFE with $M_j = M = 3$ constant over the whole element area, an efficiency reduction of ≈ 15% for a depth error of ±5% was obtained. In addition, depending on the sign of the depth error, higher or lower order focal points will by activated. A depth error of -5%, expressed by a depth scaling factor $\nu = 0.95$, leads to an additional focal point at $z \approx 380\ \mu m$ with an efficiency of 10% compared to the main focal point at $z = 250\ \mu m$. Since the measurement principle of confocal microscopy requires a well defined axial energy distribution with a high uniformity over the lens array, these effects can limit the system performance and therefore should be avoided as far as possible. In Section 3, it was shown that high phase-

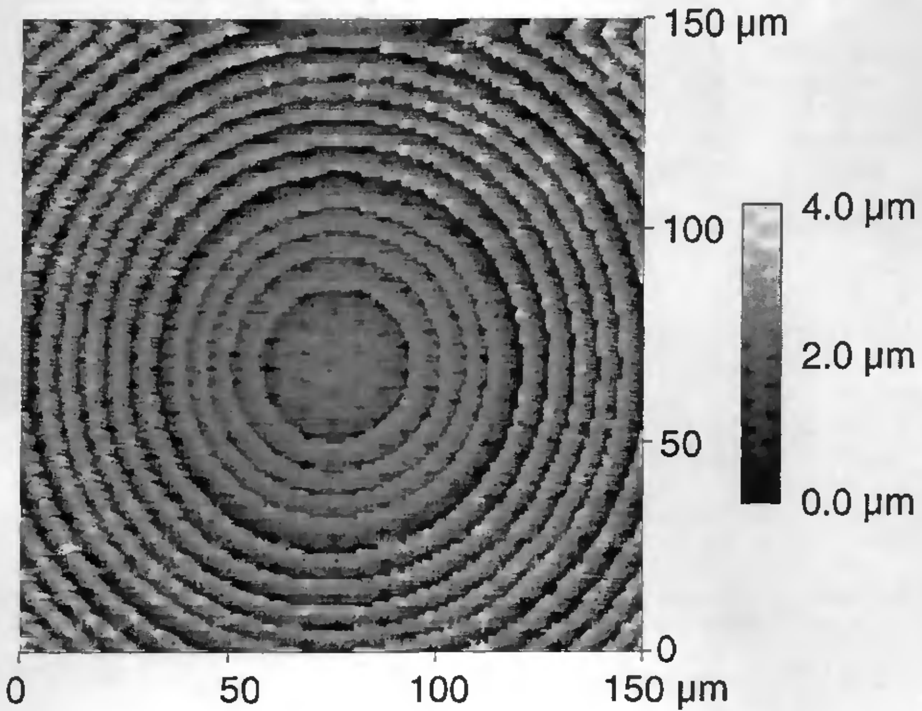

Fig. 16 AFM measurement of a PMFE designed and fabricated for application in confocal microscopy.

matching numbers increase the sensitivity on depth errors by lowering the efficiency in the main focal point and giving rise to additional foci near the designed one. Since the depth errors due to the latent image decay could not be controlled for this application, an element with values of M_j as low as possible promises a more stable behavior. Numerical simulations on such an element showed a loss of efficiency in the main focus of 8.5% and an energy of 2% in the lower order focal point at $z \approx 380$ µm by a depth error of $\nu = 0.9$, which is distinctly better than the values obtained for $M_j = 3 =$ constant.

Fig. 16 shows an AFM measurement of one single PMFE fabricated by laser beam writing in photoresist. The changes in the phase-matching number from $M_j = 1$ to $M_j = 2$ at $r = 35$ µm and from $M_j = 2$ to $M_j = 3$ at $r = 67$ µm, as well as the aliasing effects of the circular segment boundaries with the 1x1 µm raster are clearly visible. The microlens array was tested in a confocal microscopy setup at the *Institut für Technische Optik* in Stuttgart, Germany. In order to determine the focal lengths of the microlenses, a mirror with a planarity of $\lambda/20$ was measured with the confocal

microscope. The resulting profile then corresponds to the distribution of the focal lengths. A value of $\Delta l' = \pm 200$ nm with a mean deviation of $\sigma = 90$ nm was determined [50]. Due to these very small deviations, reference measurements of the microlens array were not necessary. The axial irradiance distribution showed a symmetrical form with no sidelobes, being an indication for small spherical aberrations. For the spot diameter of the confocal microscope a FWHM value of ≈ 10 µm was measured, compared to the theoretical value of 8 µm. These good optical characteristics proved that large PMFE arrays can fulfill the demanding requirements for an application such as confocal microscopy.

6.2 APPLICATION IN A TELECENTRIC OPTICAL METROLOGY SYSTEM

In an industrial project, in which a novel miniature position encoder was developed, replicated PMFEs were used as part of a prototype microoptical system. The system is based on a special microoptical telecentrical imaging system which projects an enlarged image of a scale onto a dedicated photo-detector [51] (cf. Fig. 17).

The scale is illuminated by different LEDs having a central wavelength $\lambda_0 = 880$ nm and spectral bandwidths of 30 nm, 45 nm or 80 nm. The microoptical system has to

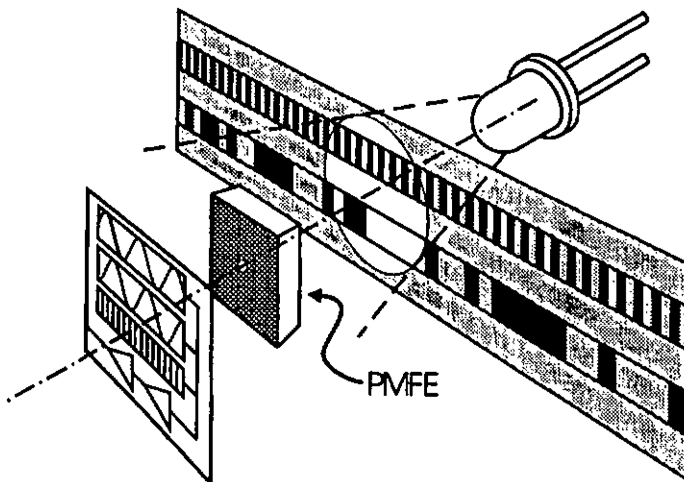

Fig. 17. Schematic setup of a novel optical position detector

magnify the scale by a factor of 8 in order to match the specially designed detector geometry. The focal length of $l' = 2$ mm of the PMFE and the diameter 360 μm of the telecentric stop results in an NA = 0.09 at the object side.

In the design of the PMFE, a phase-matching number of $M_j = 2$ for the whole area was chosen. A minimum segment width $w_{min} \approx 10$ μm and a maximum depth $h_{max} \approx 3.6$ μm resulted for an element replicated in polycarbonate. As shown in Section 3, a good profile fidelity of the laser written surface relief and therefore a reduction of stray light can be expected for these large segments. However, according to Eq. 3.7, an increased sensitivity of the element efficiency on linear surface relief errors ν introduced by fabrication inaccuracies is obtained for higher values of M_j. This potential drawback was overcome by the fabrication of an array of PMFEs where the surface relief profiles of the individual PMFEs were scaled by linear factors. The selection of the PMFE with the best profile fidelity was carried out by measuring the image contrast obtained with the different elements in a test setup of the telecentric system.

The telecentric system imaged a binary grating of 10 μm period. The fundamental spatial frequency of the grid is close to the diffraction limit. The grating image resulting with a PMFE was compared with the image obtained with a bulk spherical glass lens (Spindler & Hoyer 312002, $f_{850\ nm} = 2.05$ mm). The image contrast and the useful image field obtained with a PMFE were limited by the spectral bandwidth of the illuminating LED. Decreasing the bandwidth $\Delta\lambda$ increased the image contrast and extended the size of the useful image field. At $\Delta\lambda = 30$ nm,

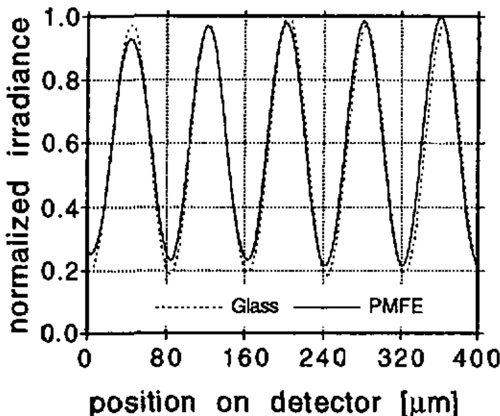

Fig. 18. Irradiance distribution of grating structure imaged by bulk glass lens (·····) and PMFE (—) in the telecentric system.

the chromatic aberrations of the diffractive leos were low enough that the image contrast as well as the image field reached values which were obtained with the glass lens.

Figure 18 shows two measurements with contrast values 0.63 for the PMFE and 0.68 for the glass lens. The image obtaioed with the glass lens showed a considerable field curvature. These aberratioos were not detected in the images obtained with the PMFE.

Due to the telecentric imaging system, the period of the imaged grating should not be affected by defocusing the grating. For a defocus $\Delta z = \pm 100$ μm a relative change in the grating period of 2% was measured for a PMFE at an illumination bandwidth of $\Delta\lambda = 30$ nm, 0.5% for a glass lens and 9% without a telecentric stop.

In this example, we have demonstrated the practical usefulness of PMFEs in an optical metrology microsystem. For a small illumination bandwidth ($\Delta\lambda \leq 30$ nm), the optical performaoce of PMFEs was comparable to the performance of the spherical classical lens. The image contrast was of the same order. For higher illumination bandwidths, the chromatic aberrations of diffractive optical elements reduce the system performance in terms of image field size, image contrast and stabilization of magnification in a telecentric setup.

6.3 LASER DIODE-TO-FIBER COUPLING / ANAMORPHIC ELEMENTS

Many applications in optics require efficient devices for interconnecting light emitters to different configurations of output ports. In recent years, parallel optical data links have attracted increasing interest in the field of data communications. Typical applications are parallel high-speed and high-capacity interconnects for optical switches, workstation clusters or even between processor chips. As an example for parallel optical interconnection, a PMFE array for laser diode-to-fiber coupling is described. Most of the other work done in the area of high NA lenses ([52], [53], [54]) uses e-beam lithography for the fabrication, requiring a set of binary masks and multiple exposures. Since the PMFE design approach locally takes into account the limitations of the technology actually used for the fabrication, we were able to achieve excellent results with direct laser beam writing in one single exposure step. The drawback of the lower lateral resolution compared to e-beam writing could be overcome by designing deeper relief structures with a continuous profile.

The aim of this project was to couple the light of a laser diode array into a multimode fiber ribbon cable compatible to the commercially available MT-connector [55]. Furthermore, the elements were designed for plastic materials, in order to be compatible with low-cost industrial replication techniques. The main requirements for this application were a high optical laser-to-fiber throughput and a low crosstalk to adjacent fibers via the lenses in the array. For the single lenslets, optimizing the optical throughput calls for (1) a high numerical aperture NA, (2)

adapting the clear aperture shape and size to the laser beam profile at the entrance pupil, and (3) achieving a high efficiency. Some important factors for crosstalk minimization in a practical device are (i) a good image quality, (ii) a large tolerance for fiber misalignment, and (iii) proper lenslet entrance pupil locations. The optimization with respect to these aspects resulted in the optical arrangement shown in Fig. 19. For the calculation of the optimal element size and the estimation of the maximum overall optical throughput, it is important to take into account the strongly inhomogenous distributions of the irradiance and the polarization state in the entrance pupil. The total fraction of transmitted light is mainly determined by the aperture size in the y-direction and the Fresnel reflection losses depending on the local polarization state. Calculations showed that the overall optical throughput saturates at 92% for elements with a y-size ≥ 300 μm. However, this estimation relies on calculations based on the scalar optical theory. Calculations using rigorous diffraction theory [56], [57], [58] showed that a significant loss in efficiency of grating structures with local periods in the range 2 - 3 times the design wavelength. In these high NA regions (r ≥ 100 μm), an optimization with vector methods would be required for a higher efficiency, which would require enormous computing power for spherical lenses of the required size.

For the design of the elements, the phase-matching number M_j was kept as low as possible and was only increased when the minimum segment size of $w_{min} = 5$ μm was achieved. In order to reduce the aliasing effects described in Section 2.3, the pixel size in the laser writing process was reduced to 250 nm. The required higher writing time was acceptable; due to the small size of the elements, it was still less than one hour. An AFM measurement of an element fabricated in photoresist is shown in Fig. 20. In order to correct for inaccuracies in the surface relief depth, the depth profile of each lens in the array was scaled by a different factor. A maximum overall optical throughput of 60% was measured.

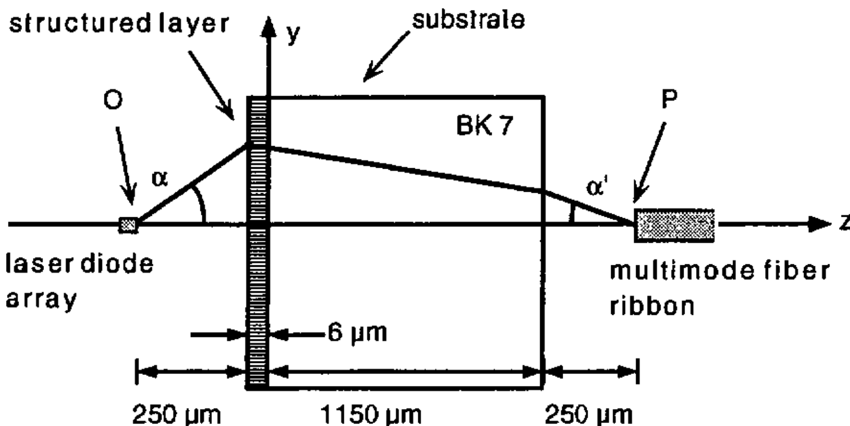

Fig. 19. Optical arrangement for laser-to-fiber coupling.

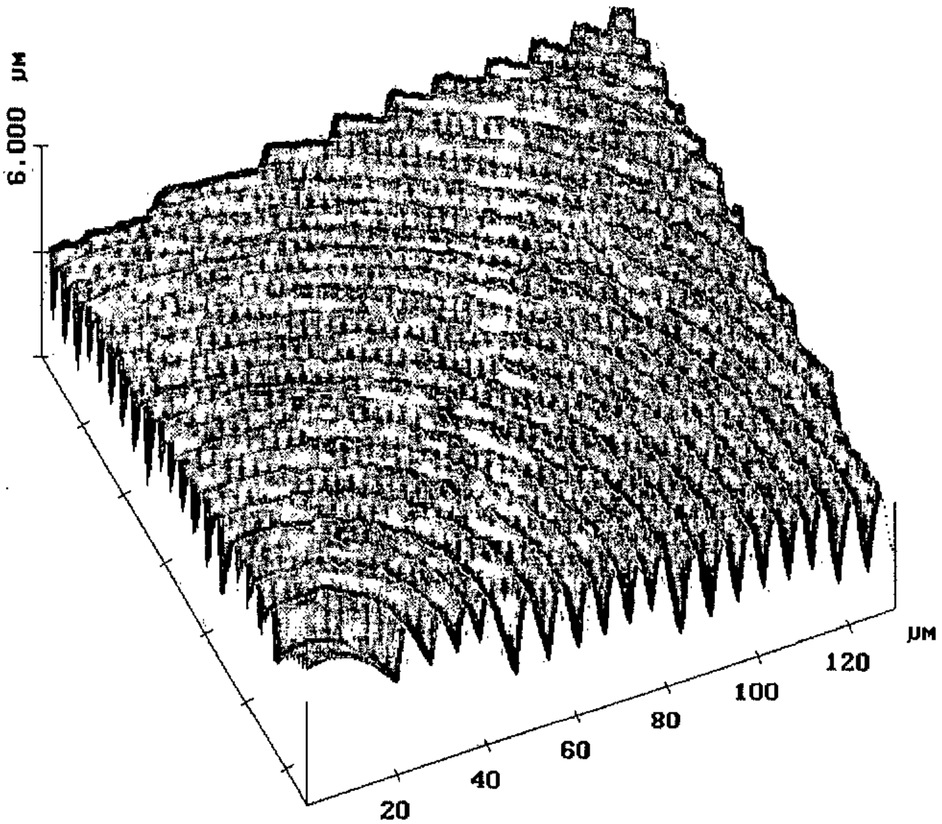

Fig. 20. AFM image of a PMFE for laser diode-to-fiber coupling

Due to the elliptical near-field and the longitudinal astigmatism of the laser diode, its image formed by a circular symmetric PMFE has also an elliptical shape. In order to adapt the image shape to the circular fiber symmetry, an anamorphic imaging element [15] was designed and fabricated.

The anamorphic microlens has different focal lengths in the parallel (x) and the perpendicular (y) direction. They were adjusted such that a circular irradiance distribution in the image plane was obtained. The beam parameters of the laser diode and of the field behind the microoptical element were determined by using an instrument (ModeMaster with silicon detector, Coherent Inc.) performing knife-edge measurements. The measurement principle and the analysis of the data are described in [38]. The results of this characterization can be summarized as follows:

1. The M^2-parameter, characterizing the beam quality does not deviate much from the values for the beam directly emitted by the laser diode, proving that the anamorphic PMFEs do not introduce significant aberrations to the laser beam.
2. In the image plane, a circularized irradiance distribution with the predicted 1/e-radius of 16 µm was measured.

These results show that PMFEs have a great potential also in many other imaging systems where an altered irradiance distribution is required. Typical examples are optical storage and sensing applications.

More information on this collaboration with the IBM Research Laboratory in Rüschlikon / Zurich can be found in paper *IV*.

6.4 REFLECTIVE PMFEs IN OPTICAL SENSOR SYSTEMS

In this industrial project, a planar focusing mirror with the potential for low-cost mass production was required for the use in an optical sensor system. The element has to image an LED with a central wavelength $\lambda_0 = 886$ nm and a spectral bandwidth $\Delta\lambda = 80$ nm on an image point O in the configuration shown in Fig. 21. In order to collect the maximum amount of light emitted by the LED, a rectangular element with a size of 12 x 17 mm^2 was needed, resulting in an f-number of 0.7 and an NA on the image side of 0.6.

The minimum segment width for fabrication by laser beam writing imposed a

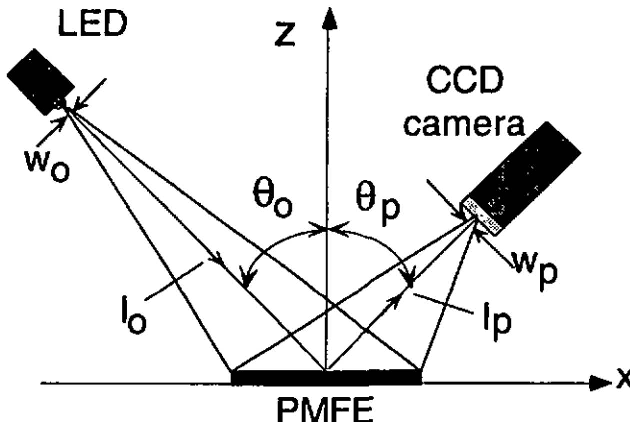

Fig. 21. Basic configuration and measurement setup for a reflective PMFE in an optical sensor ($l_O = 51.6$ mm, $l_P = 14.2$ mm, $\theta_O = \theta_P = 45°$).

maximum phase-matching number $M_j = 5$ at the element edges. For the central regions, M_j was kept as low as possible. A schematic drawing of the design is given in Fig. 4 of this overview. The PMFE was fabricated by direct laser writing in photoresist. The resulting surface microstructure was replicated by electroplating a first generation nickel shim and subsequent hot embossing in polycarbonate foil on a relatively simple laboratory apparatus. The suitability for mass production on an industrial scale was studied by combining a series of third generation shims to a larger shim for a flat bed embossing system [58]. In a trial run on such a system, good quality replicas in polyvinylchloride (PVC) foil were obtained.

For the optical characterization, the two types of PMFE replica were coated with a gold layer of ≈ 80% reflectivity. The radiating disk of the LED with a diameter of 1.2 mm was imaged on a CCD camera. For both types of elements, a spot diameter of $w_p = 360$ μm was measured [8]. This compares favorably with the value $w_{id} = 340$ μm for an ideal element. The measured efficiency of the replicas in polycarbonate was 52%, corresponding to 65% for a perfectly reflecting surface. The efficiency of the industrially fabricated PVC replicas, obtained from a third generation shim, was only 2% lower.

7. CONCLUSIONS

A novel approach for designing planar optical elements in the form of a segmented surface microrelief structure has been developed. The design of phase-matched Fresnel elements includes the optimization of the segment size, which is an important degree of freedom for combining the merits of geometrical and diffractive optical elements as well as for enhancing the suitability for the fabrication process. By this approach, the optical performance of elements with numerical apertures up to 0.5 could be optimized. The refractive and diffractive properties of these planar microoptical elements were theoretically investigated. Their behavior under fabrication errors and wavelength deviations was numerically simulated.

Laser writing in photoresist has been shown to be a viable technology for the fabrication of these planar, continuous-relief microoptical elements. Low-cost mass-production of phase-matched Fresnel elements by replication has successfully been demonstrated in a technology suitable for industrial production.

A novel concept for realizing planar focusing fan-out elements based on spatially interlaced planar lenses has been presented. For the optimization of these elements, simple and fast procedures have been developed. Excellent uniformity and a high tolerance with respect to fabrication errors have been measured.

The viability of the phase-matched Fresnel element concept was experimentally demonstrated for different types of optical components, for example point-to-point imaging elements, anamorphic lenses and focusing fan-out elements. Typical applications for these computer-generated reflective and transmissive planar optical elements are in optical imaging, illumination and detection systems as well as in micro- and planar optical systems.

Future investigations on the optical properties of these elements are aimed at optimizing phase-matched Fresnel elements for applications with broad-band illumination and spatially extended sources.

REFERENCES

[1] J. Jahns and A. Huang, "Planar integration of free-space optical components," Appl. Opt. **28**, 1602-1605 (1989).

[2] S.J. Walker and J. Jahns, "Optical clock distribution using integrated free-space optics," Opt. Commun. **90**, 359-371 (1992).

[3] M. Born and E. Wolf, *Principles of optics*, (Pergamon Press, Oxford, 1989).

[4] J.W. Goodman, *Introduction to Fourier optics*, (McGraw-Hill, San Francisco, 1968).

[5] E. Hecht and A. Zajac, *Optics*, 2nd ed. (Addison-Wesley, Reading, 1987).

[6] J.D. Gaskill, *Linear Systems, Fourier Transforms and Optics*, (J. Wiley & Sons, New York, 1978) Ch. 10-6.

[7] E.T. Whittaker, *History of the theories of aether and electricity*, Vol. 1 (Nelson, London, 1951).

[8] R.E. Kunz and M. Rossi., "Phase-matched Fresnel elements", *Opt. Comm.* **97**, 6-10 (1993).

[9] L.N. Hazra, Y. Han and C. Delisle, "Plane kinoform lenses for axial stigmatism in finite conjugate imaging," Opt. Comm. **91**, 1-4 (1992).

[10] J. Futhey and M. Fleming, "Superzone diffractive lenses," Technical Digest Series Volume 9, Diffractive Optics Workshop New Orleans, April 13-15, 1992.

[11] J.C. Marron, D.K. Angell, and A.M. Tai, "Higher-order kinoforms," in *Computer and Optically Formed Holographic Optics*, I. Cindrich and S.H. Lee, eds., Proc. SPIE **1211**, 62-66 (1990).

[12] E. Brookner (Ed.), *Practical Phased Array Antenna Systems* (Artech House, Boston, 1991).

[13] J.S. Fender, R.A. Carreras, "Demonstration of an optical phased telescope array," Opt. Eng **27**, 706-711 (1988).

[14] W.M. Neubert, K.H. Kudielka, W.R. Leeb, and A.L. Scholtz, "Experimental demonstration of an optical phased array antenna for laser space communications," Appl. Opt. **33**, 3820-3830 (1994).

[15] W.T. Welford, *Aberrations of optical systems* (Adam Hilger Ltd., Bristol, 1986).

[16] W.H. Southwell, "Ray tracing kinoform lens surfaces," Appl. Opt. **31**, 2244-2247 (1992).

[17] D.P. Hamblen, "Miniature aspheric lenses with spherical index gradients," Appl. Opt. **33**, 561-564 (1994).

[18] D. Daly, R.F. Stevens, M.C. Hutley, N. Davies, "The manufacture of microlenses by melting photoresist," Meas. Sci. Technol. **1**, 759-766 (1990).

[19] Z.D. Popovic, R.A. Sprague, and G.A. Connell, "Technique for monolithic fabrication of microlens arrays," Appl. Opt. **27**, 1281-1284 (1988).

[20] N.F. Borelli, D.L. Morse, R.H. Bellmann, and W.L. Morgan, "Photolytic technique for producing microlenses in photosensitive glass," Appl. Opt. **24**, 2520-2525 (1985).

[21] G. Hatakoshi et al, "Grating axicon for collimating Cerenkov radiation waves," Opt. Lett. **15**, 1336-1338 (1990).

[22] A.J. McDowell, P.B. Conway, A.C. Cox, R.A. Parker, C.W. Slinger, A.P. Wood, "An investigation of the defects introduced when diamond turning components for use in infrared optical systems," OSA Technical Digest Series, Vol. **11**, 99-102 (1994).

[23] T. Fujita, H. Nishihara and J. Koyama, "Blazed gratings and Fresnel lenses fabricated by electron-beam lithography," Opt. Lett. **7**, 578-580 (1982).

REFERENCES

[24] D. Zaleta, W. Daschner, M. Larsson, B.C. Cress, J. Fan, K.S. Urquhart and S.H. Lee, "Diffractive optics fabricated by electron-beam direct write methods", SPIE Critical Review Proceedings, **CR49**, San Diego, 117-137 (1993).
[25] J.M. Stauffer, Y. Oppliger, P. Regnault, L. Baraldi and M.T. Gale, "Electron beam writing of continuous resist profiles for optical applications", J. Vac. Sci. Technol. B **10**, 2526-2529 (1992).
[26] M. Ekberg, F. Nikolajeff M. Larsson, and S. Hård, "Proximity-compensated blazed transmission grating manufacture by direct-writing electron-beam lithography", Appl. Opt. **33**, (1994).
[27] E.B. Kley and W. Dorl, "Einsatz der Elektronenstrahllithographie zur Herstellung mikrooptischer Bauelemente," VDI Berichte **1012**, 531-541 (1992).
[28] M.B. Stern, M. Holz, S.S. Medeiros, and R.E. Knowlden, "Fabricating binary optics: Process variables critical to optical efficiency," J. Vac. Sci. Technol. B 9, 3117-3120 (1991).
[29] G. Gal, "Micro-optics technology and development for advanced sensors," SPIE Critical Review Proceedings, CR **49**, San Diego, 329-359 (1993).
[30] Y. Oppliger, P. Sixt, J.M. Stauffer, J.M. Mayor, P. Regnault and G. Voirin, "One-step shaping using a gray-tone mask for optical and microelectronic applications", Microelectronic Engineering 23, 449-454 (1994).
[31] M.T. Gale and K. Knop, "The fabrication of fine lens arrays by laser beam writing", *Proc. SPIE* **398**, 347-353 (1983).
[32] M.T. Gale, M. Rossi, H. Schütz, P. Ehbets, H.P. Herzig, and D. Prongué , "Continuous-relief diffractive optical elements for two-dimensional array generation", *Appl. Opt.* **32**, 2526-2533 (1993).
[33] A. Yariv, *Introduction to optical electronics* (Holt, Rinehart, Winston, 1976).
[34] M. Rossi, R.E. Kunz ad G.L. Bona, "Phase-matched Fresnel elements for optical interconnects," OSA Technical Digest Series Vol. **11**, 321-324 (1994).
[35] K. Miyamoto, "The phase Fresnel lens," J. Opt. Soc. Am. **51**, 17 (1961).
[36] D.A. Buralli, G.M. Morris, and J.R. Rogers, "Optical performance of holographic kinoforms," Appl. Opt. **28**, 976-983 (1989).
[37] G.M. Morris and D. Faklis, "Achromatic and apochromatic diffractive singlets," OSA Topical Meeting on Diffractive Optics 1994, Technical Digest Series Vol. **11**, 53-56 (1994).
[38] A.E. Siegman, *Lasers* (University Science Books, Mill Valley, 1986).
[39] N. Streibl, "Beam shaping with optical array generators," J. of Mod. Opt. **36**, 1559-1573 (1989).
[40] D. Prongué, H. P. Herzig, R. Dändliker and M.T. Gale, "Optimized kinoform structures for highly efficient fan-out elements," Appl. Opt. **31**, 5706 (1992).
[41] J. Fagerholm, J. Turunen, A. Vasara and J. Westerholm, "Computer-generated Fourier-transform holograms for optical computing," Proc. SPIE **1136**, 253 (1989).
[42] M. Rossi and R.E. Kunz, "Phase-matched Fresnel elements for fan-out applications," Proc. IEE 379, 27 (1993).
[43] M. Rossi and R.E. Kunz, "Phase-matched Fresnel reflectors for fan-out applications," Proc. SPIE Vol. **1983**, 191-192 (1993).
[44] G. Hatakoshi and M. Nakamura, "Grating lenses for optical branching," Appl. Opt. **32**, 3661 (1993).
[45] D. Wood, P. McKee and M. Dames, "Multiple-imaging and multiple-focusing Fresnel lenses with high numerical aperture," Proc. SPIE **1732**, 307 (1992).

REFERENCES

[46] T. Wilson and C.J.R. Sheppard, *Theory and Practice of Scanning Optical Microscopy* (Academic, London, 1984).
[47] K. Carlsson and N. Aslund, "Confocal imaging for 3-D digital microscopy," Appl. Opt. **26**, 3232-3238 (1987).
[48] H.J. Tiziani and H.-M. Uhde, "Three-dimensional analysis by a microlens-array confocal arrangement," Appl. Opt. **33**, 567-572 (1994).
[49] C.J.R. Sheppard, M. Gu, K. Brain, and H. Zhou, "Influence of spherical aberration on axial imaging of confocal reflection microscopy," Appl. Opt. 33, 616-624 (1994).
[50] H.J. Tiziani, private communication.
[51] K. Engelhardt and P. Seitz, "Novel Optical Absolute Position Encoder with 10 nm Resolution," Proc. EOS-Conference om+n, March 1994, Engelberg, CH.
[52] J. R. Leger, M. L. Scott, and W. B. Veldkamp, "Coherent addition of AlGaAs lasers using microlenses and diffractive coupling," Appl. Phys. Lett. **52**, 1771-1773 (1988).
[53] A. Stemmer, H. Zarschizky, F. Mayerhofer, G. Lefranc, and W. Gramann, "Diffractive coupling lenses: fabrication and measurements of silicon elements," OSA Topical Meeting on Diffractive Optics 1994, Technical Digest Series Vol. **11**, 317-320 (1994).
[54] P. McKee, J. Towers, A. Thurlow, and D. Wood, "Fresnel lens array for optical fiber semiconductor coupling," OSA Topical Meeting on Diffractive Optics 1994, Technical Digest Series Vol. **11**, 235-238 (1994).
[55] F. Ashiya, T. Satake, S. Nagasawa, "Development of multifibre connectors and their application," EFOC/LAN '91 Proceedings, 304-308 (1991).
[56] E. Noponen, J. Turunen, A. Vasara, "Electromagnetic theory and design of diffractive-lens arrays," J. Opt. Soc. Am. A **10**, 434-443 (1993).
[57] D.A. Pommet, M.G. Moharam, and E.B. Grann, "Limits of scalar diffraction theory for diffractive phase elements," J. Opt. Soc. Am. A **11**, 1827-1834 (1994).
[58] M.C. Hutley, *Diffraction gratings*, (Academic Press, London, 1982).
[59] The PVC embossings were carried out via 3D Ltd., CH-6314 Unterägeri, Switzerland.

ABSTRACTS OF PUBLICATIONS I - V

Paper I

PHASE-MATCHED FRESNEL ELEMENTS

Rino E. Kunz and Markus Rossi

A novel design method for planar optical elements in the form of segmented microstructures, combining the advantages of geometrical and diffractive optical components, is outlined. Optimizing the microstructure for fabrication is an important integral part of the design process. First elements for focusing the light emitted by an LED have successfully been fabricated by laser beam writing in photoresist and subsequent replication. Their suitability for low cost mass fabrication has been demonstrated.

Paper II

FABRICATION OF CONTINUOUS-RELIEF MICROOPTICAL ELEMENTS BY DIRECT LASER WRITING IN PHOTORESIST

Michael T. Gale, Markus Rossi, Jörn Pedersen, and Helmut Schütz

A laser writing system for the fabrication of continuous-relief microoptical elements in photoresist is described. The technology enables a wide range of planar microoptical elements to be fabricated and replicated into polymer film using Ni shims electroformed from the photoresist originals. The advantages and limitations of laser writing technology for microoptics fabrication are discussed. Examples of fabricated microoptical elements include Fresnel microlenses and microlens arrays, kinoforms and other continuous-relief phase elements.

ABSTRACTS OF PUBLICATIONS I - V

Paper III

REFRACTIVE AND DIFFRACTIVE PROPERTIES OF PLANAR MICROOPTICAL ELEMENTS

Markus Rossi, Rino E. Kunz and Hans Peter Herzig

The refractive and diffractive properties of planar microoptical elements are investigated. The transition between purely refractive and purely diffractive planar microlenses is numerically simulated for the example of differently designed phase-matched Fresnel elements. Results obtained from numerical simulations and experiments show that the refractive and diffractive types exhibit a distinctly different behavior in the presence of small fabrication errors or wavelength deviations. Based on these results, design rules for various applications, including low and high NA lenses and hybrid refractive / diffractive elements, have been derived. For a high NA (f/# = 1) lens, the experimental characterization of the irradiance distribution in the image space is presented and shown to agree well with theoretical predictions.

Paper IV

ARRAYS OF ANAMORPHIC PHASE-MATCHED FRESNEL ELEMENTS FOR DIODE-TO-FIBER COUPLING

Markus Rossi, Gian Luca Bona and Rino E. Kunz

A method for designing microlens arrays which inherently takes into account application requirements and fabrication constraints is presented. Elements with numerical apertures of up to 0.5 have been designed and fabricated by laser beam writing in photoresist and replication in plastic material. In a laser diode-to-fiber array coupling experiment, an overall optical throughput of 60% was achieved. By means of anamorphic microlens arrays, correction of the laser diode longitudinal astigmatism and circularization of the image plane irradiance distribution have been demonstrated.

ABSTRACTS OF PUBLICATIONS I - V

Paper V

FOCUSING FAN-OUT ELEMENTS BASED ON PHASE-MATCHED FRESNEL LENSES

Markus Rossi and Rino E. Kunz

A novel approach for designing and fabricating focusing fan-out elements is presented. It is based on an area-sharing arrangement of planar lenses. Due to the low number of parameters and their well-defined physical meaning, it is possible to find solutions with both a high efficiency and a low uniformity error using simple and fast optimization procedures. Results of numerical simulations and experiments agree well. Conspicuous properties include a high fabrication fault tolerance, the suitability for-low cost mass production, and the possibility of realizing very compact microoptical systems.

Paper I

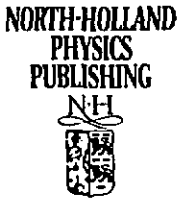

Phase-matched Fresnel elements

R.E. Kunz and M. Rossi

Paul Scherrer Institute Zurich, Badenerstrasse 569, CH-8048 Zurich, Switzerland

Received 4 September 1992; revised manuscript received 13 November 1992

A novel design method for planar optical elements in the form of segmented microstructures, combining the advantages of geometrical and diffractive optical components, is outlined. Optimizing the microstructure for fabrication is an important integral part of the design process. First elements for focusing the light emitted by an LED have successfully been fabricated by laser beam writing in photoresist and subsequent replication. Their suitability for low cost mass fabrication has been demonstrated.

Reprinted from OPTICS COMMUNICATIONS

Optics Communications 97 (1993) 6–10
North-Holland

OPTICS
COMMUNICATIONS

Phase-matched Fresnel elements

R.E. Kunz and M. Rossi
Paul Scherrer Institute Zurich, Badenerstrasse 569, CH-8048 Zurich, Switzerland

Received 4 September 1992; revised manuscript received 13 November 1992

A novel design method for planar optical elements in the form of segmented microstructures, combining the advantages of geometrical and diffractive optical components, is outlined. Optimizing the microstructure for fabrication is an important integral part of the design process. First elements for focusing the light emitted by an LED have successfully been fabricated by laser beam writing in photoresist and subsequent replication. Their suitability for low cost mass fabrication has been demonstrated.

1. Introduction

Two well-known possibilities for replacing bulk optical components by small, lightweight structures are Fresnel lenses and mirrors based on classical optics [1] and diffractive optical elements such as kinoforms [2] and holographic optical elements [3]. For conventional Fresnel elements, only coarse structures with feature details much larger than the wavelength λ of light can be properly designed, since diffractive effects are neglected. The design of diffractive optical elements is based on physical optics considerations, mainly using scalar diffraction theory. Deep structures with steep slopes are generally avoided since scalar diffraction theory is not suited to their optimization and since rigorous diffraction methods, which are able to treat deep gratings, require too large a computational effort.

In this paper, we propose and demonstrate a novel kind of planar optical element termed phase-matched Fresnel element (PMFE). Both physical and geometric optics considerations are used in the design at a moderate computational effort. The basic concept is outlined in sec. 2. The design method, which also optimizes the structure with respect to fabrication, is described in sec. 3, where some details on the fabrication are also given. In sec. 4, a PMFE is characterized by presenting first experimental results on the optical imaging properties and the surface profile measured by an atomic force microscope.

2. Basic concept

A PMFE is a segmented planar optical element with a typical segment size of several λ, which lies in the range between the feature size for classical Fresnel and diffractive optical elements. The microstructure of a PMFE is calculated by computer, providing a great flexibility for performing various optical functions, aiming for applications such as optical imaging, illumination and detection systems as well as micro- and planar optical systems [4]. In order to facilitate a concise discussion, this paper will deal with a specific example only, namely a reflective element for point-to-point imaging.

The purpose of the PMFE considered here is to focus the light emitted by a source O to an image point P in the arrangement defined in fig. 1. Each

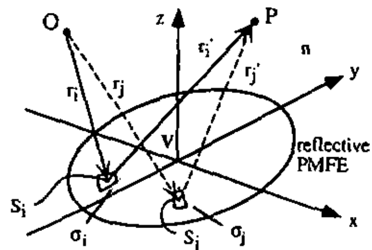

Fig. 1. Schematic of a PMFE, showing two segments σ_i and σ_j.

0030-4018/93/$ 06.00 © 1993 Elsevier Science Publishers B.V. All rights reserved.

segment σ_i acts as a reflective facet and converts a portion of the primary wave u_0 emitted from the source O into a secondary wavelet u_i directed to P. In order to calculate the contribution of the light reflected at the segment σ_i to the total light amplitude resulting in P, rays r_i and r_i' are traced from O to a point $S_i=(x_i, y_i, z_i)$ on σ_i and from S_i to P, respectively. The corresponding phase $\Phi(x_i, y_i, z_i)$ of the light amplitude in P is then calculated by means of the optical path length [5, secs. 2.1 and 11.4]:

$$\Phi(x_i, y_i, z_i) = knr_i + \Delta\Phi_i + knr_i' . \quad (1)$$

Here, $k=2\pi/\lambda$ is the wavenumber in air and n is the refractive index of the medium containing O and P. In this example, the phase shift $\Delta\Phi_i$ *due to the reflection* at S_i is assumed to be constant over the whole surface of the PMFE and independent of the local angle of incidence. The surface relief profile within one segment is defined by the condition that all rays reflected at any point S_i of a specific segment σ_i shall yield identical phases in P:

$$\Phi(x_i, y_i, z_i) = \Phi_i = \text{constant over } \sigma_i . \quad (2)$$

In the sense of a modified Huygens–Fresnel principle [6, p.393], the amplitude of the optical field at P results from the superposition of all the secondary wavelets. Therefore, in order to get constructive interference of two wavelets u_i, u_j emanating from any two different segments σ_i, σ_j, their phases Φ_i, Φ_j have to be matched to differ by an *integer* multiple of 2π;

$$\Phi_i - \Phi_j = m_{i,j} \times 2\pi, \quad m_{i,j} = 0, \pm 1, \pm 2, \dots . \quad (3)$$

The term "PMFE" was chosen because this phase matching between the different secondary wavelets is crucial for our approach. The basic concept of dividing the active area into segments with a controlled phase relation between them has its counterpart in the "phased arrays" [7] well established in microwave technology. Fulfilling the phase-match condition of eq. (3) assures that the diffractive effects will enhance the power radiated to P by constructive interference, irrespective of the specific light amplitude distribution of the secondary wavelets.

3. Design and fabrication

The feature size is a very important factor for the fabrication of any microstructure. In the design of a PMFE, the width w_i of the segments can be controlled by the phase difference

$$\Phi_i - \Phi_{i+1} = m_{i,i+1} \times 2\pi = M_i \times 2\pi , \quad (4)$$

for two neighboring segments σ_i and σ_{i+1}, i.e. by the phase-matching number M_i.

The possibility of setting $M_i > 1$ offers a powerful degree of freedom for fulfilling additional design requirements. In our case, fabrication of the PMFE by laser beam writing in photoresist [8] with a spot size of 1.5 µm imposed a minimum width $w_{min} \approx 5$ µm and a maximum depth $h_{max} \approx 3.5$ µm for the feature size of continuous microrelief structure. For the individual segments, this leads to the constraints of a minimum width $w_i \geqslant w_{min}$ and a maximum depth $h_i \leqslant h_{max}$ (cf. fig. 2).

We now consider the design and fabrication of a reflective PMFE which was used for imaging a light emitting diode (LED) in the configuration shown in fig. 3. For designing this PMFE, we started at the innermost segment $i=1$ with $M_i=1$ (cf. fig. 2). For segments $j>1$ with width w_j, the phase-matching

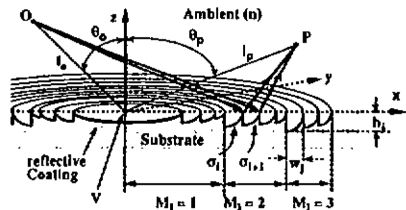

Fig. 2. Schematic drawing of a reflective PMFE structure showing regions with different phase-matching number M_i.

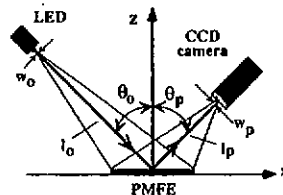

Fig. 3. Optical arrangement for measuring the light distribution in the image plane.

number M_j was kept constant as long as $w_j \geq w_{min}$, otherwise M_j was increased by 1. Repeating this process over the whole area of 12×17 mm^2 PMFE resulted in a total of 2100 segments with a maximum phase-matching number $M_{max} = 5$ at the edges of the rectangular aperture. At the center wavelength $\lambda = 886$ nm of the LED, this corresponds to an optical path length difference of 4.4 μm which is still lower than the coherence length $l_c \approx 10$ μm and therefore fulfills the requirement of coherent superposition of at least all the neighboring secondary wavelets.

For the example discussed here, it can easily be seen that eq. (3) can be fulfilled by choosing the segment boundary lines to be a set of ellipses located in the plane $z=0$ (cf. fig. 2). Their major and minor axes and center coordinates are analytical functions of the angles of incidence θ_o, θ_p and the conjugate distances l_o, l_p measured from the vertex V. The profile shape within these facets was calculated by geometrical optics ray tracing. This is adequate since the minimum facet size of 5 μm is distinctly larger than the wavelength of light. The condition imposed by eq. (2) leads to segments whose surface profiles are continuous portions of rotation ellipsoids with focal points at O and P.

In this special simple case, the PMFE can also be considered to represent a "higher order kinoform" [9] with different orders being present simultaneously, or a kind of reflective "superzone diffractive lens" [10], with the sawtooth profile being replaced by the rotation ellipsoidal surface elements. In a more general case, the PMFE structure can be interpreted to be blazed, deep, coarse and chirped diffraction grating in a region of parameter space which is usually avoided. For fabricating such elements, laser beam writing [8] is well-suited since it offers the possibility to locally vary the profile shape and also to realize any lateral shape of the segments, in contrast to other methods such as diamond turning used in ref. [10].

In order to investigate the suitability of the PMFE microstructure for low cost mass fabrication, a series of elements have been produced by laser beam writing and subsequent replication. The PMFEs have been fabricated by the programmable exposure of a 3.5 μm thick photoresist film with a focused HeCd laser beam of 1.5 μm diameter at 442 nm wavelength and 10 mm/s writing speed. The resulting photoresist surface microstructure was then used to obtain a first generation replication shim by electroplating a 100 μm thick nickel foil [11]. By means of this shim, a first series of PMFEs was successfully replicated by hot embossing in 0.75 mm thick polycarbonate sheets on a relatively simple laboratory apparatus. Next, the suitability for mass production on an industrial scale was studied, using a flat bed embossing system [12]. In a trial run on such a system [#1], good quality replicas in polyvinylchloride (PVC) foil were obtained from third generation shim derived from the original one.

4. Characterization

The surface profiles of the replicas in polycarbonate and PVC were measured by an atomic force microscope (AFM; NanoScope III, full tip vertex angle of 40°–50°). Figure 4a shows the surface profile of 3 and 2 segments for the regions $M_i = 1$ and $M_i = 2$, respectively, of a polycarbonate replica. While a good correspondence to the calculated profile is observed, two types of irregularities can be seen which are a consequence of the laser beam raster scanning process. One type is a surface ripple with an rms amplitude of 30 nm, coincident with the scan lines, and the second type are steps due to the scan raster discretization clearly visible at the segment boundaries. An AFM measurement, taken at a similar position as in fig. 4a, but for an industrially replicated PMFE in PVC, is given in fig. 4b. Closer examination of the two measurements reveals that the only distinct difference of the profile in fig. 4b is that the highest spatial frequency components of the surface profile irregularities of fig. 4a have been "smoothed" due to the processes involved in the industrial replication. A possibly positive effect on straylight reduction is presently under investigation.

The above mentioned PMFEs with 11.1 mm focal length have been optically characterized using the setup of fig. 3 with parameter values $\theta_o = \theta_p = 45°$, $l_o = 51.6$ mm, $l_p = 14.2$ mm. These f/0.7 elements were used at a numerical aperture of 0.6 on the image side. The radiating disk with diameter $w_o = 1.2$

[#1] The PVC embossings were carried out by 3D Ltd., CH-6314 Unterägeri, Switzerland.

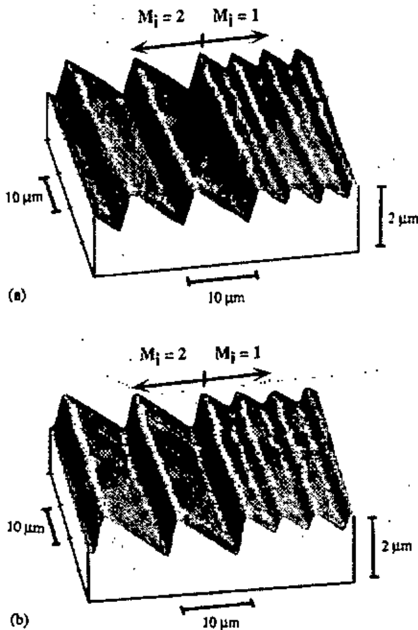

Fig. 4. Surface profiles of PMFE replicas (a) in polycarbonate and (b) in PVC foil, measured by an atomic force microscope.

mm of an LED with 80 nm spectral bandwidth was imaged for both types of replicas into a spot of diameter $w_p = 360$ µm on a CCD camera. This compares favorably with the value $w_{id} = 340$ µm for an ideal element. In order to match the optical setup requirements imposed by the short focal length, we used a Philips CCD camera, Model NXA 101-41, with the CCD sensor chip moved fully to the front and the electronics boards rearranged and recessed. With a gold layer of 80% reflectivity sputtered onto the replicas, the measured efficiency of the PMFE replicas in polycarbonate was 52%, corresponding to 65% for a perfectly reflecting surface. The efficiency of the PVC replicas, industrially produced from a third generation shim, was only 2% lower.

5. Conclusions

A novel approach for designing planar optical elements in the form of a segmented surface microrelief structure has been outlined. This design method includes the optimization of the segment size, which is an important degree of freedom for combining the merits of geometrical and diffractive optical elements as well as for enhancing the suitability for the fabrication process. Laser writing has been shown to be appropriate for producing the master microrelief, since it provides the flexibility for realizing continuous relief segments, each with a specific profile shape. The suitability of this type of optical element for low cost mass production by embossing in polycarbonate and PVC foil has been demonstrated.

As computer generated microstructures, the phase-matched Fresnel elements provide a great flexibility for performing much more complex function than the point-to-point imaging example described in this paper. Typical applications for reflective and transmissive elements are optical imaging, illumination and detection system as well as micro- and planar optical systems.

Acknowledgements

The authors gratefully acknowledge the help of and discussions with M.T. Gale, R. Dändliker (Institute of Microtechnology, Neuchâtel), J. Pedersen, C. Appassito, H. Schütz and Th. Jung.

References

[1] O.E. Miller, J.H. McLeod and W.T. Sherwood, J. Opt. Soc. Am. 41 (1951) 807.
[2] L.B. Lesem, P.M. Hirsch and J.A. Jordan, IBM J. Res. Develop. 13 (1969) 150.
[3] P. Hariharan, Optical Holography (Cambridge Univ. Press, Cambridge, 1984) Sec. 12.11.
[4] J. Jahns and A. Huang, Appl. Optics 28 (1989) 1602.
[5] W.T. Welford, Aberrations of optical systems (Adam Hilger, Bristol, 1986).
[6] E. Hecht and A. Zajac, Optics, 2nd Ed. (Addison-Wesley, Reading, 1987).
[7] E. Brookner, ed., Practical phased array antenna systems (Artech House, Boston, 1991).

[8] M.T. Gale, G.K. Lang, J.M. Raynor and H. Schütz, Proc. SPIE 1506 (1991) 65.
[9] J.C. Marron, D.K. Angell and A.M. Tai, Proc. SPIE Vol. 1211 (1990) 62.
[10] J. Futhey and M. Fleming, Technical Digest Series Volume 9, Diffractive Optics Workshop New Orleans, April, 1991.
[11] M.T. Gale, M. Rossi, H. Schütz, P. Ehbets, H.P. Herzig and D. Prongué, Applied Optics (1992) accepted for publication.
[12] B. Kluepfel and F. Ross, eds., Holography market place (Ross books, Berkeley, 1991).

Paper II

Fabrication of continuous-relief micro-optical elements by direct laser writing in photoresists

Michael T. Gale, MEMBER SPIE
Markus Rossi
Jörn Pedersen
Helmut Schütz
Paul Scherrer Institute
Badenerstrasse 569
CH-8048 Zürich, Switzerland
E-mail: gale@cvax.psi.ch

Abstract. A laser writing system for the fabrication of continuous-relief micro-optical elements in photoresist is described. The technology enables a wide range of planar micro-optical elements to be fabricated and replicated into polymer film using Ni shims electroformed from the photoresist originals. The advantages and limitations of laser writing technology for micro-optics fabrication are discussed. Examples of fabricated micro-optical elements include Fresnel microlenses and microlens arrays, kinoforms, and other continuous-relief phase elements.

Subject terms: micro-optics; planar optical elements; direct laser writing; replication.

Optical Engineering 33(11), 3556-3566 (November 1994).

1 Introduction

Planar micro-optical elements can be found in an increasing number of applications in optical systems and are expected to play a major role in future systems. They offer the potential of compact, lightweight optics that can be mass-produced in polymeric materials by low-cost replication techniques. With the trend toward miniaturization, these features are becoming highly attractive, for example, in the areas of optical sensors and optical metrology.

Figure 1 shows examples of some planar micro-optical elements. Typical elements for application at visible and near-infrared (NIR) wavelengths can be realized as surface-relief microstructures with a maximum relief depth of about 5 μm. Such microstructures can be mass-produced using current replication technologies such as hot-embossing, moulding, and casting. The fabrication and replication of deeper microstructures becomes increasingly more difficult and is not discussed in this paper. Micro-optical elements can be refractive (e.g., hemispherical lenslets and lenslet arrays), diffractive (kinoforms, grating microstructures, etc.) or a combination of both (e.g., Fresnel microlenses). They can be realized as continuous surface-relief microstructures[1,2] or as binary or multilevel reliefs,[3,4] the latter usually being referred to as "binary" optics (from the binary mask lithography steps used to fabricate the multilevel structures).

In most practical cases, the optical performance (efficiency and image uniformity in particular) of continuous-relief micro-optical elements is superior to that of their binary optical counterparts, the performance of which generally improves with increased complexity and number of levels. On the other hand, the fabrication of the original continuous-relief microstructure can present considerable experimental problems. Binary optical elements are fabricated using modern, high-resolution semiconductor fabrication technology, for which a variety of processes and equipment is available. In contrast, fabrication technology for continuous-relief micro-optics has not benefited from the massive semiconductor technology effort and is still in its infancy. Simple microstructures can be fabricated by diamond milling,[5] but limited resolution restricts applications to relatively smooth, slowly varying relief structures. Direct writing in photoresist by a focused laser beam, in which accurate control of the process parameters enables a complex continuous-relief microstructure to be fabricated in a single exposure scan and development step, has been shown to produce excellent results.[2,6] A similar approach using e-beam writing has also been demonstrated[7,8] but requires significantly more complex (expensive) equipment and, with the exception of high-resolution microstructures with submicrometer feature sizes, has not shown any significant advantage over laser writing for the fabrication of micro-optical elements. The imaging of half-tone masks, fabricated by e-beam writing, onto a photoresist film using a standard lithographic stepper has been shown to give good results,[9] although the application to high-quality, high-resolution microstructures has still to be demonstrated. The ablation of polymer film using a UV laser has also been demonstrated for producing continuous-relief structures,[10] but resolution and depth control are not yet sufficient for practical microstructure fabrication.

This paper describes progress in the fabrication of continuous-relief micro-optical elements by direct laser writing and presents examples of fabricated elements. The work described was carried out at the Paul Scherrer Institute, Zurich (PSIZ), using a laser writing system set up[11] in the early 1980s and continuously improved in subsequent years.[2,12,13] The technology developed enables a wide range of micro-optical elements to be fabricated, including Fresnel microlenses and lens arrays, kinoform elements, and general micro-relief phase structures for a variety of applications in optical

Paper MO-010 received Mar. 25, 1994; accepted for publication June 16, 1994. This paper is a revised version of a paper presented at the SPIE Symposium on Holography, Microstructures, and Laser Technologies, August 1993, Quebec, Canada. The paper presented there appears (unrefereed) in SPIE Proceedings Vol. 2045.
© 1994 Society of Photo-Optical Instrumentation Engineers. 0091-3286/94/$6.00.

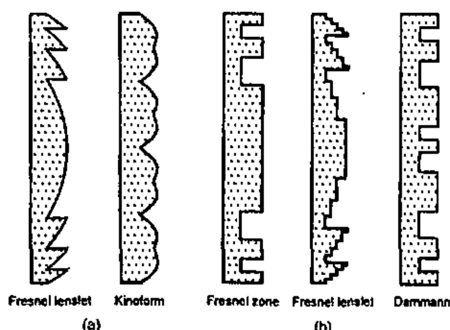

Fig. 1 Planar micro-optical elements: (a) examples of continuous-relief micro-optics fabricated by direct laser writing in photoresist and (b) binary micro-optics fabricated by binary semiconductor mask lithography.

systems. The paper concentrates on the practical aspects of the laser writing approach and discusses the advantages and limitations of the technology. Measurements on the fidelity of the replication process, which involves the fabrication of a nickel copy of the surface-relief microstructure and its replication into polymer material, are also presented and discussed.

2 Fabrication Technology

The original microstructures for continuous-relief micro-optical elements are fabricated by direct laser writing in photoresist. Following development of the exposed, raster-scanned photoresist film, the resulting surface relief is electroformed to produce a nickel shim from which multiple copies can be generated by replication into polymer or epoxy materials. Figure 2 shows an overview of the fabrication steps.

2.1 *Laser Writing System*

The basic laser writing system is shown schematically in Fig. 3. It has been described in detail elsewhere[13] and is only summarized here. A photoresist-coated substrate is exposed by xy raster scanning under a focused HeCd laser beam ($\lambda = 442$ nm), synchronously controlled in intensity to write a fully programmable, 2-D exposure pattern. Development of the resist then results in a continuous-relief microstructure of the desired surface profile. The (positive) photoresist material and film preparation, as well as the development process, are chosen and optimized to give a relatively linear dependence of the developed relief height on the exposure dose (see Sec. 2.2), which is fully characterized by calibration runs. Because writing times can be relatively long (many hours for typical microstructures of 1 cm^2 area), an effective decay of the written exposure pattern (latent image decay) may be significant and is ideally compensated in the exposure data.

The fidelity of the developed microstructure is determined by a number of factors, including the surface roughness of the coated and developed photoresist films, the profile of the focused laser spot, the accuracy of the exposure dose, and the positional accuracy of the raster scan. In practice, the latter factor, essentially the line straightness and the accuracy

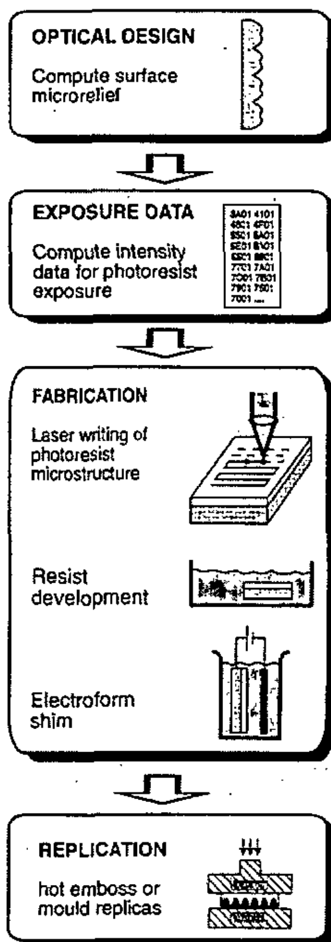

Fig. 2 Fabrication steps for continuous-relief micro-optical elements.

of the interline distance of the raster scan on the substrate, dominates the current experimental errors in the writing process. The PSIZ writing system uses a precision xy stage gliding on four air-bearing legs over a granite base, driven by linear motors with interferometer position measurement. The stage travel of 300×300 mm was originally chosen to satisfy the requirements of a number of applications; in practice, continuous-relief micro-optical elements are limited to a maximum size of about 50×50 mm by the writing times required. The dynamic positioning accuracy, defined as the y position held for typical line scan in the x direction at 10 mm/s, is about ± 150 nm rms. Vibrations from the building and from the table movement are dampened by com-

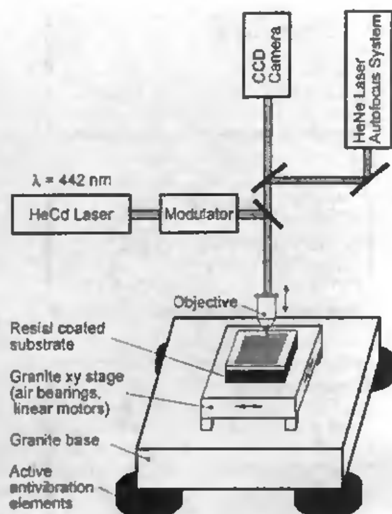

Fig. 3 Schematic of laser writing system for the fabrication of continuous-relief micro-optical elements.

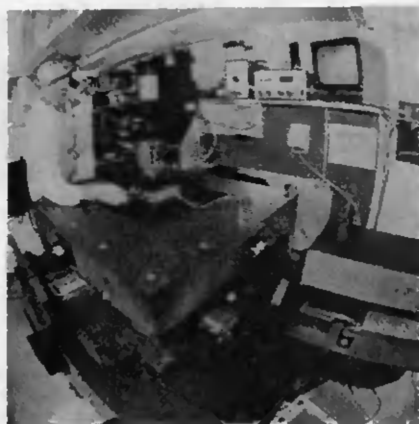

Fig. 4 Laser writing system.

mercial antivibration isolation elements in combination with in-house-developed active antivibration modules.[14] Figure 4 shows a picture of the current laser writing system.

The writing system is controlled by a PC, with custom hardware to set the laser intensity (exposure) via an acousto-optic modulator. The pixel intensity data (8 bits) is stored in a line buffer and clocked out by the interferometer pulses during the constant velocity line scan. The hardware enables the pixel length to be set in units of the interferometer pulses ($\lambda/32 \sim 20$ nm) from 20 nm to about 1.3 mm. The basic pattern can be programmed from 1 to 64k elements and can be repeated as required along the scan line. An autofocus system dynamically holds focus over the scan area during the writing procedure.

Typical writing parameters are an interline spacing of 1 μm, a focused spot size of at least 1.5 μm (diameter at $1/e$ intensity points), and a writing speed of 10 mm/s. The spot size is controlled by the choice of focusing objective, and is chosen as large as possible for a given microstructure relief. A large spot leads to smoother profiles but a loss in feature resolution, whereas a small spot results in unwanted surface modulation on the relief surface. The spot size, exposure, and interline spacing are interrelated and must be chosen accordingly; a discussion of the interdependence can be found in Ref. 11. Typical writing times are relatively long, up to 12 h for a 10×10 mm^2 area micro-optical element, but this is not of major significance because the final elements are usually replicated from an electroformed Ni shim.

2.2 *Photoresist Processing*

The exposure data required for the fabrication of a given surface-relief micro-optical element are computed from the required microrelief and the photoresist development characteristic. The latter describes the relief height of the resist film after development as a function of the exposure dose. It is determined by carrying out a calibration run and measuring the depth of areas of varying exposure doses using a surface profilometer. It is a function of the resist film preparation, writing and processing parameters, and in general must be uniquely determined for the following:

- resist type, film thickness, and prebake conditions
- writing parameters—spot size (focusing objective) and scan interline spacing
- development procedure—developer type, dilution, temperature, etc.

The majority of planar micro-optical elements are currently fabricated in resist films of up to about 5 μm thickness. The resist used is usually Shipley AZ 1400-37 or, more recently, Microposit S1828 (a product of Shipley Co., Inc., Newton, Massachusetts), spin-coated onto glass substrates. A spinning speed of 3000 rpm (for 1 min) gives a film thickness of about 3.3 μm. Thicker resist films (up to about 15 μm) can be obtained using lower spinning speeds for shorter times (although this results in some degradation in film quality) or by using other resist formulations. After coating, the films are baked either in an oven at 100°C for 1 h or on a hotplate at 100°C for 1 min.

Development is carried out using Shipley Microposit AZ 303 developed at a dilution of typically 1:7 or 1:10 with deionized water. This gives a relatively linear development characteristic; other developers can give much steeper, nonlinear development characteristics, which are less suitable for reproducible microrelief fabrication. AZ 303 concentrations stronger than about 1:10 can result in a significant removal of unexposed resist during the development process (an effective offset of the development characteristic); this must be taken into account in choosing the resist film thickness required for a given microstructure.

The photoresist development characteristic is determined by writing an exposure pattern consisting of a series of exposure steps, typically 12 equally spaced steps chosen to cover the full thickness range available for the given film. After development, the relief steps are measured using a profilometer and the data are typically fitted to a five-parameter equation relating the developed resist relief depth to the required exposure. These parameters are used in the computation of the exposure data for the micro-optical element. Figure 5(a) shows a typical development characteristic for Shipley S1828 resist and AZ 303 developer. The development characteristic shown in Fig. 5(a) can be represented as

$$E=a_0+a_1t+a_2t^2+a_3t^3+a_4t^4+a_5t^5 \ ,$$

where

E = exposure in arbitrary units 0 to 255

t = developed relief depth in nanometers

$a_0,\ldots,a_5$ = fit parameters.

Typical values for the fit parameters for 30-s development of S1828 resist film in 1:10 AZ 303 developer [Fig. 5(a)] are

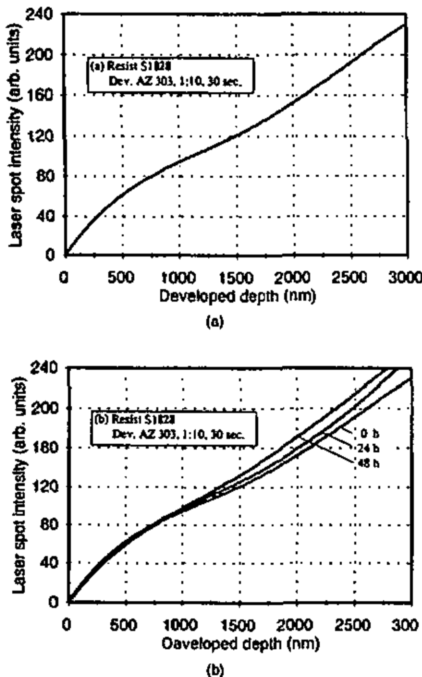

Fig. 5 Development characteristics for Shipley S1828 photoresist: (a) typical measured development characteristic and (b) example of latent image decay after 24 and 48 h.

$a_0=0.67$, $a_1=169\times10^{-2}$, $a_2=-1.17\times10^{-4}$, $a_3=4.87\times10^{-8}$, $a_4=6.61\times10^{-12}$.

For long writing runs, a dependence of the development characteristic on the time between exposure and development should be taken into account. This effect, a decay in the latent image exposure, becomes significant for writing times of more than about 12 h. Figure 5(b) shows measured development data illustrating the effect. It can be compensated by precorrecting the exposure data.

Good experimental reproducibility of the development characteristic requires careful control over the coating and development procedures. In practice, an accuracy and reproducibility of about ±5% in average relief height is relatively straightforward, a tolerance of ±2% requires considerable effort. The developed microreliefs are checked by writing a test calibration pattern beside every micro-optical element and comparing the developed depths with the programmed values. For elements requiring a very accurate relief structure, the most practical approach is to write a group of elements with the exposure varied by a small scaling factor (~2%) and to select the best microstructure after development. An automatic spray development system with optical monitoring to achieve a reproducible development end point by measuring the diffracted order intensity from an additional written grating microstructure is currently being installed. A target reproducibility of ±1% has been set for the improved development system.

2.3 *Data Preparation and Writing Parameters*

Figure 6 shows an overview of the data preparation and handling procedures. Most micro-optical elements (typical elements of recent and current interest include Fresnel microlenses and lens arrays, kinoforms, and phase plates) are currently designed by custom programs. The data are first prepared in a "standard" format that defines the surface relief microstructure in terms of the relief height in a 3-D pixelated structure. Compressed versions of the data format are available for microstructures containing repeat elements (for example, gratings and other periodic microstructures). These relief data are then combined with the measured resist development characteristic to produce a data file containing (8-bit) intensity data that define the effective exposure for the given resist preparation and for the writing and development conditions. In the writing procedure, the *xy* stage is moved in the appropriate raster scan while the line intensity data are synchronously clocked out to the modulator by the real-time interfereometer pulses. Software has also been written to compute the intensity data on a workstation and transfer it line-for-line (real time) to the PC controller during the writing process.

2.4 *Replication*

A major attraction of planar micro-optical elements lies in the potential of mass production by replication technology. This technology is already well established for the production of diffractive foil, display holograms, and holographic security features,[15] for which microrelief structure with typical grating periods of 0.5 to 1 μm with a maximum depth of about 1 μm is produced on a hot roller press in rolls of plastic

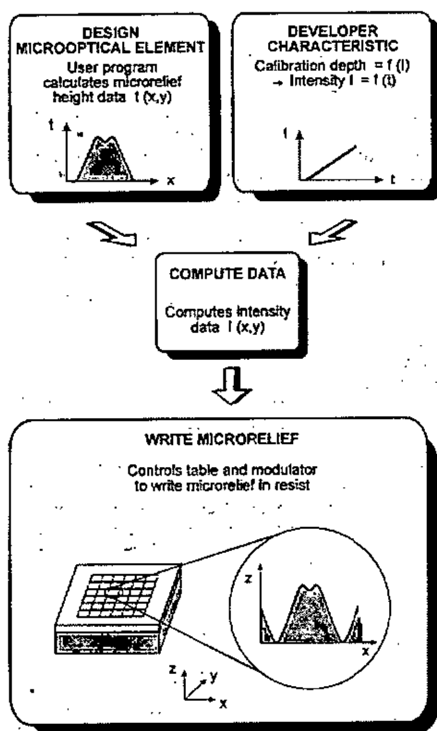

Fig. 6 Data preparation procedures.

up to 1 m wide and thousands of meters in length. Deeper microrelief structures currently require other replication technologies, such as a reciprocating hot-press, casting, or moulding techniques. In all cases, the first step is to fabricate a metal (usually Ni) shim by electroplating the surface of the microstructure, followed by recombination of a number of small-area shims to produce the larger shim (~1 m^2 or larger) required for commercial replication machinery.

Figure 7 illustrates the steps involved in the fabrication of replication shims. The recorded surface-relief microstructure in photoresist is first made conducting, either by the evaporation of a thin (~100-nm) film of Au or Ag, or using a commercial electroless Ni deposition bath. A Ni foil is then built up by electroplating this structure to a thickness of about 300 μm. Finally, the Ni is separated from the resist/substrate and cleaned to give the master (first-generation) replication shim. This master shim can be used directly for laboratory replication, typically by hot embossing or casting. It can also be supplied to a commercial shim facility for recombination to produce a large-area production shim.

The first-generation shim can also be used to generate multiple copies by electroplating further generations. The Ag or Ni surface is first passivated by immersion in a dichromate

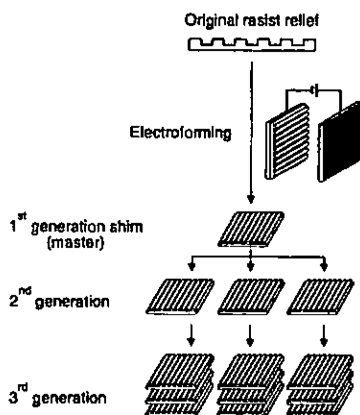

Fig. 7 Fabrication of replication shims.

solution or by O_2 plasma treatment, followed by further electroplating to form a copy that can readily be separated. In this way, numerous copies can be made from a single recorded microrelief. Measurements on the surface roughness of the shim reproduction and replication process are given in the following.

3 Surface Roughnees and Profile Fidelity

The quality of micro-optical elements fabricated by laser writing in photoresist followed by electroforming and replication depends on a number of experimental factors. The best surface quality achievable is limited by the surface roughness of the resist film and degradation occurring in the replication process. Unwanted surface structure introduced by the writing process is strongly dependent on the focused laser spot size, the scan line separation, and the positional accuracy of the scan lines. Profile errors are also introduced by the finite spot size, which limits the steepness of profile steps. Finally, the replication process itself can lead to surface relief profile errors in the fabricated replica microstructures. The ultimate test of a micro-optical element is, of course, its optical performance in terms of light distribution, efficiency, and scattered light.

In this section, we present measurements on some of the underlying quality parameters for the surface-relief structures. A distinction is made between the surface roughness, resulting from "inherent" factors such as the resist film quality and the replication process and the (unwanted) surface modulation resulting from the laser writing process itself. Fabricated surface-relief profiles were characterized mainly by line profilometer measurements and by using an atomic force microscope (AFM) to measure and visualize the surface roughness and profile.

3.1 *Surface Roughness*

Figure 8 summarizes the surface rms roughness measurements on small areas (~5×5 μm^2) at various stages of the fabrication. The glass substrates were standard

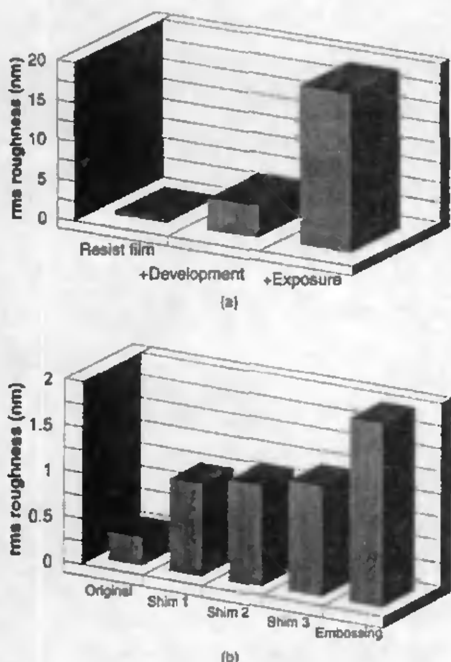

Fig. 8 Measured rms area roughness for (a) photoresist and (b) Ni shim surfaces.

$50\times50\times1$ mm^3 glass (Schott B270) substrates with a measured roughness of about 2 nm. After coating with a 3- to 5-μm layer of Shipley AZ 1400 photoresist, the surface quality improved to better than 0.5-nm roughness. Development in 1:7 or 1:10 AZ 303 developer resulted in a surface roughness in unexposed areas of about 4 nm. This represents the limiting roughness for the microrelief structures. Exposed areas are progressively worse (~25 nm and greater for typical micro-optical elemenst, see later) primarily because of surface modulation introduced by the raster scan and, above all, by positioning error in the individual scan lines.

The situation at the replication level is also shown in Fig. 8. The electroformed Ni shim, fabricated in this case from a quartz substrate with an rms surface roughness of less than 0.3 nm, has a measured roughness of about 1 nm. Subsequent generations of electroformed shims have progressively higher roughness, but even the third-generation is well below the 2-nm miniimum value measured for the original resist film. Replicas fabricated by hot embossing into polycarbonate (PC) film using a first-generation shim also showed a roughness of about 2 nm after embossing.

3.2 *Surface Modulation and Profile Fidelity*

The basic process is thus capable of producing replica elements with an rms surface roughness of about 4 nm, which is more than adequate for the majority of applications in micro-optics. Surface-relief modulation resulting from the writing process is currently about an order of magnitude greater, and depends on the spot size and interline spacing parameters, as well as the positioning errors in the raster scan. The relation between these parameters was analyzed in an earlier paper.[11]

The main parameter that can be easily varied and optimized for a given microstructure is the spot size, determined by the focusing objective lens. The interline spacing can be set from the control program but, as discussed in Sec. 2.1, does not in practice have a major influence on the (unwanted) surface modulation. On the current PSIZ system, coarse microstructures (lateral feature sizes of ~100 μm and greater) are written with a relatively large spot size (~8 μm), resulting in a measured surface modulation down to about 25 nm rms. For finer microstructures, written with a spot size of about 1.5 μm, significantly higher modulation values are obtained, typically up to about 100 nm rms. An improved xy stage with better dynamic line-positioning accuracy (currently in excess of ±150 nm) should reduce this value considerably, and is the basis of a next-generation system currently being constructed.

Even for perfect scan positioning with optimized interline spacing, the finite spot size limits the fidelity with which a surface-relief profile can be fabricated. All but the smoothest profiles will contain errors caused by the finite spot size, in particular at steep slopes and narrow profile features. This gives the limits of the laser writing process; although in practice experimental errors such as scan line positioning accuracy are usually considerably larger than the inherent limitations in the process. The fidelity of the replication process is difficult to assess objectively; results to date indicate that no significant increase in surface roughness or loss of surface-relief profile is observed for typical micro-optical elements and that optical performance is not degraded by the replication process. The next section shows examples of micro-optical elements that have been realized with the current writing system.

3.3 *Resolution Considerations*

An important parameter in the design and fabrication of planar micro-optical elements such as Fresnel lenses is the lateral size of the smallest realizable segment. Together with the maximum relief height, this effectively sets the maximum lens numerical aperture (NA) attainable. In the current writing system, the HeCd laser beam can readily be focused down to a spot size below 0.5 μm, and corresponding linewidths in resist can be achieved for single lines exposed and developed through to the substrate. However, as explained, the effective limitation is not the spot size but the straightness of the scan lines, and a spot size below 1 μm does not bring any improvement for continuous-relief microstructures. The minimum segment size that can be written with acceptable relief continuity using a spot size and line spacing of 1 μm has been determined to be about 5 μm. The steepness of the relief step is determined by the spot size and the bandwidth of the intensity modulator; for the current system and typical relief depths of 3 to 5 μm it corresponds to an angle of about 70 deg.

Figure 9 illustrates the situation for a Fresnel lens microstructure. For a given phase step (step height) at the segment

boundaries, the segment size decreases toward the edge of the lens [Fig. 9(a)] and the NA of the lens is limited by the minimum segment size of about 5 μm. If the phase step is increased by 2π, the segment width increases accordingly. Thicker resist films allowing larger phase steps thus enable higher NA lenses to be fabricated. Figure 9(b) shows the dependence of the minimum segment size on the lens NA for various phase steps, computed for lenses fabricated in polymer of refractive index $n = 1.58$ (polycarbonate) and a readout wavelength of $\lambda = 633$ nm.

High-aperture Fresnel lenses with NAs approaching 0.5 require careful design and optimization. Planar microlenses are designed as phase-matched Fresnel elements (PMFEs) with segment profiles and phase steps optimized to maintain proper phase relationships at the design wavelength.[16] Such micro-optical elements combine the advantages of geometrical and diffractive optical components and their optical characteristics can be considered as resulting from a combination of refractive and diffractive behavior, depending on the dimensions of the Fresnel segments. The minimum segment size can be maximized by choosing the largest phase step possible within the limits of the resist thickness—a 0.5 NA lens with 8π phase step requires a resist thickness of at least 4.4 μm. On the other hand, the performance of structures with high phase steps is more sensitive to errors in the relief profile. This leads to microstructures of the type shown in Fig. 9(c), in which the phase step is increased by 2π each time the segment size approaches the limiting value as the radius increases.

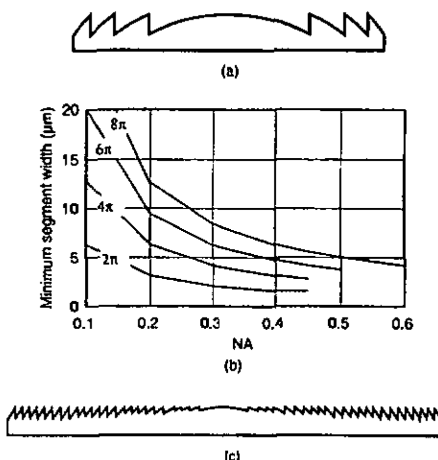

Fig. 9 Basic Fresnel lens microstructure (a) and dependence of the segment width on lens NA for phase-matched Fresnel elements (PMFEs) (b); a phase step of 2π corresponds to a 1.1-μm relief step for PC lenslets in air at $\lambda = 633$ nm. A PMFE with multiple phase steps is shown in (c).

4 Fabricated Micro-Optical Elements: Experimental Results

Examples and performance data are presented here of various micro-optical elements that have been fabricated for applications in a variety of projects using the described laser writing system. The writing data were generated in a number of different ways, most commonly by dedicated user programs computing the optimum surface-relief profile for a given application.

4.1 *Microlenses*

PMFEs offer a considerable degree of functional flexibility, with typical applications in monochromatic (laser) or narrowband (LED) imaging and illumination systems. Microlenses with sizes varying from about 30 μm up to 1 cm have been fabricated for a wide variety of applications. The lenslets may have a maximum relief depth corresponding to the resist film thickness, typically about 5 μm. Low-NA lenslets can generally be fabricated using an 8-μm spot size, resulting in smooth surface-relief profiles with low scatter. High-NA lenslets correspond to deeper relief microstructures and are fabricated using a writing spot size of about 1.5 μm. The resulting surface-relief structures show various degrees of unwanted surface modulation caused by the writing process; they are nevertheless useful in the many applications where a certain amount of stray light can be tolerated.

Figure 10 shows an AFM image of the surface profile of a fabricated microlens of 5-mm diameter and 10-mm focal length (NA = 0.24), replicated into polycarbonate film. The microlens was designed for use at a wavelength of $\lambda = 633$ nm and had a measured efficiency (transmitted energy focused into the central spot) of 70% at this wavelength. Optical performance was essentially diffraction limited for on-axis focusing applications.

Figure 11 shows an AFM image of a similar lens with 100-μm diameter and 500-μm focal length (NA = 0.1). The microlens has four Fresnel segments with a phase step of 2π (~ 1.1 μm at $\lambda = 633$ nm) and was fabricated using a 1.5-μm writing spot size. Limitations in the fabrication process are clearly visible as unwanted structure on the microlens surface, mainly in the direction normal to the scan lines and resulting from positioning errors in scan. This results in reduced efficiency of the microlens and stray light outside the focused spot. Such microlenses have nevertheless found applications in optical microsystems for numerous illumination and imaging applications. Microlenses have been fabricated with NAs up to 0.5 and with measured efficiencies in the range 60 to 90%, depending on the lens design and microstructure.

A more complex PMFE microstructure with segments of varying phase steps of 2π up to 8π is shown in Fig. 12. The lenslet has a size of 250×300 μm and NA ~ 0.5. The figure shows an AFM image of the fabricated microstructure and an enlargement of a section showing a phase step change from 2π to 4π. The measured efficiency of this lenslet was about 60%.

4.2 *Microlens Arrays*

Laser writing allows the fabrication of arrays of refractive and diffractive microlenslets with effectively zero dead space between the lenslets. Figure 13 shows a scanning electron microscope (SEM) image of a section of an array fabricated for Shack-Hartmann wavefront sensor for the European Southern Observatory (ESO) for use in astronomical telescopes.[17] The lenslets have a focal length of 22.5 mm and a

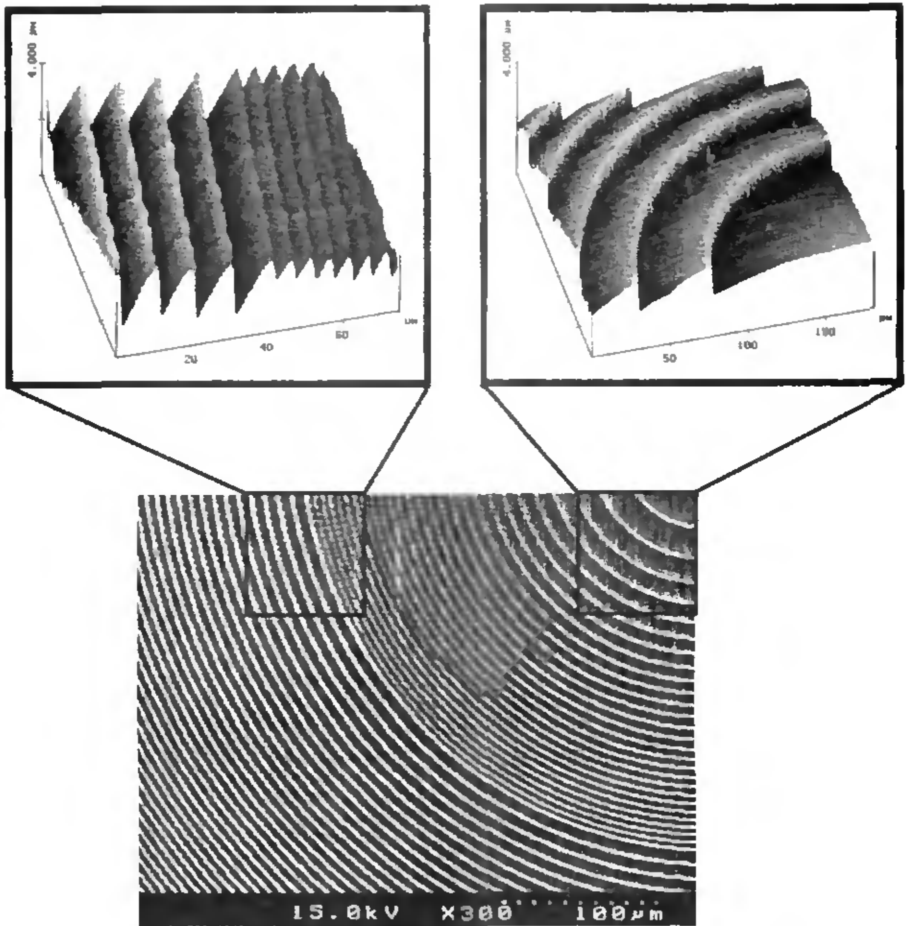

Fig. 10 Microlens structure—AFM image of a section of a PMFE with 5-mm diameter and 10-mm focal length (NA = 0.24). The microlens had a measured efficiency of 70% at λ = 633 nm.

size of 500×500 µm^2. They essentially consist of a single Fresnel segment, except at the extreme corners where a step of about 2 µm is required. Dead space between lenslets is essentially zero. The low NA of 0.01 allowed the use of a writing spot size of ~8 µm with a scan line spacing of 2 µm, resulting in much lower surface microstructure than that shown in Figs. 10 to 12 and much reduced stray light. Arrays of up to 80×80 lenslets have been fabricated, electroformed into nickel shims, and replicated into thin optical epoxy films on glass substrates to produce high-quality replica elements of good mechanical stability.

Further microlens arrays have been fabricated for applications in optical interconnects, multiple spot scanning microscopy, laser-to-fiber imaging, and numerous other areas in which geometrically precise arrays of planar microlenses are required. Figure 14 shows an SEM image of an array of PMFEs of 250-µm focal length and 150- × 150-µm lenslet size.

Continuous relief microlens arrays can be fabricated by a number of alternative techniques, in particular by the reflow of photoresist islands.[18] Reflow techniques can produce lenslets of high NA with spherical profiles of very high surface

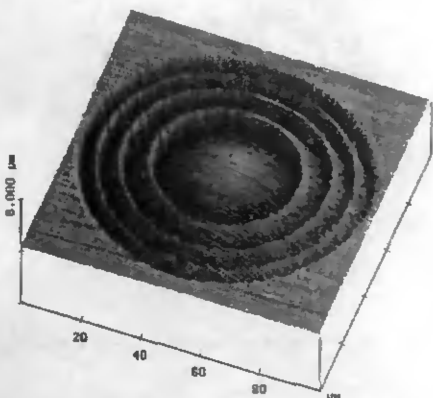

Fig. 11 Microlens structure—AFM image of a PMFE with 100-µm diameter and 500-µm focal length (NA = 0.1).

quality. Laser writing is in general not currently able to produce microlenses with comparable imaging and stray light properties, but has advantages in other aspects that can be of significant practical importance. The laser written microlens arrays can have very small dead space between lenslets of any desired shape and profile (including aspheric forms). Fresnel lens microstructures allow the fabrication of truly planar structures with maximum relief height limited to micrometer dimensions, which has major advantages for many mass-production replication technologies. As the laser writing technology improves, the quality of the microlenses will approach that of reflow structures.

4.3 *Kinoforms and Diffractive Optical Elements*

Laser writing allows the fabrication of surface-relief microstructures with complex profiles of any desired form within the resolution limitations. A good example of the flexibility of this approach is the fabrication of kinoform and other diffractive optical element (DOE) microstructures.

Figure 15 shows an AFM image of a 2-D 9×9 fan-out kinoform element. The design was computed at the Institute of Microtechnology, University of Neuchâtel, and fabricated at PSIZ by laser writing in resist followed by electroforming of a Ni shim and replication into epoxy. The performance

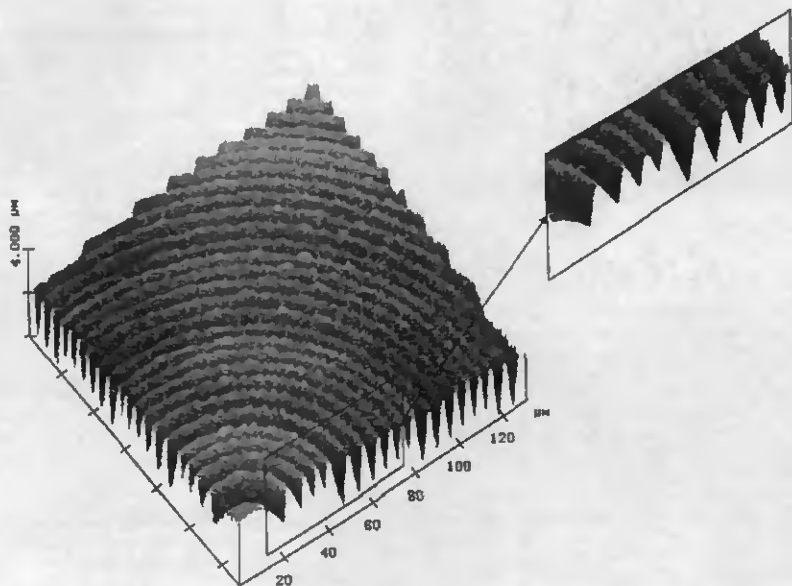

Fig. 12 PMFE structure—AFM image showing a section of a microlens 250×300 µm size and NA ~0.5. The enlargement shows a change in phase step from 2π to 4π.

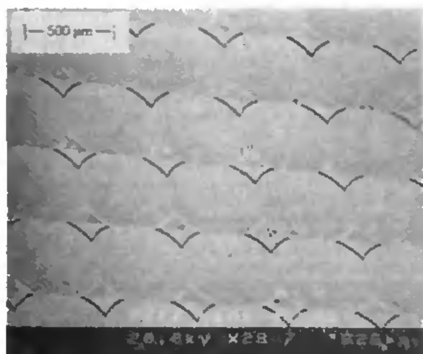

Fig. 13 SEM micrograph of a microlens array for a Shack-Hartmann wavefront sensor. The lenslets have a focal length of 22.5 mm and a size of 500×500 μm²; they were written with an 8-μm laser spot size (from Ref. 1).

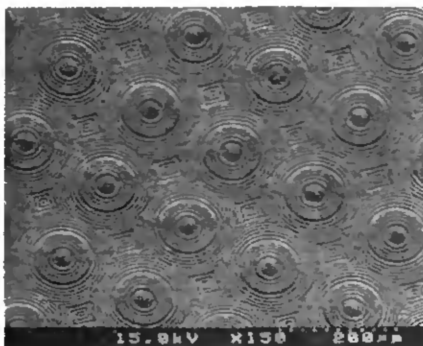

Fig. 14 SEM micrograph of an array of PMFEs (150- × 150-μm size, 250-μm focal length).

was excellent—measured efficiency for resist recordings (after correction for reflection losses) was better than 94% and overall uniformity better than ±8% of the average spot intensity; replicas in epoxy had the same efficiency and a uniformity of ±15% (with the lower uniformity caused by a known error in the recording of the corresponding relief structure). The figure shows the central portion of the fabricated microstructure. Further details on the kinoform design and performance can be found in Ref. 2.

DOEs with nonperiodic phase structures have been also fabricated for applications as low-pass filters and other modulation transfer function (MTF) control filters in optical processing systems. Optical filters with a Gaussian point spread function have been fabricated as surface-relief structures and incorporated into liquid crystal cells to produce electrically switchable optical filters.[19] Typical surface-relief structures for this application have a maximum relief modulation of up

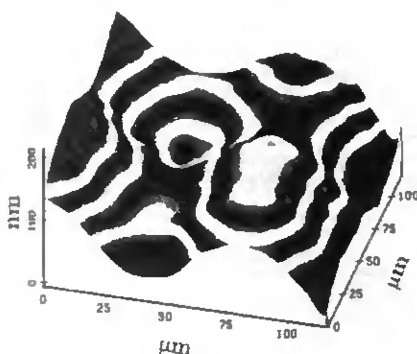

Fig. 15 AFM image showing a section of fabricated microstructure for a 9×9 fan-out continuous-relief kinoform (from Ref. 2).

to 7 μm and are fabricated in arrays of 8×8 elements of 1.6- × 1.6-mm size.

5 Conclusions

Laser writing in photoresist has been shown to be viable technology for the fabrication of planar, continuous-relief micro-optical elements. Microstructures with relief depths of up to about 5 μm can be fabricated directly in photoresist. Replicas of the microstructures can be produced from electroformed Ni shims of the recordings by hot-embossing, casting, and moulding techniques. The planar optical elements, with typical efficiencies varying from 60 to over 90%, are of practical interest for a large number of applications in which the attraction of low-cost, compact elements of flexible design outweighs the current limitations in efficiency and stray light. These limitations in surface quality and profile fidelity are of experimental origin and can be expected to be further reduced with improvements in the fabrication process, in particular higher accuracy in the raster scan during the writing step itself. A next-generation writing system with significant improvement in this area is under construction at PSIZ.

A number of examples of fabricated continuous-relief micro-optical elements have been described, including Fresnel microlenses and lens arrays, kinoforms, and other DOEs. Replicas have so far been produced mainly in small quantities using laboratory replication equipment. Ongoing work aimed at demonstrating an effective link to industrial replication processes such as hot embossing and injection moulding will provide a low-cost, high-volume source of micro-optical elements, with applications in a wide variety of areas.

Acknowledgments

The authors gratefully acknowledge numerous discussions with R. E. Kunz and his contributions to the design and development of PMFEs. They are also indebted to C. Appassito, L. Baraldi, M. Kuhn, G. K. Lang, J. M. Raynor, and R. Stutz for their contributions in the development of the laser writing system and replication technology. Many helpful discussions with K. Engelhardt, K. Knop, and M. Stalder at PSIZ, and

with R. Dändliker, P. Ehbets, and H. P. Herzig at the Institute of Microtechnology, University of Neuchâtel, are gratefully acknowledged. Micro-optical elements for optical interconnects were designed and characterized in collaboration with G. L. Bona at the IBM Research Center, CH-8803 Rüschlikon. Shim recombination was carried out by 3D Ltd., CH-6314 Unterägeri. This work was supported in part by the Swiss Priority Program OPTIQUE and other programs of the Board of the Swiss Federal Institutes of Technology.

References

1. M. T. Gale, M. Rossi, and H. Schütz, "Fabrication of 2-dimensional continuous-relief diffractive optical elements," *Proc. SPIE* **1732**, 58–66 (1993).
2. M. T. Gale, M. Rossi, H. Schütz, P. Ehbets, H. P. Herzig, and D. Prongué, "Continuous-relief diffractive optical elements for two-dimensional array generation," *Appl. Opt.* **32**, 2526–2533 (1993).
3. W. B. Veldkamp, "Overview of micro-optics: past, present and future," *Proc. SPIE* **1544**, 287–299 (1991).
4. M. B. Stern, M. Holz, and T. R. Jay, "Fabricating binary optics in infrared and visible materials," *Proc. SPIE* **1751**, 85–95 (1992).
5. G. Hatakoshi, M. Kawachi, K. Terashima, Y. Uematsu, A. Amano, and K. Uedo, "Grating axicon for collimating Cerenkov radiation waves," *Opt. Lett.* **15**, 1336–1338 (1990).
6. P. Ehbets, H. P. Herzig, D. Prongué, and M. T. Gale, "High-efficiency continuous surface-relief gratings for two-dimensional array generation," *Opt. Lett.* **17**, 908–910 (1992).
7. J. M. Stauffer, Y. Oppliger, P. Regnault, L. Baraldi, and M. T. Gale, "Electron beam writing of continuous resist profiles for optical applications," *J. Vac. Sci. Technol.* **B10**(6), 2526–2529 (1992).
8. M. Larsson, M. Ekberg, F. Nikolajeff, and S. Hård, "Successive-development optimization of resist kinoforms manufactured with direct-writing electron-beam lithography," *Appl. Opt.* **33**, 1176–1179 (June 1994).
9. Y. Oppliger, P. Sixt, J. M. Stauffer, J. M. Mayor, P. Regnault, and G. Voirin, "One-step shaping using a gray-tone mask for optical and microelectronic applications," *Microelectron. Eng.* **23**, 449–454 (1994).
10. S. Mihailov and S. Lazare, "Fabrication of refractive microlens arrays by excimer laser ablation of amorphous Teflon," *Appl. Opt.* **32**, 6211–6218 (1993).
11. M. T. Gale and K. Knop, "The fabrication of fine lens arrays by laser beam writing," *Proc. SPIE* **398**, 347–353 (1983).
12. M. T. Gale, G. K. Lang, J. M. Raynor, and H. Schütz, "Fabrication of microoptical elements by laser beam writing in photoresist," *Proc. SPIE* **1506**, 65–70 (1991).
13. M. T. Gale, G. K. Lang, J. M. Raynor, H. Schütz, and D. Prongué, "Fabrication of kinoform structures for optical computing" *Appl. Opt.* **31**, 5712–5715 (1992).
14. J. R. Sandercock, "A dynamic antivibration system," *Proc. SPIE* **732**, 157–165 (1987).
15. B. Kluepfel and F. Ross, Eds., *Holography Market Place*, Ross Books, Berkely, CA (1991).
16. R. E. Kunz and M. Rossi, "Phase-matched Fresnel elements," *Opt. Commun.* **97**, 6–10 (1993).
17. D. Enard, "The European Southern Observatory Very Large Telescope," *J. Opt., Paris* **22**, 33–50 (1991).
18. D. Daly, R. F. Stevens, M. C. Hutley, and N. Davies, "The manufacture of microlenses by melting photoresist," *Meas. Sci. Technol.* **1**, 759–766 (1990).
19. M. Stalder and P. Ehbets, "Electrically switchable diffractive optical element for image processing," *Opt. Lett.* **19**, 1–3 (1994).

Michael T. Gale is the head of the Optics Section at the Paul Scherrer Institute (PSI), Zürich, Switzerland. He received the BA degree in physics from Cambridge University, England, in 1968 and the MSc degree in optoelectronics from Essex University, England, in 1969. On subsequently joining Laboratories RCA Ltd., Zürich, he worked on a number of holographic and applied optics projects, including surface-relief micro-images, laser-writing lithography, fabrication and applications of diffractive surface relief structures, development of a single-chip CCD color camera, and applications of CCD imagers in surveillance and metrology. More than 50 technical publications and 18 issued patents have accompanied this work. Since the transfer of the laboratories to PSI in 1987, his research interests have also included fabrication and applications of planar micro-optical structures by direct laser writing and replicated integrated optics.

Markus Rossi received his MSc degree in physics at the Swiss Federal Institute of Technology (ETH), Zürich, Switzerland, in 1990. He is currently working at the Paul Scherrer Institute in Zürich on his PhD thesis on the design, fabrication, and characterization of micro-optical elements. This work includes the study of novel types of planar optical elements in the form of phase-matched Fresnel elements and their fabrication by laser beam writing. Special interest is devoted to applications of micro-optical elements for optical interconnection systems.

Jörn Pedersen was trained as an optician. Since joining the Paul Scherrer Institute Zürich in 1991, he has worked on a variety of integrated optics and micro-optics projects, in particular the development of integrated optical devices based on nonlinear polymers and the replication of surface-relief microstructures for optical components. His current work involves the development of control software for a new laser-writing system for the fabrication of continuous-relief micro-optical elements.

Helmut Schütz joined Laboratories RCA Ltd., Zürich, in 1965, and has worked on a wide range of projects in the areas of holography, diffractive optics, and micro-optics. Since the transfer of the laboratories to the Paul Scherrer Institute in 1987, he has worked primarily on the fabrication of submicron surface-relief gratings for diffractive optics and integrated optics, and on the development of a laser-writing system for the fabrication of continuous-relief micro-optical elements. His current work is concentrated on the construction and application of a next-generation laser-writing system.

Paper III

Refractive and diffractive properties of planar microoptical elements

M. Rossi, R.E. Kunz and H.P. Herzig*

Paul Scherrer Institute, Badenerstrasse 569, CH-8048 Zurich, Switzerland

* Institute of Microtechnology, University of Neuchâtel, Switzerland

submitted 23 December 1994.

The refractive and diffractive properties of planar microoptical elements are investigated. The transition between purely refractive and purely diffractive planar microlenses is numerically simulated for the example of differently designed phase-matched Fresnel elements. Results obtained from numerical simulations and experiments show that the refractive and diffractive types exhibit a distinctly different behavior in the presence of small fabrication errors or wavelength deviations. Based on these results, design rules for various applications, including low and high NA lenses and hybrid refractive / diffractive elements, have been derived. For a high NA (f/# = 1.0) lens, the experimental characterization of the irradiance distribution in the image space is presented and shown to agree well with theoretical predictions.

1. Introduction

Classical lenses and mirrors consisting of macroscopic surface relief structures are designed using the laws of geometrical optics, treating light propagation by the refraction and reflection of geometrical rays at optical interfaces. The eikonal equation as the basis of geometrical optics can be derived from Maxwell's equations in the limit where the wavelength tends to zero [1]. Therefore, no wavelength dependent properties, apart from those due to material dispersion, are observed. However, due to the large structure size, these elements are often not appropriate for the integration in optical and optoelectronical microsystems. One possibility for miniaturization is the classical Fresnel lens, obtained by a simple dissection of the geometrically calculated profile. Although the eikonal equation yields a locally correct phase distribution, the laws of geometrical optics do not reckon the interference effects of the waves emanating from the different segments. Due to the resulting incoherent superposition of different waves, the resolution of a classical Fresnel lens is limited by the size of individual segments.

In contrast, holographic optical and diffractive optical elements (DOEs) do consider these effects. In general, DOEs are designed based on the wave nature of light, expressed by the laws of wave optics. An example of such an element is the Fresnel zone plate. The diffraction limited focusing function of these binary phase or amplitude gratings can be explained only by the coherent superposition of different waves. Since diffraction effects are strongly dependent on the wavelength of light, the imaging properties of DOEs typically suffer from severe chromatic aberrations. In order to obtain a high efficiency in one or several specific grating diffraction orders, a precisely controlled phase profile is required for DOEs.

Therefore, the optical properties of planar microoptical elements consisting of grating structures combined with continuous surface relief profiles between the grating lines are of great interest. Depending on the sizes of the surface relief features, the laws of geometrical optics can also be adequate for the description of their behavior. The aim of this paper is to show under which conditions the effects of refraction and diffraction are dominant. We will especially concentrate on the consequences of typical fabrication inaccuracies and wavelength deviations and give some fabrication-related design rules.

The analysis will be carried out on phase-matched Fresnel elements (PMFEs) [2], since they offer a generalized approach for the design and fabrication of planar microoptical elements. In particular they offer degrees of freedom for

choosing the weights of the refractive and diffractive contributions to the overall optical properties. In the next Section we will outline the concept of the PMFE design, which is based upon both geometrical and wave optics. The mathematical models for the numerical simulation of the refractive and diffractive properties of PMFEs will be introduced in Section 3. In Section 4, the optical behavior of differently designed planar microoptical elements in the presence of fabrication errors and illumination wavelength deviations will be treated for examples of lenses with numerical apertures NA = 0.05 (f/# = 10) and NA = 0.45 (f/# = 1.0). In order to demonstrate the feasibility of the PMFE design and fabrication, an experimental spot characterization on an NA = 0.45 lens is presented. As a special combination of refraction and diffraction, the limits of operation for a hybrid achromat will be derived.

2. Phase-matched Fresnel element concept

For the combination of refractive and diffractive properties, a general approach for the design is chosen. The following discussions will concentrate on imaging elements, however, the PMFE concept is not limited to this class of elements. We start with the statement, that a PMFE is equivalent to a *segmented micro relief structure* [2].

Each segment acts as a transmissive or reflective facet, so that an incoming primary wave u_0 is split into secondary wavelets u_j. In a first approximation, we do not consider the calculation of the exact mathematical form of the secondary wavelets u_j, which would require rigorous diffraction theory. The surface relief profile of each segment is designed to perform the desired optical function in the sense of geometrical optics. An equivalent formulation of this condition is that the optical path length W_j [3] between the object and image points for any ray r_j crossing the segment σ_j is constant (cf. Fig. 1). For the calculation of the optical path length W_j, the dispersive refractive indices n_0, n' and n in object and image space and the PMFE layer, respectively, have to be taken into account. In this paper n_0 and n' will be set to the constant value of 1. The size and the relative arrangement of the individual segments will be determined by additional design requirements and constraints originating from fabrication techniques.

For the calculation of the segment boundaries, the wave nature of light is taken into account. In the sense of a modified Huygens-Fresnel principle, which gave rise to using "Fresnel" in the term "phase-matched Fresnel elements", the amplitude of the optical field in the far field is given by the superposition of all sec-

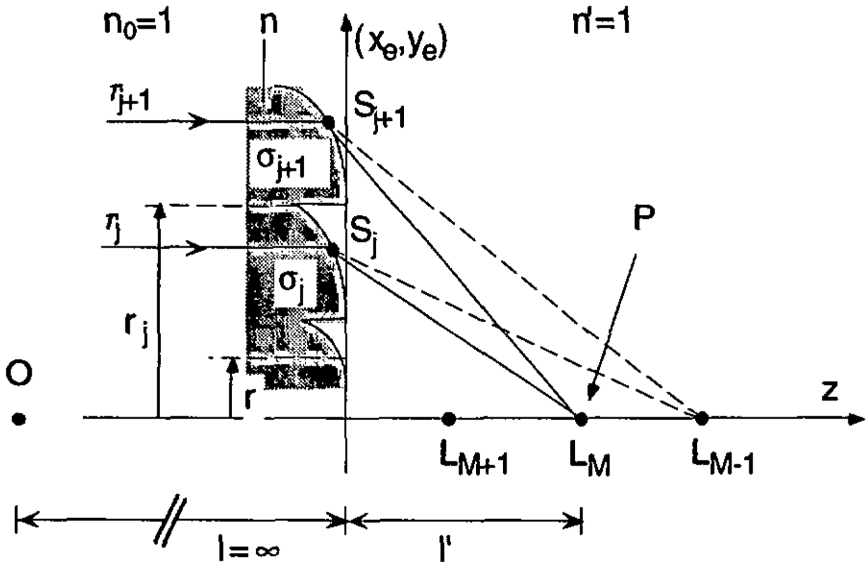

Fig. 1. Definitions of PMFE segments and focal points of different orders.

ondary wavelets u_j [2]. In order to take advantage of interference effects (be it constructive or destructive) of these wavelets, we establish a *controlled phase relation* between the wavelets emanating from all segments, using phase-sensitive ray tracing algorithms [3] with the concept of geometrical wavefronts. As an example we consider the imaging of a point source O into an image point P, where the object distance l is taken to be infinite as shown in Fig. 1 This is achieved by choosing the segment boundaries in a manner that the optical phase difference ΔW_j in L' of two rays r_j and r_{j+1}, crossing neighboring segments σ_j and σ_{j+1} is an integer multiple M_j of 2π (cf. Fig. 1). The equivalent expression for the optical path length is:

$$\Delta W_j = W\left(\overline{OS_{j+1}P}\right) - W\left(\overline{OS_jP}\right) = M_j\lambda \ , \qquad (1)$$

where λ is the wavelength in air. The fact that the integer M_j, called the phase-matching number, may be locally different from one boundary to another is an important degree of freedom for the design of these elements.

Since the approach presented in the previous paragraph is a rather general one, the width w_j and depth h_j of the segments and the exact form and position of their boundaries are not uniquely determined. Specific design strategies are characterized by the alignment of the segments and the local values of the phase-matching number M_j. The choice of the alignment of the segments, e.g. top or bottom aligned (cf. Fig. 2), will be influenced by the fabrication technology and becomes relevant in the high NA regions of planar lenses. The value of M_j determines the width and depth of the segments. One possible strategy is to choose M_j so that the segment width w_j remains above a minimal value w_{min} for a given fabrication technology [4]. This special case corresponds to the approach used by Futhey [5] in the design of "superzone diffractive lenses" and by Marron et al. [6] for their "higher order kinoforms". Besides the aspect of segment width and depth, the refractive and diffractive properties are a function of the number of illuminated segments. With the variation of M_j, the element can behave in the two extreme cases as a purely diffractive ($M_j = M = 1$, number of illuminated segments $Q >> 1$) or refractive (M large enough to get only one segment, i.e. $Q = 1$) element.

The design procedure presented here, which locally optimizes the surface relief, does not rely on any approximations other than on the validity of the scalar theory. Particularly, good results can be obtained for lenses with high numerical aperture [4], since the calculations are not restricted to the paraxial domain [7]. Due to the direct calculation of a locally optimized surface relief instead of a phase function in a plane, no complex corrections for the profile are required as e.g. in [8].

The approach of using a segmented surface relief structure for interfering and phase-matching the secondary wavelets in the image space can also be interpreted as representing a miniature implementation of an "optical phased-array" [9].

The PMFE microstructures can be fabricated by any technology which enables one to produce the segments with a sufficient accuracy. The segments can be formed as continuous surface reliefs by means of direct laser [10] or e-beam writing [11], or as binary optical [12] structures. In this paper, we will concentrate on elements fabricated by direct laser writing in photoresist.

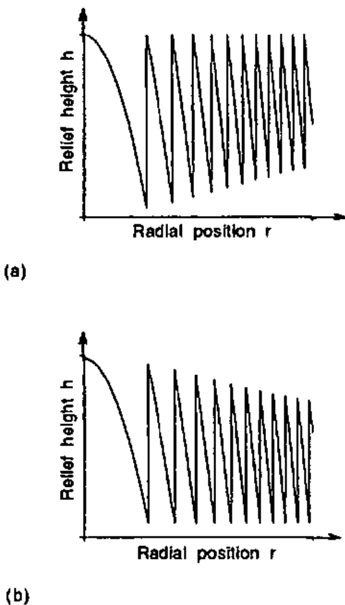

Fig. 2. Schematic design examples for top-aligned (a) and bottom-aligned (b) PMFE microstructures.

3. Theoretical description

For the theoretical description of the PMFE behavior, two different models will be used. In a first approach, the diffraction patterns will be

calculated in the Fresnel diffraction regime. These calculations give reliable results for lenses with NA ≤ 0.05 (f/# ≥ 10) [7] and will give a good intuition for the basic processes. More precise results can be obtained from the subsequent calculations in the Rayleigh-Sommerfeld approximation. These numerical simulations take also into account the finite thickness of the PMFE surface relief and determine the diffraction pattern of the structures designed using the algorithms in Section 2.

The PMFE concept combines geometrical and wave optics in a way, that the segment boundary pattern locally acts as a diffraction grating having the M_jth order focus at the position $l' = L_M$, and that the segment relief shape is optimized for the geometrical optical refraction of light rays into the point L'. Besides this main focal point L' of the diffraction grating, there exist additional positions L_N on the z-axis where the optical path difference ΔW_j is an integer multiple N of λ with $N > M_j$ or $N < M_j$ (cf. Fig. 1). The values L_N for these higher and lower diffraction orders can be obtained by solving Eq. (1) with M_j replaced by N. A plot of these positions L_N for lenses with an NA = 0.05 and different values of M_j is given in Fig. 3. The density of higher and lower diffraction orders on the optical axis apparently rises with increasing values of M_j and is an important factor for the behavior of planar microoptical elements in the presence of surface distortions and wavelength deviations.

Whereas the above calculations determine the positions where constructive interference of the different secondary wavelets u_j occurs, the surface relief profile of the segments determines the amount of light at these positions. A first estimation of the intensity distribution among these various diffraction orders can be obtained assuming that a paraxial description [13], [7] is valid. In this case, Eq. (1) can be transformed to:

$$r_j^2 = 2jM_j\lambda_0 l', \tag{2}$$

where r_j is the distance of the segment boundary from the origin and λ_0 is the design wavelength in air. The phase-shift introduced by the continuous surface relief segments at an arbitrary position r is approximated by a quadratic function

$$\Phi_j(r) = \alpha M_j \cdot 2\pi\left(j - \frac{r^2}{2M_j\lambda_0 l'}\right),$$
$$\text{for } r_j \le r < r_{j+1}, \tag{3}$$

where the parameter

$$\alpha = \frac{\lambda_0\left(n(\lambda_1)-1\right)}{\lambda_1\left(n(\lambda_0)-1\right)}. \tag{4}$$

quantifies the phase delay for an illumination wavelength $\lambda_1 \neq \lambda_0$ (cf. [7]). In addition to chromatic effects, we will also treat the influence of fabrication inaccuracies in the form of relief profile scaling errors. A typical distortion of an original surface relief profile h(r) is expressed by a term μ as

$$h'(r) = \mu \cdot h(r). \tag{5}$$

Since the required phase shift is realized by a surface relief profile using the relation

$$h(r) = \frac{\lambda_0}{2\pi\left[n(\lambda_0)-1\right]}\Phi(r), \tag{6}$$

we also introduce the multiplicative factor μ in Eq. (3) for modelling relief height errors.

We now introduce a new variable $\xi = r^2 / 2\lambda_0 l'$. The segment transmission function $t(\xi) = \exp[i\Phi(\xi)]$ is then periodically extended and describes a Fresnel lens with an infinite number of segments and a constant phase-matching number $M_j = M$. $t(\xi)$ is a periodic function with a period T = 1 and can be approximated by a Fourier series

$$t(\xi) = \sum_{N=-\infty}^{\infty} \exp\left[-i\pi(\alpha\mu M - N)\right] \times \mathrm{sinc}(\alpha\mu M - N)\cdot \exp\left[-i2\pi N\xi\right] \tag{7}$$

or

$$t(r) = \sum_{N=-\infty}^{\infty} \exp\left[-i\pi(\alpha\mu M - N)\right] \times \mathrm{sinc}(\alpha\mu M - N)\cdot \exp\left[-\frac{i\pi N r^2}{M\lambda_0 l'}\right], \tag{8}$$

where the *sinc*-function is defined as:

$$\mathrm{sinc}(x) = \frac{\sin(\pi x)}{\pi x}. \tag{9}$$

The expansion (8) requires a large number of segments j for being valid. The following numerical simulations in Sections 4.2 and 4.3 will indicate that already for 4 illuminated segments, the optical behavior of a microlens can be de-

scribed by Eq. (8) with a good accuracy. As comparison, the transmission function for a lens with only *one* segment, designed for a focal length f and a wavelength λ_1, is given by [14]

$$t(r)=\exp\left[-\frac{i\pi r^2}{\lambda_1 f}\right]. \qquad (10)$$

This equation describes a purely refractive lens with one single focal point and a wavelength dependence given by the material disperison $n(\lambda)$ (cf. Eq. (6)), remembering that we have set $n_0 \equiv 1$ and $n' \equiv 1$. Comparing Eqs. (8) and (10), the transmission function of a paraxial Fresnel lens can then be interpreted as a summation over the transmission functions of a series of lenses with focal lengths

$$l_N=\frac{Ml'}{N}\cdot\frac{\lambda_0}{\lambda_1}. \qquad (11)$$

The normalized energy in these focal points is proportional to the squared modulus of the Fourier coefficient:

$$\eta_N=\mathrm{sinc}^2(\alpha\mu M-N). \qquad (12)$$

If the illumination wavelength λ_1 is not equal to the design wavelength λ_0, the position of the focal points l_N and their efficiency η_N will be changed according to Eqs. (11) and (12). A profile height error $(\mu-1)\neq 0$ will not affect the position of the foci l_N, but will alter the energy distribution among them. From the *sinc*-function in Eq. (12) follows that only *two* diffraction orders N simultaneously can have an efficiency of more than 5%, independent of the values of α, μ and M. This fact that only two values of η_N are in the central *sinc*-lobe, is similar to the behavior of blazed gratings working in higher diffraction orders [15], which can be interpreted as special, non-focusing cases of PMFEs.

As a further consequence of Eq. (12), the probability that an other than the designed diffraction order M gets the most efficient one, i.e. $\eta_N > \eta_M$ for $N \neq M$, increases for higher values of M. This can also be explained with refraction based considerations. Since the higher and lower diffraction orders N move nearer to the nominal focal point L' for higher values of M (cf. Fig. 3), it takes smaller profile deviations to *refract* the light at these positions L_N of constructive interference and therefore rise their efficiency η_N.

The existence of additional focal points and their behavior under wavelength or fabrication inaccuracies are the most important differences in the properties of purely refractive and diffractive lenses. The following investigations will concentrate on these effects in the *transition region* between the two extremes. As a consequence, we will encounter cases where the assumption of a high number of segments j in Eq. (8) is no longer fulfilled. In addition, these paraxial equations are not suited for the numerical simulation of high NA lenses. Therefore, the Rayleigh-Sommerfeld diffraction formulas [16] are used here for the quantitative evaluation of these PMFE diffraction patterns:

$$u_2(x,y)=\iint_{-\infty}^{\infty}u_1(x_e,y_e)\left(\frac{z_{12}}{i\lambda r_{12}^2}\right)e^{jkr_{12}}\,dx_e\,dy_e$$

$$=\int\int_{-\infty}^{\infty}u_1(x_e,y_e)\times\frac{\exp\left\{ikz_{12}\left[1+\left(\frac{x-x_e}{z_{12}}\right)^2+\left(\frac{y-y_e}{z_{12}}\right)^2\right]^{1/2}\right\}}{i\lambda z_{12}\left[1+\left(\frac{x-x_e}{z_{12}}\right)^2+\left(\frac{y-y_e}{z_{12}}\right)^2\right]}dx_e\,dy_e \qquad (13)$$

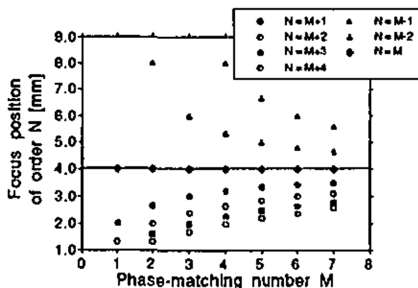

The variable $u_1(x_e,y_e)$ is the complex amplitude distribution in the tangential plane (x_e,y_e) to the microoptical surface relief (cf. Fig. 1), and is calculated by taking into account both the phase shift of the PMFE relief and the refraction of the rays at the curved surface. With this equation, the finite depth of the surface relief profile is correctly taken into account. The complex amplitude distribution in some plane (x,y), which fulfills the Rayleigh-Sommerfeld conditions ($z_{12} >> \lambda$) is given by $u_2(x,y)$; z_{12} is the distance of the planes (x_e,y_e) and (x,y). Since the radial

distribution of the relief data points resulting from the PMFE design is dependent on the local profile structure, we did not make use of Fast Fourier algorithms for the evaluation of Eq. (13) and solved it by direct numerical integration.

4. Experiments and numerical simulations on the refractive / diffractive behavior

4.1. General remarks

In Section 2, it was shown that the phase-matching number M_j and *the strategy of its variation over the element surface* are the most important features of the design procedure for PMFEs. The value $M_j(x_e,y_e)$ determines essentially the width and the depth of the microlens segments. One important way of using this parameter is the adaptation of the segment size to the limits imposed by the fabrication technology. Moreover, also the optical characteristic of microlenses can depend on the phase-matching number. Especially when small fabrication errors occur or when the microoptical element is illuminated by a wave with a wavelength $\lambda_1 \neq \lambda_0$, where λ_0 is the design wavelength, the irradiance distribution and the efficiency of the microlenses depends on the number and the size of the illuminated segments. We will first show some basic effects concerning the refractive and diffractive behavior of planar microlenses at representative examples. At the end of this Section we will give a summary and list some design rules for typical applications.

The following numerical simulations were performed on a series of 8 different PMFEs, which focus a collimated HeNe laser beam (wavelength $\lambda_{HeNe} = \lambda_0 = 632.8$ nm) at a distance $l' = 4.0$ mm. These lenses have a numerical aperture NA = 0.05 (f/# = 10), their phase-matching numbers ($M_j = M =$ constant) have been varied from M = 1 to M = 8. The PMFE with M = 1 consists of Q = 8 segments (cf. Fig 4) and because of the 2π phase steps it represents the purely diffractive case [17]. Due to the clamped finite aperture, the case of a purely refractive microlens is reached by the element with M = 8. According to the increasing size of contiguous surface relief areas and the decreasing number of segment boundaries, the elements with phase-matching numbers ranging from M = 2 to M = 7 can be described as having both refractive and diffractive attributes. The element with M = 2 has Q = 4 complete segments, the one with M = 4 has Q = 2 complete segments. The PMFEs with M = 5 to M = 7 all include exactly 1 segment boundary, the area of the second, outer segment decreasing relative to the

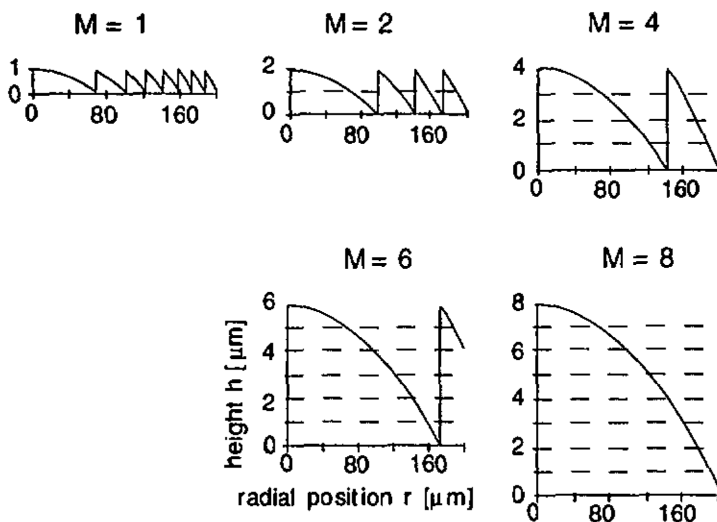

Fig. 4. PMFE surface relief elements for numerical simulations

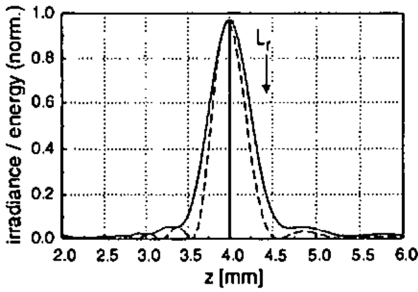

e) M = 1, Q = 8, NA = 0.05

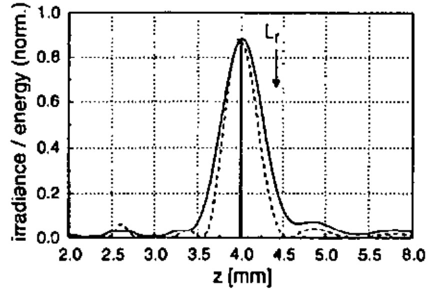

b) M = 2, Q = 4, NA = 0.05

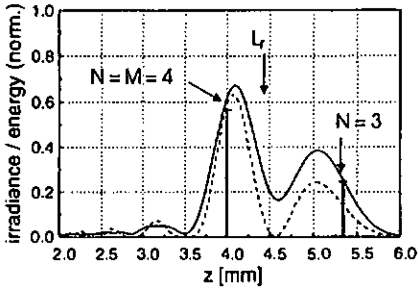

c) M = 4, Q = 2, NA = 0.05

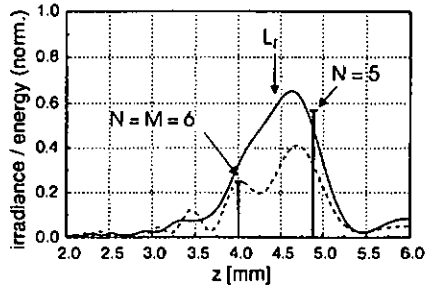

d) M = 6, Q = 2, NA = 0.05

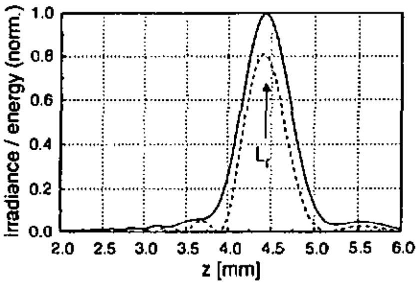

e) M = 8, Q = 1, NA = 0.05

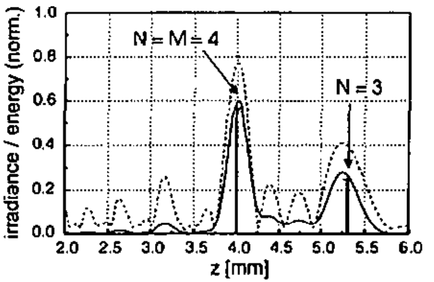

f) M = 4, Q = 4, NA = 0.1

Fig. 5. Calculated distribution of irradiance (----) and encircled energy (—) along the optical axis $z = z_{12}$ for PMFEs with (a) M = 1, (b) M = 2, (c) M = 4, (d) M = 6, (e) M = 8 and a depth scaling factor of $\mu = 0.9$; (f) shows the curves for an element with M = 4 and NA = 0.1. The vertical lines show the positions and efficiencies of the focal points calculated with Eqs. (11) and (12).

area of the inner segment. All these PMFEs are compatible with fabrication technologies such as laser beam writing [10], although resist films thicker than 5 µm require non-standard processing.

4.2. Monochromatic applications

Provided that the wavelength λ_1 of the monochromatic illumination wave is equal to the design wavelength λ_0, the microlens performance is mainly determined by the fabrication accuracy. The *lateral pattern* of the microlenses, i.e. the position of the segment boundaries, can be realized with very small tolerances using photolithographic fabrication techniques such as laser or e-beam writing. Interferometric control of the writing stages and modern mask aligners as used for binary optics guarantee a very high lateral precision for the segment boundaries. The *vertical shape* of the surface relief profile is more difficult to fabricate with a good reliability. For the fabrication of the elements by direct laser beam writing, relief height errors in the range of several percent, due to irregularities of the photoresist films, the exposure dose and the wet etching process, are typical. The consequences of surface relief errors are analyzed by considering elements whose original relief depth is multiplied by a constant factor μ.

In order to demonstrate the most important effects, a relatively high surface relief error of 10% ($\mu = 0.9$) was chosen. The results obtained with the Rayleigh-Sommerfeld integrals are shown in Figs. 5a - e. For each microlens, the irradiance on the optical axis and the energy encircled by a disk with the Airy radius q_a of the undistorted lens ($q_a \approx 1.22 \cdot f' \cdot \lambda_0 / 2a = 7.7$ µm, with 2a = lens aperture = 400 µm) are plotted as a function of the distance z_{12} from the micro-optical element on the optical axis. Irradiance and energies of the distorted PMFEs were normalized by the corresponding values obtained for $\mu = 1.0$. For this ideal case, all different design variants showed identical diffraction patterns. The bold vertical lines in Figs. 5a - d indicate the position and the efficiency of the discrete focal points, which are calculated under the assumption of a large number of illuminated segments with Eqs. (11) and (12).

The irradiance distribution along the optical axis is governed by two effects: (i) the variations with a $sinc^2$ - dependence for one single focal point as described in [18] and [19] and (ii) the diffraction of light in higher order focal points introduced by the surface relief distortions.

In the case where the surface relief profile is distorted by a factor $\mu = 0.9$, the focus point calculated by the refraction of rays is at $L_r \approx 4440$ µm for all different design variants. However, wave optics determines where constructive interference between the secondary wavelets of the different segments occurs. For the purely diffractive lens (M = 1, Q = 8), there is no lower order focus point near this refractive focus L_r (cf. Fig. 3). Consequently, no additional focus with notable efficiency will occur, exactly as it is predicted by the paraxial equations for diffractive lenses. The same applies for the PMFE with M = 2, where Q = 4 segments are illuminated. This proves that a PMFE with only 4 segments still shows the properties of a diffractive optical element. For higher values of M, and consequently lower numbers of Q, two types of consequences get relevant. First, the axial density of higher and lower order focal points is increasing. In the presence of surface relief errors, this can lead to a change in the focal length of the element, i.e. another than the Mth diffraction order can get the most efficient one (cf. Fig. 5d). In the purely refractive case (here for M = 8), there is again only one single focus point observed, with an efficiency that approaches 100% (cf. Fig. 5e). Its position is shifted by $\Delta z = 440$ µm, which coincides exactly with the value obtained by fitting a spherical lens through the distorted relief and subsequent calculation of the geometrical optical focus.

The second consequence of a high phase-matching number is that, in the transition region between refractive and diffractive elements, the assumption of a high Q for the expansion (8) is no longer fulfilled. This leads to deviations of the Rayleigh-Sommerfeld diffraction patterns from the results obtained by Eqs. (11) and (12), which are drawn as vertical lines in Figs. 5a - d. Particularly, a deviation of the axial position of maximum encircled energy from the focal point $L_{par.}$ calculated with the paraxial equations is observed. For the case with M = 1 and Q = 8, the position of maximum energy $L_{R.S.}$, obtained with the Rayleigh-Sommerfeld integrals, exactly coincides with $L_{par.}$. For M = 2 (Q = 4), the position of maximum energy is shifted by $\Delta z_2 = L_{R.S.} - L_{par.} = 30$ µm in direction to the refractive focus L_r. These deviations increase for lower numbers Q of illuminated segments (e.g. $\Delta z_4 = 100$ µm, $\Delta z_6 = -180$ µm, both having Q = 2).

In order to demonstrate that the transition between refractive and diffractive behavior depends on the number of illuminated elements only, the same simulations were performed for an element with M = 4 and a doubled aperture

Table 1. Focus width (FWHM values) for PMFEs with varying values for M and v. The theoretical FWHM value for an Airy disk with $q_a = 7.7\ \mu m$ is $q_{FWHM} = 6.6\ \mu m$. (*: PMFE with $\mu = 1.0$ / +: PMFE with M = 8, designed for $l' = 4440\ \mu m$).			
PMN	focus position [µm]	depth scal. factor µ	focus width [FWHM]
1*	4000	1.00	6.7
1	4006	0.90	6.7
2	4026	0.90	6.7
3	4038	0.90	6.7
4	4108	0.90	6.9
8	4436	0.90	7.5
8+	4440	1.00	7.5

size (i.e. Q = 4). The axial diffraction pattern and energy distribution of this PMFE with 4 illuminated segments are compared with those of the element with M = 4 and Q = 2 (cf. Figs. 5c and 5f). Whereas in the case Q = 2 the behavior differs significantly from the one of a diffractive lens, for Q = 4 a good coincidence with the results of a paraxial diffractive lens is obtained.

In contrast to the energy and the axial position of their maxima, the width of the focal spots showed no change. In Table 1, the FWHM values of the foci for different PMFEs are compared. The widths for M = 1 are equal in the two cases $\mu = 1.0$ and $\mu = 0.9$. For higher values of M, an increasing spot width is observed besides the focal shift. But a comparison with the FWHM of an undistorted element, that was designed for the shifted focus position, proves that this spot broadening completely occurs due to longer focal length.

4.3. Brief discussion of polychromatic applications

The treatment of polychromatic applications will be limited to the case of $\lambda_1 \neq \lambda_0$. A full discussion of the behavior under broad-band illumination would go beyond the scope of this paper. In the paraxial domain, Eqs. (11) and (12) will be used, with a factor α given by (4). The positions L_N of constructive interference and especially the designed diffraction order M will be shifted on the z-axis due to the chromatic aberrations of diffraction gratings. The refractive focus, which would be obtained by geometrical optics and which determines the energy distribution among the different diffraction orders, remains at the originally designed position, apart from a small deviation due to material dispersion. In analogy to the case of surface distortions, this mismatch will result in a reduction of the efficiency in the main focal point and a rise of the energy in the higher or lower diffraction orders. According to previous considerations, the focal point L_N situated nearest to the refractive focus will be the most efficient one.

For small values of wavelength deviations $\Delta\lambda = \lambda_1 - \lambda_0$, only a small decrease of efficiency will occur in all various design variants. A value of $\Delta\lambda = 70$ nm would be needed for a factor $\alpha = 0.9$ in order to significantly change the energy distribution among the different diffraction orders. More important is the axial chromatic aberration, which is linear to $\Delta\lambda$ for small values of α. Similar numerical simulations as presented in the last Section revealed that this diffractive effect becomes dominant as soon as more than 2 secondary wavelets interfere. Fig. 6a shows that the transition between the purely diffractive and the purely refractive chromatic behavior occurs between the cases of M = 4 and M = 7, i.e. when only two segments are illuminated. Furthermore, the encircled energy in a focal point decreases, the higher the absolute value of

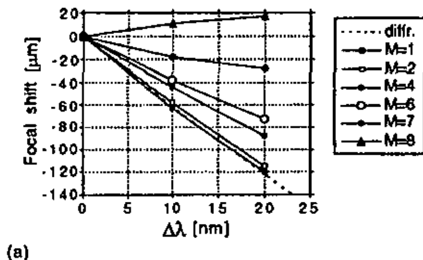

(a)

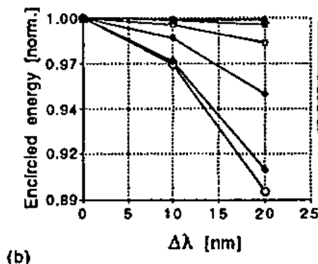

(b)

Fig. 6. Wavelength dependence of (a) focal length l' and (b) encircled energy. The broken line in (a) shows the values for a purely diffractive lens calculated with Eq. (11).

$\Delta\lambda$ is (cf. Fig. 6b). As in the previous Chapter, it could be demonstrated, that the transition effects shown in Figs. 6a and 6b only depend on the number of illuminated segments and not on the absolute value of M.

For the case of a high number of illuminated segments (i.e. $Q \geq 4$), the efficiency in the higher or lower diffraction orders can be calculated with Eq. (12). For a suitable choice of the values of $\Delta\lambda$, M and N they can be moved to the originally designed focal point L' with 100% efficiency. This case was described under the name "multiple order diffractive lenses" in [20] and allows the achromatization of planar lenses for a series of discrete wavelengths. The achromatization for a continuous, broad-band wavelength range with diffractive optics is described in the following Section.

4.4. Achromatization of classical lenses

The previous paragraphs showed that the refractive properties of planar microlenses become important when only a few segments are illuminated and when the incoming light has an extended spectrum. An example where the exact distinction between refractive and diffractive behavior is of great importance is the hybrid achromat, which combines a refractive lens with a diffractive lens. The two lenses can be combined in one lens, as shown in Fig. 7. The advantage of such a system is that the axial chromatic aberration of the refractive component can be corrected by a diffractive component with positive focusing power due to the negative dispersion of the DOE. In a traditional achromatic doublet a refractive element with negative focusing power is needed. Consequently, the required focusing power of the refractive component is greatly reduced in the case of the hybrid lens, thus reducing the magnitude of the higher order aberrations.

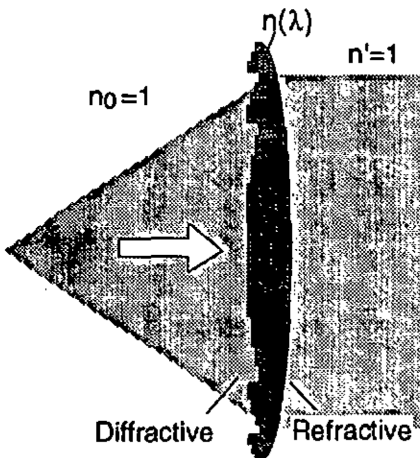

Fig. 7. Hybrid (refractive / diffractive) lens.

The design of a hybrid achromat is based on geometrical ray-tracing. For calculating the influence of the diffractive surface, the law of refraction is replaced by the law of grating diffraction [21]. This approach implies that the diffractive element shows a purely diffractive chromatic behavior, as it corresponds to the curves M = 1 and M = 2 in Fig. 6. In the following, we will use paraxial equations for estimating the critical dimensions of a hybrid achromat.

The focal length f of a thin doublet is given by [22]

$$\frac{1}{f} = \frac{1}{f_r} + \frac{1}{f_d}, \tag{14}$$

where in our case f_r and f_d are the focal lengths of the refractive and the diffractive lens, respectively.

The condition for an achromat is then [23]

$$f_r v_r + f_d v_d = 0, \tag{15}$$

where the dispersions of the refractive lens and the diffractive lens are characterized by the Abbe number v_r and v_d, respectively. For a refractive lens the Abbe number is given by

$$v_r = \frac{n_1 - 1}{n_2 - n_3}, \tag{16}$$

where n_i are the refractive indices for the wavelengths λ_i. Equation (15) requires that the focal length f of the achromat is the same for the wavelengths λ_2 and λ_3. The central wavelength is λ_1. The definition requires that $\lambda_2 < \lambda_1 < \lambda_3$. In the case of a diffractive lens the optical power is proportional to the wavelength, therefore the Abbe number is given by

$$v_d = \frac{\lambda_1}{\lambda_2 - \lambda_3}. \tag{17}$$

Note, the Abbe number of a refractive lens is positive, i.e. $v_r > 0$, whereas for a diffractive lens $v_d < 0$.

From Eqs. (1) and (2) we can calculate f_d as

$$f_d = f\left(1 - \frac{v_r}{v_d}\right). \quad (18)$$

The phase function $\Phi(r)$ of a thin diffractive lens with focal length f_d is described by

$$\Phi(r) = \frac{2\pi}{\lambda_l}\frac{r^2}{2f_d}. \quad (19)$$

For a lens of radius a, the number Q of illuminated segments is then given by

$$Q = \frac{\Phi(a)}{2\pi M} = \frac{1}{\lambda_l}\frac{a^2}{2f_d M}. \quad (20)$$

From Eqs. (18) and (20), we obtain an estimation for the number Q of illuminated segments of the diffractive component. Q is a function of the focal length f and the f-number ($f/\# = f/2a$) of the hybrid lens, namely

$$Q = \frac{f}{8\lambda M\,(f/\#)^2}\frac{v_d}{v_d - v_r}, \quad (21)$$

Figure 8 shows a graphical representation of Eq. (21). The example uses an optical glass BK7 and is designed for the wavelength range of 650 nm ± 25 nm, i.e. $\lambda_l = 650$ nm, $\lambda_2 = 625$ nm, and $\lambda_3 = 675$ nm. If only a few segments of the achromat are illuminated, then the achromat will not work properly, because the achromatization is based on purely diffractive behavior of the diffractive component. As can be seen in Fig. 6a, the chromatic aberrations of an element start to differ from the purely diffractive case, when less than 4 segments are illuminated. The number of illuminated segments depends on both the phase-matching number M and the aperture of the element. Figure 8 shows that even for $M = 1$, problems occur already for focal lengths shorter than 10 - 20 mm. The main reason for the low number of segments Q is that the dispersion of a refractive component is much smaller than the dispersion of a diffractive component ($v_r \approx 10\, v_d$). Consequently, the diffractive lens needs only a low optical power to compensate the chromatic aberrations of the refractive component [see Eq. (15)]. Another reason for preferring low values of M in a hybrid achromat is given by efficiency considerations. Due to the broad band illumination, some light will be diffracted in the unwanted diffraction orders of the diffractive lens. Following Eq. (12) with $\alpha_2 = 1.04$ and $\alpha_3 = 0.96$, the efficiency in unwanted diffraction orders will rise for higher values of M.

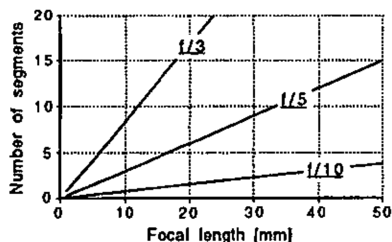

Fig. 8. Hybrid achromat ($M = 1$): number of diffractive segments versus focal length.

4.5. Experimental results for high NA lenses

So far we have treated the case of low NA lenses, where the number of illuminated segments can be very low and the purely refractive case is a solution still relevant for planar fabrication techniques. In order to demonstrate the potential of the PMFE approach we investigate the effects of small surface distortions for the example of a PMFE with NA = 0.45 ($f/\# = 1.0$). The same design wavelength $\lambda_0 = 632.8$ nm as in Sec. 4.1 was chosen, the focal length was set to $f' = 2.0$ mm.

Although the PMFE design procedure is not limited to the paraxial domain, as with many other approaches, and inherently includes the effects of the profile depth, the theoretical maximum efficiency will not reach 100%, as predicted by scalar theory. If we chose $M_j = M = 1$ for the whole PMFE, a minimum segment width of $w_{min} \approx 1.3\,\mu m$ would result at the aperture edges. Due to results based on electromagnetic theory [24], structures designed by scalar theory will no longer yield high efficiencies in this regime and an optimization would need very computing intensive rigorous diffraction calculations. This efficiency reduction will also occur for the larger but deeper segments of an element with $M > 1$ and was not yet taken into account in the design procedure.

As in the previous Sections, different design variants were investigated. For the fabrication by laser beam writing, a design strategy was chosen which started with a value of $M_j = 1$ in the center of the PMFE, and increased the phase-matching number M_j each time when the minimum segment size for laser beam writing (here: $w_{min} = 5\,\mu m$) was reached [4]. A maximum value of $M_j = 4$ resulted at a radius of $a = 1.0$ mm. The diffraction pattern of such a

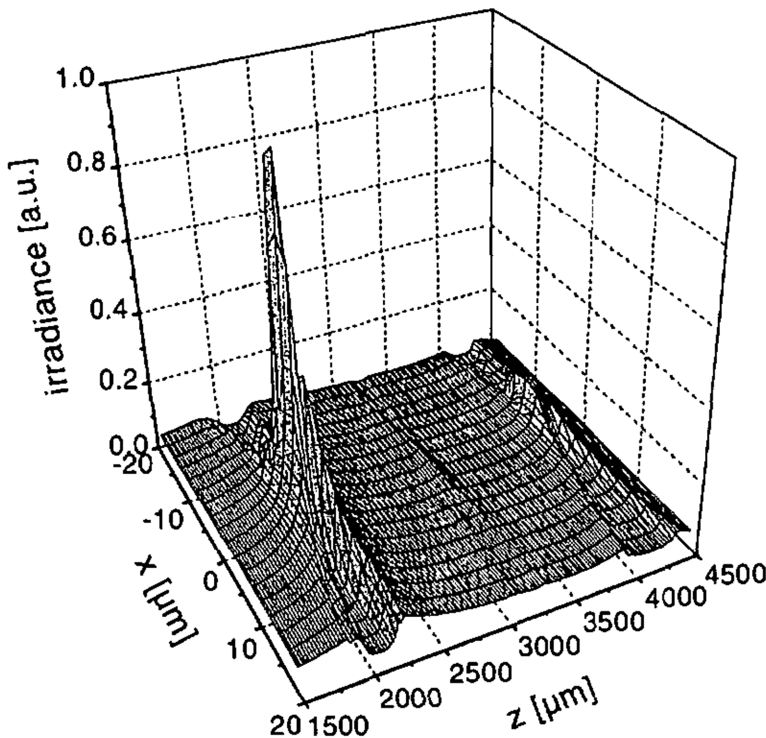

Fig. 9. Measured irradiance distribution in the image space on an f/1 PMFE.

PMFE, fabricated by laser beam writing in photo resist, is shown in Fig. 9. It was measured by scanning a photodiode masked with a small slit in the x-direction at various distances z from the microoptical element. The FWHM of the spot at a distance of $z_{12} = z = 2.0$ mm was measured to be ≈ 1.5 µm, compared to the theoretical value of 1.0 µm obtained with numerical simulations. The spot diameter measurements were performed by scanning a pinhole of 2 x 2 µm^2 size in the focal plane imaged by a 20x microscope objective. The deviation of the experimental from the theoretical beam diameter can be explained by inaccuracies in this measurement setup. A maximum efficiency of $\approx 70\%$ was measured for these PMFEs. The second, small peak at $z \approx 4.0$ mm in Fig. 9 occurs due to deviations in the surface relief profile and corresponds to a lower diffraction order of the structures with $M_j > 1$ in the outer regions of the PMFE.

The most important differences in the behavior compared to low NA lenses can be summarized as follows: First, well defined higher and lower order focal points do no longer occur in the irradiance distribution on the optical axis for α and / or $\mu \neq 1.0$ occur. As an illustration, the axial energy distribution of a PMFE with $M = 4$ is shown in Fig. 10. A depth scaling error of $\mu = 0.9$ leads to the diffraction of light in the 3rd order focus, which is spread out on the z-axis. The main reason for these large aberrations is that the points L_N, which fulfill the optical phase condition (1) between rays r_j and r_{j+1}, depend on the radial distance of the rays for lenses with a high NA. An aberration free focal point will only result for the designed diffraction order M at the design wavelength λ_0 and a perfect surface relief. In addition, steep surface relief slopes which occur at large radii are much more sensitive to depth errors. With geometrical

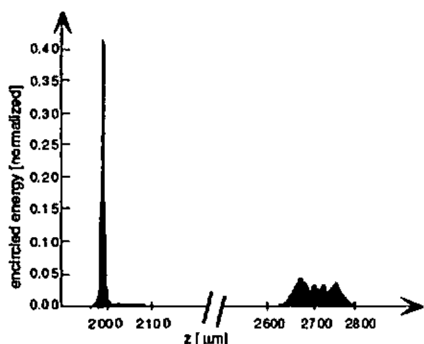

Fig. 10. Calculated axial distribution of the encircled energy of an f/1-lens with a depth scaling factor of $\mu = 0.9$.

optical considerations one can see that the focal shift due to a certain depth error is a monotonically increasing function of the relief slope. A second difference to the behavior of paraxial lenses is that the energy reduction in the main focus due to α and / or $\mu \neq 1.0$ is much higher than predicted by the paraxial equations. In the example of Fig. 10, Eq. (12) would give an efficiency of $\eta_M = 0.57$ for an error factor $\mu = 0.9$, whereas numerical simulations with the Rayleigh-Sommerfeld integrals result in a value of $\eta_M \approx 0.41$.

4.6. Discussion

The results of the above investigations show that diffraction effects are dominant as soon as at least two independent segments of a microoptical surface relief are illuminated. The laws of wave optics determine the points in the image space where the diffraction at some segment boundary pattern leads to constructive interference. The energy distribution among these diffraction orders is controlled by the phase shift introduced by the relief structure between the segment boundaries and can be obtained by solving the wave equations, e.g. in the Rayleigh-Sommerfeld approximation. Nevertheless, the laws of geometrical optics can be used to get a rough estimation on the effect of typical fabrication inaccuracies.

In the PMFE design, the refractive and diffractive behavior of planar microlenses can be adjusted via the phase-matching number M_j, mainly in the sense that the size of contiguous surface relief elements can be varied over the elements' area. Elements with different M_j, whose theoretical optical function is identical, behave differently when small fabrication errors occur or polychromatic applications are considered. Therefore, the design of a specific element has to take into account fabrication constraints, as well as the most important requirements of an application. Some design rules can be given for different ranges of numerical apertures:

For low numerical apertures, elements with a constant $M_j = M$ can be designed having either purely refractive or purely diffractive properties. In the paraxial approximation, the number Q of illuminated segments is given by:

$$Q \approx \frac{l'(NA)^2}{2M\lambda_0}. \qquad (22)$$

Therefore, with a suitable choice of M both types of behavior are accessible: either a refractive element with low chromatic aberrations, but with a focus position which is strongly dependent on the exact surface relief profile, or a diffractive planar optical element showing large chromatic aberrations, but having a focus position which is not very sensitive on the surface relief profile. For any practical realization, the upper limit for M is given by the maximum available profile depth, whereas the lateral resolution imposed by the fabrication technology determines the minimum value of M. The different design examples of an NA = 0.05 lens with l' = 4 mm presented in this Section represent the actual limits for the fabrication by direct laser beam writing.

As soon as more than a few segments of planar microlenses are illuminated (a typical number is $Q \geq 4$), their behavior under typical fabrication and wavelength inaccuracies corresponds to a diffractive optical element. Nevertheless, the variation of the parameter M_j offers some important perspectives for the fabrication and also for the design of new types of elements. As an advantage of the diffractive behavior, the focal position of such microlenses is not affected by small surface relief errors, whereas chromatic aberrations are very strong. However, elements with a high M have an increased density of possible focal points along the z-axis and therefore can react with an axial shift of the most efficient focal point in the presence of fabrication errors concerning the relief depth. Nevertheless, these designs are not necessarily worse than the case of M = 1. The most important consequences of a design with a high value of M are the larger lateral feature sizes and consequently the lower lateral resolution required for their realization. For many technologies, e.g. laser beam writing, the fabrication

of high NA elements is only made possible with the PMFE concept. In addition, a reduction of optical losses may be achieved by the lower number of segment boundaries, which are the main sources for stray light. A potential drawback of elements which use the full depth available by a high M, may be the need for a higher *relative* fabrication accuracy in the vertical dimension. Since for all interference effects (be it in the first or the Mth order), the relative optical path differences in fractions of the wavelength λ_0 are relevant, each profile step at a segment boundary requires the same absolute depth accuracy.

5. Conclusions

The refractive and diffractive properties of planar microoptical elements were investigated for the example of phase-matched Fresnel elements. Their design locally optimizes the surface relief profile, takes into account the finite profile depth, and is only limited by the validity of the scalar theory. By the variation of the phase-matching number, the width and depth of the surface relief segments can be adjusted locally. The optical properties of a series of design variants were compared. By variation of the number of illuminated segments at a constant numerical aperture, the transition between purely refractive and diffractive lenses was numerically simulated. While all these designs perform exactly the same optical function in theory, their refractive or diffractive characteristic becomes obvious when fabrication inaccuracies or wavelength deviations occur. The main result of the numerical simulations in the Rayleigh-Sommerfeld approximation is that the diffractive behavior of a planar microlens is dominant when more than about 4 segments are illuminated. In the paraxial region, their behavior under typical fabrication and application conditions can then be described by the use of a Fourier series which is identical to a sum over refractive lenses with different focal points and efficiencies. For a number of different applications, including low and high NA lenses and hybrid achromats, fabrication-oriented design rules have been given.

Acknowledgments

The authors gratefully acknowledge the helpful discussions with R. Dändliker and M.T. Gale. This work was supported in part by the Swiss Priority Program OPTIQUE of the Board of the Swiss Federal Institute of Technology.

References

[1] M. Born and E. Wolf, *Principles of optics*, (Pergamon Press, Oxford, 1989), chap. 3.1, p. 109.

[2] R. E. Kunz and M. Rossi, "Phase-matched Fresnel elements," Opt. Comm. 97 (1993) 6-10.

[3] W. T. Welford, *Aberrations of Optical Systems*, (Adam Hilger, Bristol, 1986), chap. 2.1, p. 11.

[4] M. Rossi, R. E. Kunz ad G. L. Bona, "Phase-matched Fresnel elements for optical interconnects," OSA Technical Digest Series Vol. 11 (1994) 321-324.

[5] J. A. Futhey and M. Fleming, "Superzone diffractive lenses," OSA Topical Meeting on Diffractive Optics 1992, Technical Digest Series Vol 9 (1992) 4-6.

[6] J. C. Marron, D. K. Angell, and A. M. Tai, "Higher-order kinoforms," in *Computer and Optically Formed Holographic Optics*, I. Cindrich and S. H. Lee, eds., Proc. SPIE 1211 (1990) 62-66.

[7] D. A. Buralli, G. M. Morris, and J. R. Rogers, "Optical performance of holographic kinoforms," Appl. Opt. 28 (1989) 976-983.

[8] L. N. Hazra, Y. Han and C. Delisle, "Plane kinoform lenses for axial stigmatism in finite conjugate imaging," Opt. Comm. 91 (1992) 1-4.

[9] J. S. Fender, R. A. Carreras, "Demonstration of an optical phased telescope array," Opt. Eng 27 (1988), 706-711.

[10] M. T. Gale, M. Rossi, J. Pedersen, and H. Schütz, "Fabrication of continuous-relief microoptical elements by direct laser writing in photoresist," Opt. Eng. 33 (1994) 3556-3566.

[11] D. Zaleta, W. Daschner, M. Larsson, B. C. Cress, J. Fan, K. S. Urquhart, and S. H. Lee, "Diffractive optics fabricated by electron-beam direct write methods", SPIE Critical Review Proceedings, CR49, San Diego (1993) 117-137.

[12] G. J. Swanson, W. B. Veldkamp, "Diffractive optical elements for use in infrared systems," Opt. Eng. 28, (1989) 605 -608.

[13] H. Dammann, "Blazed synthetic phase-only holograms," Optik 31 (1970) 95-104.

[14] J. W. Goodman, *Introduction to Fourier optics*, (McGraw-Hill, San Francisco, 1968), chap. 5.1, p. 80.

[15] S. Sinzinger, M. Testorf and W. Singer, "The transition between diffractive and re-

fractive microoptical components," OSA Topical Meeting on Diffractive Optics 1994, Technical Digest Series Vol. 11 (1994) 143-146.
[16] J. D. Gaskill, *Linear Systems, Fourier Transforms, and Optics*, (Wiley, New York,1978), chap. 10.2, p. 363.
[17] K. Miyamoto, "The phase Fresnel lens," J. Opt. Soc. Am. 51 (1961) 17.
[18] J. J. Stamnes, *Waves in Focal Regions*, (Adam Hilger, Bristol, 1986), chap. 12.1, p. 255.
[19] ref. 1, chap. 8.8, p. 441.
[20] G. M. Morris and D. Faklis, "Achromatic and apochromatic diffractive singlets," OSA Topical Meeting on Diffractive Optics 1994, Technical Digest Series Vol. 11 (1994) 53-56.
[21] ref. 3, chap. 11.3, p. 216.
[22] ref. 3, chap. 10.2, p. 193.
[23] E. Hecht, A. Zajac, *Optics*, (Addison-Wesley, Reading, 1987), chap. 6.3, p. 233.
[24] E. Noponen, J. Turunen, A. Vasara, "Electromagnetic theory and design of diffractive-lens arrays," J. Opt. Soc. Am. A 10 (1993) 434 - 443.

Paper IV

Arrays of anamorphic phase-matched Fresnel elements for diode-to-fiber coupling

M. Rossi, G.L. Bona* and R.E.Kunz

Paul Scherrer Institute, Badenerstrasse 569, CH-8048 Zurich, Switzerland

* IBM Research Laboratory, Säumerstrasse 4, CH-8803 Rüschlikon, Switzerland

submitted 27 July 1994; accepted for publication 27 October 1994.

A method for designing microlens arrays which inherently takes into account application requirements and fabrication constraints is presented. Elements with numerical apertures of up to 0.5 have been designed and fabricated by laser beam writing in photoresist and replication in plastic material. In a laser diode-to-fiber array coupling experiment, an overall optical throughput of 60% was achieved. By means of anamorphic microlens arrays, correction of the laser diode longitudinal astigmatism and circularization of the image plane irradiance distribution have been demonstrated.

1. Introduction

Many applications in optics require efficient devices for interconnecting light emitters to different configurations of output ports. In recent years, parallel optical data links have attracted increasing interest in the field of data communications. Typical applications are parallel high-speed and high-capacity interconnects for optical switches, workstation clusters or even between processor chips.

In this paper, experimental and theoretical results are presented for novel, single element optical interconnects based on phase-matched Fresnel elements (PMFEs) [1]. These are planar surface microrelief structures which are well suited for low-cost mass replication. Laser diode-to-fiber connecting lens arrays with high numerical apertures NA have been designed and fabricated. Most of the other work done in the area of high NA lenses ([2], [3], [4]) uses e-beam lithography for the fabrication, requiring a set of binary masks and multiple exposures. Since the PMFE design approach locally takes into account the limitations of the technology actually used for the fabrication, we were able to achieve excellent results with direct laser beam writing in one single exposure step. The drawback of the lower lateral resolution compared to e-beam writing could be overcome by designing deeper relief structures with a continuous profile. Furthermore, our elements were designed for plastic materials, in order to be compatible with low-cost industrial replication techniques. In Section 2, the most important fundamentals for the design of PMFEs are outlined. Section 3 lists the special requirements for a specific laser diode-to-fiber coupling application, the design parameters for the microlens arrays and first experimental results. Section 4 deals with the possibility of circularizing the elliptical image of the laser diode by means of anamorphic microlenses.

2. Design of Phase-matched Fresnel elements

The design of PMFEs aims at structuring the surface of a thin layer in order to image an object point source O on an image point P through an arbitrary number of different media, including curved interface planes and reflective arrangements and bases on a phase-sensitive ray tracing algorithm [5]. For conciseness, we only deal with the specific example of laser- to-fiber array coupling (see Fig. 1). The design procedure starts with a principle ray for which the optical phase Φ_P in the image point is calculated as

$$\Phi_P = \sum_k 2\pi \cdot n_k r_k / \lambda, \qquad (1)$$

where λ is the optical wavelength in air, n_k is the index of refraction of the medium k and r_k is the geometrical path length of a ray traversing it. Next, a ray which is shifted by a small increment along a radial line in the yz-plane is propagated from O to P. At the actual ray position, a curved surface element is calculated such that the phase Φ_P in the image point is kept constant up to an integer multiple of 2π. This leads to a segmentation of the surface relief. For the resulting

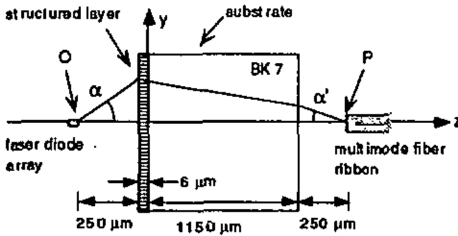

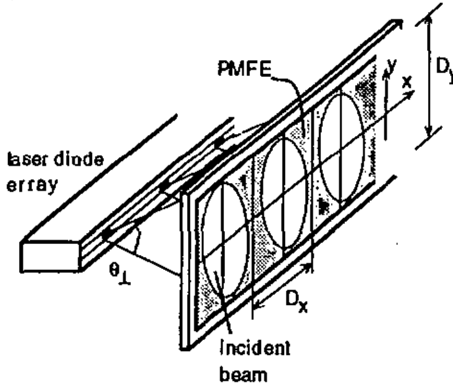

Fig. 1. Optical arrangement for laser-to-fiber coupling: (a) vertical (yz) plane cross-section, (b) illumination of PMFE structured layer by the laser diode array.

microoptical surface, the phase Φ_P is (i) constant for any two rays which cross the same segment and (ii) differs by an integer multiple of 2π for two rays crossing different segments. The phase difference $M \cdot 2\pi$ between neighboring segments is given by the phase-matching number M, which is a powerful design parameter for optimizing the optical performance within the constraints imposed by the fabrication process [1]. Related design schemes are described under the names "superzone diffractive lenses" and "higher-order kinoforms" in [6] and [7], respectively.

For fabricating the PMFEs, we used a direct laser writing process in photoresist [8], in contrast to other more frequently used techniques such as e-beam writing or diamond turning. A photoresist-coated sample is raster scanned under an intensity-modulated focused laser beam. The exposure pattern consists of $1 \times 1\ \mu m^2$ pixels, each with 256 grey levels. In order to allow for this resolution, the size of any individual surface relief segment was constrained to be $w_i > w_{min} = 5\ \mu m$ [1]. A higher value of M leads to wider and deeper segments. One design strategy was to minimize the locally varying phase-matching number M in order to keep the surface relief depth h_i below the photoresist thickness h_{max} and maintaining the condition $w_i > w_{min}$ for all segments i. The resulting computer-generated PMFEs can be considered to represent a generalized type of Fresnel microlens whose zones have a locally varying depth.

A major advantage of the PMFE approach is that arrays of planar elements with very high numerical aperture and an arbitrary clear aperture shape can easily be generated and mass fabricated on a single substrate. Therefore, PMFEs were chosen for accomplishing the compact parallel optical interconnection of a laser diode array to a fiber ribbon cable.

3. Laser Diode-to-Fiber Coupling Application

The main requirements for this application were a high optical laser-to-fiber throughput $T_n = P_{F,n}/P_{L,n}$ and a low crosstalk $T_{nm} = P_{F,n}/P_{L,m}$, where $P_{F,n}$ is the power incident on fiber No. n in the (x',y') image plane, and $P_{L,m}$ is the total power emitted by laser m. For the single lenslets, optimizing T_n calls for (1) a high numerical aperture NA, (2) adapting the clear aperture shape and size to the laser beam profile at the entrance pupil, and (3) achieving a high efficiency $\eta_n = P_{F,n}/P_{E,n}$ where $P_{E,n}$ is the power incident on the clear aperture of lenslet n. The above definition of the efficiency η_n is valid under the assumption of a negligible crosstalk T_{nm}. Some important factors for crosstalk minimization in a practical device are (i) a good image quality, (ii) a large tolerance for fiber misalignment, and (iii) proper lenslet entrance pupil locations. For the present example, the most important design parameters and experimental results can be summarized as follows.

Each laser emitted an astigmatic beam with divergence angles $\theta_{//} = 8°$ and $\theta_\perp = 28°$ (FWHM) in the parallel (xz) and perpendicular (yz) planes, respectively, at a wavelength of 831 nm [9]. The MT-connector [10] compatible ribbon cable consisted of 12 multimode fibers having 250 µm pitch with numerical apertures $NA_F = 0.21$ and diameters $\O_{co} = 50\ \mu m$ of the core and $\O_{cl} = 125\ \mu m$ of the cladding.

Optimization with respect to the above aspects (1-3) and (i-iii) resulted in the optical arrangement as shown in Fig. 1. The object and image distances were $l = 250\ \mu m$ and $l' = 1400\ \mu m$, respectively. The transversal magnification factor was 4, yielding theoretical image radii ($1/e^2$-values) of $w'_{0,x} \approx 16.4\ \mu m$ and $w'_{0,y} \approx 5.4\ \mu m$.

For the PMFE, Fresnel reflection losses at the microoptical surface relief structure can cause a decrease of transmittance especially for large angles of incidence. The polarization-dependent transmittance is plotted in Fig. 2a. The polarization of the laser diode

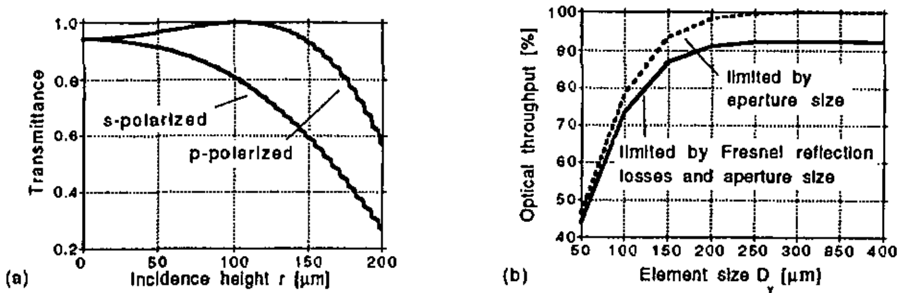

Fig. 2 (a) Position-dependent transmittance through the PMFE surface for s- and p-polarized beams. The ripple in the curves results from the depth steps at the segment boundaries. (b) Integrated aperture and reflection losses.

is parallel to the xz-plane with an extinction ratio of 250:1. For the calculation of the optimal element size and the estimation of the maximum overall optical throughput, it is important to take into account the strongly inhomogeneous distributions of the irradiance and the polarization state in the entrance pupil. The total fraction of transmitted light, which is mainly limited by the aperture size in the y-direction and the Fresnel reflection losses depending on the local polarization state, is plotted in Fig. 2b. These calculations show that the overall optical throughput saturates at 92% for elements with a size of $D_y \geq 300$ µm. No anti-reflection coating was applied to the PMFE which would allow to increase the optical throughput beyond 92%. A further reduction from this theoretical maximum efficiency has to be expected due to the limited validity of the scalar theory, which is the basis for the design. Calculations using rigorous diffraction theory

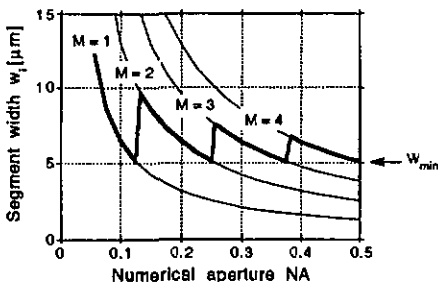

Fig. 3. Dependence of the PMFE segment width on the numerical aperture NA for various values of M. The thick line indicates the design rule which minimizes M.

as in [11] showed a significant loss in efficiency of grating structures with local periods in the range 2 - 3 times the design wavelength. In these high NA regions ($r \geq 100$ µm), an optimization with vector methods would be required for a higher efficiency. However, for spherical lenses of the size presented here, this would require an enormous computing power.

A PMFE prototype consisted of a 6 µm thick structured photoresist layer on a BK7 substrate. The value of 6 µm is given by the maximum thickness range for standard photoresist processing and for replication by embossing or casting techniques. Up to this thickness, no degradation of the surface relief profile in the replication step was observed. In addition to the parameter values directly given in Fig. 1, widths D_x = 250 µm and D_y = 300 µm were chosen for the rectangularly shaped PMFE lenslets. While D_x is equal to the inter-laser and inter-fiber spacing, D_y corresponds to an object side NA = sin α = 0.51. The image side numerical aperture NA' = sin α' = 0.13 of this arrangement is still smaller than the numerical aperture of the fiber NA_F, ensuring an optimal coupling efficiency. As described in Section 2, the design of microlenses having these high values of NA and being compatible to current laser beam writing technologies, requires special algorithms.

Fig. 3 shows how the segment width w_i depends on the numerical aperture NA of the element for different values of the phase-matching number M. It was obtained by using the PMFE design programs based on the algorithms described in Section 2. A series of microlenses was calculated using different design strategies, resulting in different surface relief segment dimensions and number depending on the set of values chosen for M versus the NA. These elements were fabricated by laser beam writing in photoresist and

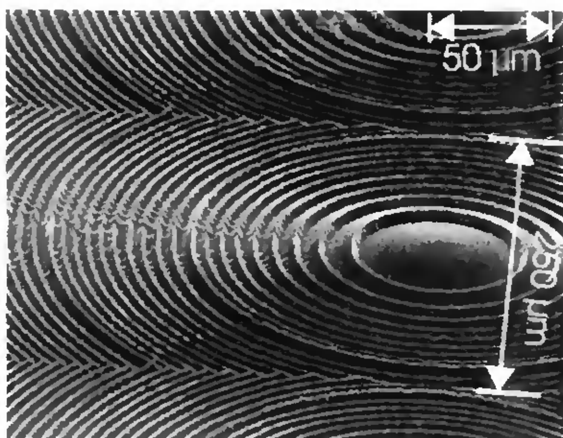

Fig. 4: SEM picture of a PMFE array fabricated in photo resist following the "minimum number of segments" design rule.

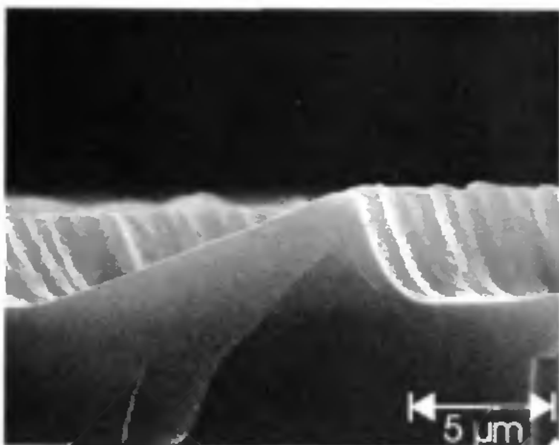

Fig. 5. SEM picture of a single PMFE segment replicated in epoxy.

compared by measuring their imaging quality and efficiency.

Two different design strategies were evaluated and are discussed briefly now. For the PMFE shown in Fig. 4, the phase-matching number M was kept everywhere at the maximum value imposed by the photoresist depth of 6 µm. At the center of the PMFE, $M = 4$ is the highest possible value and leads to segments with a depth of $h \approx 5.9$ µm. But since the depth of the segments decreases for increasing numerical apertures at constant M, M could be incremented for higher PMFE radii. The first change of $M = 4$ to $M = 5$ occurs at a radius of $r \approx 105$ µm and is clearly visible in Fig. 4. This strategy leads to a PMFE with a minimum number of segments. However, the best results were obtained for elements designed by keeping the phase-matching number M as low as possible everywhere. This design rule corresponds to the thick line in Fig. 3. Such an element was fabricated in epoxy by a uv-replication technique [12]. Fig. 5 shows a single PMFE segment near its center. For obtaining the SEM micrograph, the microlenses had to be coated with a thin Au layer. The overall optical throughput of $T_n = 60\%$ measured for a first prototype corresponds to the diffraction efficiencies obtained for e-beam fabricated elements [3]. The efficiency measurements were performed by means of a 20X microscope objective imaging the focal plane of the PMFE onto a masked photodiode. Crosstalk to adjacent fibers via the lenses in the array were determined to be negligible.

4. Design of anamorphic Microlenses

Due to the elliptical near-field and the longitudinal astigmatism of a laser diode, its image formed by a circular symmetric PMFE of the kind described in the previous Sections has also an elliptical shape. In order to adapt the image shape to the circular fiber symmetry, an anamorphic imaging element [13] was designed and fabricated.

The anamorphic microlens had different focal lengths in the parallel (x) and the perpendicular (y) direction. The focal distance l'_x in the parallel direction was left at the previously calculated value of 1400 µm. By calculating the Gaussian beam parameters [14] separately in the x- and y-direction, the transverse focal distance l'_y was adjusted such that the transverse beam width $\mathcal{W}'_y(l'_x)$ at the distance l'_x was identical to the parallel beam width $\mathcal{W}'_{0x}(l'_x)$ (see Fig. 6). This leads to a circular irradiance distribution in the image plane and corresponds to the introduction of a longitudinal astigmatism. Based on measured

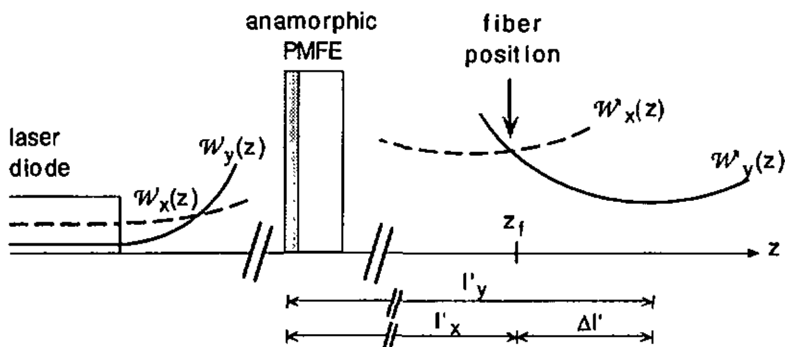

Fig. 6. Scheme of the optical setup for anamorphic imaging.

data of the laser diodes, the focal distance l'_y had to be shifted by $\Delta l' = 81$ µm in the positive z-direction. The transversal microlenses also corrected for the longitudinal astigmatism of ≈ 2 µm of the laser diode.

The raster scan data for the laser beam writing of all the PMFEs are calculated simultaneously during the writing process on an external Sun Sparc station. The combination of the two different lenses to one anamorphic element was performed by the same principle forming an ellipsoidal rather than a circular surface.

The value of Δl' is determined by the laser diode divergence angles $\theta_{//}$ and $\theta_{\perp}$, which have tolerances of at least 0.5°. Therefore, the ability to introduce a longitudinal astigmatism with anamorphic microlenses was investigated systematically, and a series of elements with varying values of Δl' was fabricated and characterized. The beam parameters of the laser diodes and of the field behind the microoptical element were determined by using an instrument (ModeMaster with silicon detector, Coherent Inc.) performing knife-edge measurements. The analysis of the measured data was done following Refs. [15], [16]. In Table 1, the determined values for the $\mathcal{M}^2$ parameters [17], the longitudinal astigmatism Δl' and the transversal magnification factors $m = \mathcal{W}'_{0,x} / \mathcal{W}_{L,x}$ are listed. The measured values of Δl' differed by + 0..15% from the design values $\Delta l'_d$. The beam waist $\mathcal{W}'_{0,x}$ in the x-direction is very close to the theoretical value of 16.4 µm, leading to a good coincidence between the calculated and measured magnification factor m, whereas the measured value of $\mathcal{W}'_{0,y}$ is larger than expected. The $\mathcal{M}^2$ beam parameter, derived from the product of waist size and divergence angle, indicates how closely the beam properties match the ones of an ideal Gaussian beam. The measured $\mathcal{M}^2$ values reported in Table 1 do not deviate much from the values for the beam directly emitted by the laser diode, proving that the anamorphic PMFEs do not introduce significant aberrations to the laser beam. The slightly increased values of $\mathcal{M}^2_y$ and $\mathcal{W}'_{0,y}$ can be explained as follows: since the laser diode polarization is in the xz-plane, the reflection losses in the y-direction are higher than along the x-direction (see Fig. 2a). Combined with the strongly elliptic far-field shape, this leads to a reduced effective aperture in the y-direction and a broadening of the spot width $\mathcal{W}'_{0,y}$. In addition, most of the stray light of the PMFEs is concentrated along the y-axis, which is a direct consequence of the laser beam writing raster scan [8] and can lead to small inaccuracies in the knife-edge measurements. Furthermore, it turned out that these knife-edge experiments are *very sensible* to *misalignment* of the microlenses. For instance, a small vertical tilt of the elements can reduce the beam quality expressed by the $\mathcal{M}^2$ parameters substantially.

Table 1. Measured values of the $\mathcal{M}^2$ parameters, Δl' and magnification m for anamorphic microlenses.

Element type	$\mathcal{M}^2_x$	$\mathcal{M}^2_y$	Δl' (measured)	transversal magnification m
laser diode	1.2	1.35	2	–
PMFE, $\Delta l'_d = 0$ µm	1.3	1.8	5	4.16
PMFE, $\Delta l'_d = 40$ µm	1.3	1.8	48	3.96
PMFE, $\Delta l'_d = 60$ µm	1.2	1.6	70	4.97
PMFE, $\Delta l'_d = 80$ µm	1.3	1.7	88	4.37
PMFE, $\Delta l'_d = 100$ µm	1.2	1.35	102	4.58

Fig. 7 shows a contour plot of the circularized

irradiance distribution in the image plane z_f measured with a CCD camera. The radius at the $1/e^2$ value is $\approx 16\ \mu m$ which clearly shows that the elliptical near-field irradiance distribution of the laser diode with $\mathcal{W}_{L,x} = 4.1\ \mu m$ and $\mathcal{W}_{L,y} = 1.4\ \mu m$ is circularized by the anamorphic PMFE.

5. Conclusions

Experimental and theoretical results have been presented for novel, planar element optical interconnects. It has been shown that phase-matched Fresnel elements are suitable for realizing parallel optical interconnections of a laser diode array to a fiber ribbon cable. By this approach, the optical performance of elements with a high numerical aperture of up to 0.5 can be optimized, taking into account the constraints imposed by the fabrication process. The computer-generated surface microreliefs were fabricated by a direct laser writing process. For investigation purposes, elements fabricated in photoresist were used. In addition, the replication in polymer materials was successfully demonstrated. For the first prototypes, an overall optical throughput of 60% was measured. The possibility of circularizing the irradiance distribution in the image plane was demonstrated by using anamorphic microlenses. This shows that the PMFEs have a great potential also in many other imaging systems where an altered irradiance distribution is required. Typical examples are optical storage and sensing applications. These compact planar optical elements lend themselves to low-cost mass production by replication in plastic materials.

Acknowledgments

The authors gratefully acknowledge M.T. Gale and H. Schütz for their support in the fabrication by laser beam writing, R. Stutz for the replication of the micro-optical elements, and R. Germann, H. Richard and P. Vettiger for their assistance in the characterization of the elements. This work was supported in part by the Swiss Priority Program OPTIQUE of the Board of the Swiss Federal Institute of Technology.

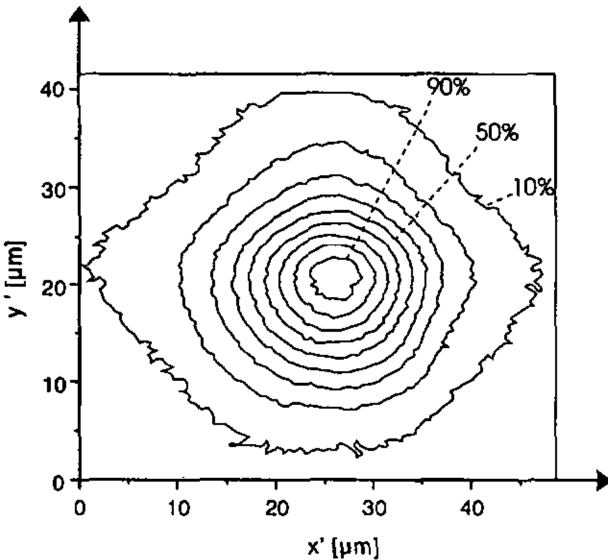

Fig. 7. Contour plot of circularized irradiance distribution in the plane of the fiber. The contour line spacing is 10% and the radius at $1/e^2$ is $16\ \mu m$.

References

1. R. E. Kunz and M. Rossi, "Phase-matched Fresnel elements," Opt. Comm. 97, 6-10 (1993).
2. J. R. Leger, M. L. Scott, and W. B. Veldkamp, "Coherent addition of AlGaAs lasers using microlenses and diffractive coupling," Appl. Phys. Lett. 52, 1771 - 1773 (1988).
3. A. Stemmer, H. Zarschizky, F. Mayerhofer, G. Lefranc, and W. Gramann, "Diffractive coupling lenses: fabrication and measurements of silicon elements," OSA Topical Meeting on Diffractive Optics 1994, Technical Digest Series Vol. 11, 317 - 320 (1994).
4. P. McKee, J. Towers, A. Thurlow, and D. Wood, "Fresnel lens array for optical fiber semiconductor coupling," OSA Topical Meeting on Diffractive Optics 1994, Technical Digest Series Vol. 11, 235 - 238 (1994).
5. W. T. Welford, Aberrations of optical systems (Hilger, Bristol, 1986), chap. 2, p. 11.
6. J. A. Futhey and M. Fleming, "Superzone diffractive lenses," OSA Topical Meeting on Diffractive Optics 1992, Technical Digest Series Vol. 9, 4 - 6 (1992).
7. J. C. Marron, D. K. Angell, and A.M. Tai, "Higher-order kinoforms," in *Computer and Optically Formed Holographic Optics*, I. Cindrich and S.H. Lee, eds., Proc. SPIE 1211, 62-66 (1990).
8. M. T. Gale, M. Rossi, J. Pedersen, and H. Schütz, "Fabrication of continuous-relief micro-optical elements by direct laser writing in photoresist," Opt. Eng. 33, 3556-3566 (1994).
9. H. Jaeckel, G. L. Bona, P. Buchmann, H. Meier, P. Vettiger, W. Kozlovsky, and W. Lenth, "Very high power AlGaAs SQW-GRINSCH ridge laser with frequency doubled output," IEEE J. Quantum Electron 27, 1560-1567 (1991).
10. F. Ashiya, T. Satake, S. Nagasawa, "Development of multifibre connectors and their application," EFOC/LAN '91 Proceedings, 304 - 308 (1991).
11. E. Noponen, J. Turunen, A. Vasara, "Electromagnetic theory and design of diffractive-lens arrays," J. Opt. Soc. Am. A 10, 434 - 443 (1993).
12. M. T. Gale, M. Rossi and H. Schütz, "Fabrication and replication of continuous-relief DOEs," IEE conference publication No. 379, 66-70 (1993).
13. Ref. 2, Chap. 11, p. 211.
14. A. Yariv, Introduction to optical electronics (Holt, Rinehart, Winston, 1976), chap. 3.2.
15. D. Wright, P. Greve, J. Fleischer, L. Austin, "Laser beam width, divergence and beam propagation factor - an international standardization approach," Opt. and Quant. Elect. 24, S993 - S1000 (1992).
16. R. D. Jones, T.R. Scott, "Error propagation in laser beam spatial parameters," Opt. and Quant. Elect. 26, 25 - 34 (1994).
17. A. E. Siegman, Lasers (University Science Books, Mill Valley, 1986), chap. 17, p. 697.

Paper V

ELSEVIER

1 December 1994

OPTICS COMMUNICATIONS

Optics Communications 112 (1994) 258-264

Focusing fan-out elements based on phase-matched Fresnel lenses

M. Rossi, R.E. Kunz

Paul Scherrer Institute Zurich, Badenerstrasse 569, CH-8048 Zurich, Switzerland

Received 16 May 1994; revised manuscript received 1 August 1994

Abstract

A novel approach for designing and fabricating focusing fan-out elements is presented. It is based on an area-sharing arrangement of planar lenses. Due to the low number of parameters and their well-defined physical meaning, it is possible to find solutions with both a high efficiency and a low uniformity error using simple and fast optimization procedures. Results of numerical simulations and experiments agree well. Conspicuous properties include a high fabrication fault tolerance, the suitability for low-cost mass production, and the possibility of realizing very compact microoptical systems.

1. Introduction

Fan-out elements are important components for optical computing and interconnection applications. Many different algorithms have been developed for their design, leading to elements with a high efficiency and a good uniformity [1]. The purpose of these elements is to split an incoming planar wave into an array of quasiparallel waves. Therefore, additional optical components are needed in typical point-to-point interconnection schemes. Furthermore, their optical performance is strongly dependent on a very accurate realization of the theoretically calculated surface relief profile [2,3].

In this paper, a concept is presented for combining the focusing and the splitting function into one single element and simultaneously reducing the dependence of their performance on fabrication tolerances. Moreover, the approach provides the possibility of deriving a concise design procedure for focusing fan-out elements. Very efficient computer algorithms can be derived for the modelling procedure, since only a relatively low number of parametres is used, most of them with a well-identified physical meaning.

Sect. 2 states the fundamentals for the design of focusing fan-out elements based on spatially interlaced planar lenses. After a general introduction to this concept, a theoretical modelling approach and algorithms for the optimization of such focusing fan-out elements are presented. In Sect. 3, the description of this approach in terms of a phase function and the comparison with other types of fan-out elements are summarized. Experimental results are listed and first estimations and measurements of the fan-out performance on the fabrication tolerances are presented in Sect. 4.

2. Fan-out elements based on spatially interlaced planar lenses

A focusing fan-out element simultaneously has to perform two functions usually provided by different elements, namely that of focusing and beam splitting. The basic optical configuration for an element connecting a point source O to an array of output ports P_j is shown in Fig. 1. In the approach presented here, the focusing part will be realized in the form of *phase-*

0030-4018/94/$07.00 © 1994 Elsevier Science B.V. All rights reserved
SSDI 0030-4018(94)00460-9

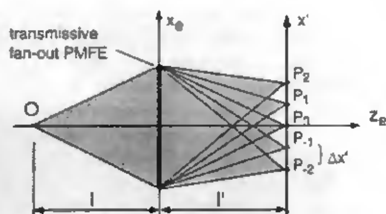

Fig. 1. Optical configuration for a transmissive focusing fan-out element.

matched Fresnel elements (PMFEs) 34]. These are computer-generated surface micro-relief structures whose design inherently takes into account fabrication constraints. They are suitable for low-cost mass production by laser beam writing and subsequent replication techniques. As a first possibility, for an interconnection from one object point source to an array of N image points at positions x'_j, N different PMFEs are used, one for each interconnection channel. In principle, these different PMFEs could be arranged as whole units in an array configuration. However, for point-to-point connections with a non-uniform illumination of the element plane, a spatially interlaced arrangement of splitted elements in an area-sharing pattern is favourable.

Therefore, each one of the N different lenses is split into a subarray, representing only a non-contiguous part of the original PMFE. The complete PMFE fan-out structure is then obtained by interlacing the N different subarrays, denominated as $(\bar{C}, \bar{B}, A, B, C)$ in Fig. 2, which shows the Atomic Force Microscope (AFM) picture of a portion of an element fabricated in photoresist. For the design and optimization, the diffraction patterns of the different PMFE subarrays have to be calculated and coherently superposed. For these calculations, each PMFE subarray structure is treated as being a thin transmission object located in the (x_e, y_e)-plane of a lens (cf. Fig. 3). Point P_0 in the output plane represents the image of the light source O obtained in the 0th diffraction order. The optical effect of the subarray structure of type j is described by a transmission function

$$t_j(x_e, y_e) = a_j(x_e, y_e) \exp(i\Delta\varphi_j) . \quad (1)$$

The aperture function a_j is used to mask the portions of the original PMFE type j which are to be occupied

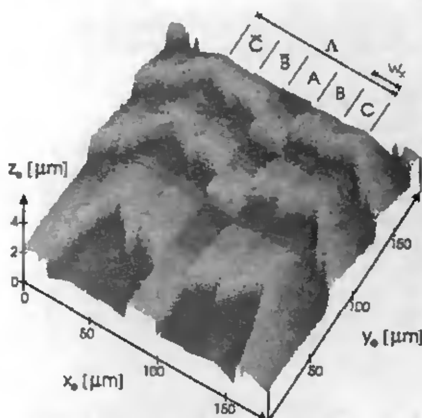

Fig. 2. Atomic Force Microscope (AFM) picture of the surface relief for one complete subarray period of a 5×1 planar fan-out element.

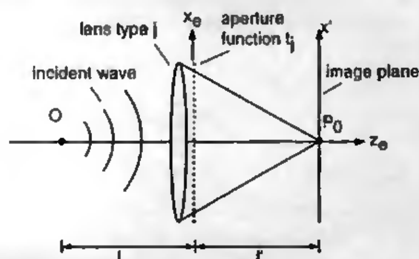

Fig. 3. Basic optical arrangement used for modelling the fan-out PMFEs.

by the other lenses. An arbitrary phase shift $\Delta\varphi_j$ can be added to each PMFE. It represents an important optimization parameter. When this structure is illuminated by a wave $u_0(x_e, y_e)$, the diffraction pattern

$$u'_j(x', y') = AB \frac{\exp(ikl')}{i\lambda l'} q_j\left(x', y'; \frac{1}{\lambda l'}\right) \times \mathcal{F}\{u_0(x_e, y_e)\, t_j(x_e, y_e)\}|_{x'/\lambda l', y'/\lambda l'} , \quad (2)$$

in the image plane of the lens is basically given by the Fourier transform $\mathcal{F}$ of the transmission function t_j multiplied by u_0, assuming that the Fresnel approximations are valid [5,6]. The lens of type j is characterized by the quadratic-phase factor

$$q_j\left(x', y'; \frac{1}{\lambda l'}\right) = \exp\left(\frac{i\pi}{\lambda l'}\left[(x'-x'_j)^2 + y'^2\right]\right) \quad (3)$$

and the constants A and B. A describes the magnitude and the phase of the incident wave, B is a constant that accounts for the finite thickness of the element and any losses due to reflection and absorption. In the approach presented here, the subarray aperture function a_j is assumed to correspond to a periodic arrangement of rectangular apertures with a period Λ (cf. Fig. 2). According to the basic properties of the Foureir transform in Eq. (2), it is evident that the diffraction pattern of a structure with period Λ has a periodicity of

$$d' = l' \lambda / \Lambda \quad (4)$$

in the image plane, if the illuminating amplitude distribution u_0 is slowly varying.

The first step of the design procedure aims at achieving a mutual coincidence between the bright spots of the diffraction patterns of the different subarrays and the array of the desired image points. This requires

$$d' = \Delta x', \quad (5)$$

where $\Delta x'$ is the pitch of the image point array (cf. Fig. 1), and leads to a periodicity of

$$\Lambda = l' \lambda / \Delta x' \quad (6)$$

for all subarray types. For the cases where the approximations for the Fresnel diffraction regime are not valid, subarray structures with a *locally varying* "periodicity" have to be used. A preliminary account of this concept including two-dimensional and reflective PMFE fan-out elements has been given in Ref. [7].

Thus, the whole fan-out PMFE structure is completely characterized by N interlaced, different PMFEs focusing at points P_j with corresponding aperture functions a_j and phase offsets $\Delta\varphi_j$. Whereas the aperture functions a_j are determined by the conditions of Eq. (6), the N phase offsets $\Delta\varphi_j$ may be chosen without any restrictions. The only constraint for the N positions x'_j of the focus points P_j of the different PMFEs results from the condition that they have to match the linear array of periodicity d' given by Eq. (4). The relative arrangement of their subarray structures is an additional design paramcter, whose influence on the performance of an optimized fan-out element is, however, small. Often, the effective number of design parameters can be reduced to $<2N$ by means of symmetry considerations.

A frequent case is a fan-out element whose purpose is to produce a uniform symmetric output array. A symmetric irradiance distribution in the image plane is exclusively obtained by a symmetric or antisymmetric phase function in the element plane. An antisymmetric phase function would require an odd Fourier transform in Eq. (2), which in consequence calls for an odd symmetry of the complex function $u_0 t_f$. Since this is not achievable with plane or spherical wave illumination, we only take into account those configurations representing a symmetric arrangement of the different subarrays with symmetric phase offsets. The appropriate figures of merit for the optimization procedures are the uniformity error

$$\sigma = \frac{P_{max} - P_{min}}{P_{max} + P_{min}}, \quad (7)$$

and the efficiency

$$\eta = \frac{\sum_{j=1}^{N} P_j}{P_0}, \quad (8)$$

where P_j are the peak powers in the image points, P_{max} and P_{min} their maximum and minimum values, respectively, and P_0 the illuminating power incident on the total PMFE area. Depending on the application, a combination of σ and η can be used to construct an appropriate merit function.

The parameter set investigated first is related to the N values x'_j of the focus positions given by the different PMFEs. For a symmetric image plane irradiance, both the location of the N focus points and the arrangement of the corresponding PMFEs forming the interlaced subarray structure have to be symmetric with respect to P_0 and the center of the whole element, respectively. Depending on the size of N, either a systematic variation of the possible arrangements or a choice of reasonable configurations will be considered. In this section, the design and optimization of $N \times 1$ fan-out elements based on N interlaced planar lenses is described. However, solutions with $L > N$ or $L < N$ different PMFEs are also valid and, depending on the application, can lead to even better results, as will be shown in Sect. 4 for the example of a 5×1 fan-out element. The notation $(\bar{C}/\bar{B}/A/B/C) = (-2/$

$-1/0/1/2$) for a subarray configuration with $L=5$ different PMFEs means that the type $\bar{C}$ subarray corresponds to a PMFE focusing at the point $(-2)\Delta x'$ on the x'-axis (cf. Figs. 1 and 2), for example.

The next step consists of optimizing the values of the phase offsets $\Delta\varphi_j$ for a given configuration of the subarrays. Instead of using an optimization procedure without any a priori knowledge of the values for uniformity error and efficiency versus the phase offsets, a *systematic* scan in the $(L-1)/2$ dimensional parameter space is performed for identifying the relevant regions. Figs. 4a and 4b show the figure-of-merit "surfaces" for the uniformity error and the efficiency, respectively, for a 5×1 fan-out. This PMFE structure has only two independent phase parameters, namely $\Delta\varphi_2=\Delta\varphi_5$ and $\Delta\varphi_3=\Delta\varphi_4$, once the configuration of the subarrays has been chosen. The aim is to find the global optimum for the fan-out performance, i.e. $\sigma\to0$ and $\eta\to1$, corresponding to the bright regions in both Figs. 4a and 4b. The last step of the optimization procedure is then restricted to regions of the parameter space where local minima of the uniformity error coincide with high efficiency regions. This requirement is fulfilled near the uniformity error minimum at the point $\Delta\varphi_2=\Delta\varphi_5\approx0.45\times2\pi$ and $\Delta\varphi_3=\Delta\varphi_4\approx0.95\times2\pi$ (cf. Fig. 4a), since it is also located in a high efficiency region with $\eta>80\%$ (cf. Fig. 4b). Starting from this point, the uniformity error of the fan-out is minimized using simple and fast converging methods, such as steepest gradient algorithms.

A more detailed analysis of Figs. 4a and 4b reveals that, for a given PMFE subarray configuration, several regions with a low uniformity error exist. All of them have a minimum with a vanishing uniformity error, but not necessarily combined with a high efficiency, since a large fraction of the total energy can be diffracted in points outside the desired image point array. However, by choosing an appropriate PMFE subarray configuration (e.g. one where the focal points of the PMFEs are identical to the fan-out image point array), the *global* optimum of the merit function can be determined. It has a theoretical uniformity error $\sigma=0$ at an efficiency of about 90%.

The calculation effort for designing fan-out PMFEs can be reduced even further for many applications, since the main function of the different types of lenses is to produce shifted image points. In the approximation of a slowly varying illuminating wave u_0, this can also be realized by calculating only one type of lens, but shifting its position in the aperture plane by integer multiples of the value $\Delta x'$.

3. The fan-out PMFE phase function

The model given in Sect. 2 can be generalized by describing the operation of fan-out PMFEs by the phase shift of a single transmission object. This facilitates a direct comparison to other approaches for modelling fan-out elements. Due to the twofold function of a focusing fan-out element, its total phase variation $\Omega_{tot}(x_e, y_e)$ is a combination of a focusing $\Omega_{foc}(x_e, y_e)$ and a splitting $\Omega(x_e)$ phase function in the sense of Ref. [8]. These two phase terms can be

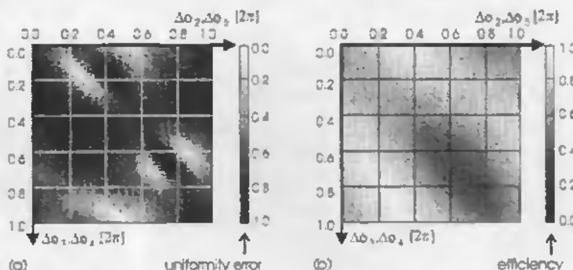

Fig. 4. Merit function variation with respect to the uniformity error (a) and the efficiency (b) for a 5×1 fan-out based on the symmetric subarray configuration $(-2/-1/0/1/2)$.

identified also for the fan-out PMFE structure introduced in Sect. 2.

The focusing part $\Omega_{foc}(x_e, y_e)$ is given by the phase shift resulting from the local surface relief structure within the PMFE lenses, whereas the splitting phase function $\Omega(x_e)$ corresponds to the subdividing and interlacing operation applied on the different types of PMFEs. In this Section, we discuss the special case where the different types of PMFEs are approximated by identical but shifted lenses. Due to the basis Fourier transform properties [5], the Fourier transform of the function $u_0 t_j$ shifted by $\Delta x_j'$ is identical to the transform of the unshifted function multiplied by a linear-phase factor. Hence, according to Eqs. (2)-(6), the interlaced subarray structure of N spatially shifted lenses corresponds to a splitting function $\Omega(x_e)$ with a period identical to the subarray period Λ and function values which vary linearly within N discrete subintervals. This piecewise linear splitting function is an approximation to the continuous phase functions demonstrated in Ref. [1], calculated by applying diffractive optics.

While this might appear to be a drawback at first sight, several reasons emphasize the benefit of such a fan-out PMFE approach *for practical applications*. First, as shown in Sect. 2, the design and the optimization of these focusing fan-out elements rely on a low number of parameters, and only a relatively small calculation effort is needed for fan-out elements having a theoretically vanishing uniformity error. The second, even more significant advantage, is the extremely low sensitivity of the fan-out performance in terms of uniformity error with respect to fabrication errors. For achieving a good uniformity, an exact realization of the splitting function is most important. The technologies for the fabrication of these elements, e.g. laser and e-beam writing, typically guarantee a high lateral precision, whereas inaccuracies in the vertical dimension are more likely to occur. Theoretical and experimental investigations have revealed a remarkable fault tolerance for the type of fan-out elements with a piecewise linear splitting function, as considered here. Depth scaling errors present in the (mass produced) replicated elements primarily reduce the fan-out efficiency with only little effect on the uniformity.

4. Experimental results and discussion

For demonstrating the design and fabrication of a fan-out PMFE, the example of a transmissive element which focuses a collimated HeNe laser beam (wavelength $\lambda = 632.8$ nm) into a linear array of 5 image spots, equally spaced by 67 μm, is considered here. The focal length was 10 mm, leading to a subarray period $\Lambda = 100$ μm (cf. Eq. 6). Different design variants for this problem will be treated.

In the design procedure described in Sect. 2, we dealt with the case of a $N \times 1$ fan-out realized by N different subarray structures. However, it is also viable to use a greater or smaller number L of different interlaced PMFEs. Table 1 shows theoretical and experimental results for the efficiency and the uniformity error of a fan-out PMFE in 5 different design variants. The experimental values were determined by measuring the powers P_j of the image spots by a photodetector masked with a slit.

For $L = N = 5$ the theoretical uniformity error can be optimized to zero, the calculated efficiency of such

Table 1
Theoretical and experimental results for a 5×1 fan-out: optimized phase offsets $\Delta\phi_p$, uniformity error σ and efficiency η for different subarray configurations

Configuration (...$\bar{B}/A/B$...)	L	Phase offsets [2π] ($\Delta\phi_A = 0$)	σ_{theor} [%]	σ_{exp} [%]	η_{theor} [%]	η_{exp} [%]
(−2/−1/0/1/2)	5	$\Delta\phi_{\bar{B},B} = 0.973$, $\Delta\phi_{\bar{C},C} = 0.484$	0.0	1.6	88.4	85.1
(−3/−1/0/1/3)	5	$\Delta\phi_{\bar{B},B} = 0.383$, $\Delta\phi_{\bar{C},C} = 0.068$	0.0	2.2	86.2	82.3
(−1/0/1)	3	$\Delta\phi_{\bar{B},B} = 0.614$	1.5	5.0	87.0	83.9
(1/0/−1)	3	$\Delta\phi_{\bar{B},B} = 0.008$	1.5	4.4	87.0	85.3
(−2/−1/−1/0/1/1/2)	7	$\Delta\phi_{\bar{B},B} = 0.477$, $\Delta\phi_{\bar{C},C} = 0.246$, $\Delta\phi_{\bar{D},D} = 0.017$	0.0	1.0	92.1	91.1

an element is $\eta_{th} \approx 88\%$. If, for some application, the requirements for the uniformity are less stringent, the efficiency can be increased at the cost of the uniformity by changing the two independent phase offset parameters according to the simulation results shown in Fig. 4. Assuming a maximal uniformity error of 15% to be tolerable, a solution with an efficiency $\eta_{th} \approx 95\%$ can be found for the first example of Table 1. An alternative way for achieving a higher efficiency is the design of a fan-out PMFE with $L > N$ different subarrays. The $(L-1)/2$ dimensional parameter space has additional degrees of freedom and therefore allows for better optimization of both the efficiency and the uniformity error, at a correspondingly increased computing effort. The use of $L < N$ subarrays requires much less computation time for the optimization, but is resulting in elements with a uniformity $\sigma > 0$ and a slightly decreased efficiency. However, it is favorable to minimize L, if the width

$$w_x = A/L \tag{9}$$

of the individual subarray elements tends to values below the limit provided by the fabrication technology, especially in case of large image point separations and small focal lengths.

The fan-out PMFEs used for these investigations were fabricated by laser beam writing in photo resist layers on glass substrates [9]. A previously designed contiguous PMFE, fulfilling the task of focusing the laser beam into one image point, was the basis for realizing these elements. The element was writen using a laser beam spot size of 1.5 μm. The maximum depth of the microstructure was 1.0 μm and the minimum segment width was 6 μm. The numerical aperture of this PMFE with a size of 1.6×1.6 mm^2 was NA = 0.08. Elements with an NA of up to 0.5 have already been demonstrated and can also be used for fan-out applications. The data for the fan-out structure were calculated in *real-time* during the writing process on a Sun Sparc station and transmitted via DecNet to the control PC. For the data preparation, the original PMFE was divided into L different subarrays, each one with elements of equal width w_x in x_e-direction. The subarray structures were individually shifted along the x_e-direction, provided with a phase offset $\Delta\phi_j$, and finally combined to form the whole fan-out PMFE structure. The efficiencies η_r of the fan-out PMFEs were measured relative to the efficiency of a single, unsplitted PMFE, whose typical absolute values was $\eta_s \approx 70\%$. For $L = N = 5$ an experimental uniformity error of 1.6% at an efficiency close to the theoretical value of $\eta_r \approx 88\%$ was achieved. Experiments with $L = 7$ demonstrated a uniformity error of $\sigma = 1.0\%$ and an efficiency of $\eta_r = 91.1\%$ for the 5×1 fan-out element under consideration. Fig. 5 shows a scan through the irradiance distribution in the image plane of an element with the configuration $(-3/-1/0/1/3)$, measured by a CCD camera. A good agreement with the theoretical values, calculated using the formalism presented in Sect. 2, was observed. The maximum power into an off-spot was in the range of 10% of the average on-beam power. These results, as well as the low calculation effort in the design procedure, compete favorably with results presented elsewhere [8,10].

An interesting and attractive feature of fan-out elements based on interlaced PMFEs is their large tolerance to depth scaling errors. Purely diffractive suface relief fan-out elements suffer from a considerable degradation of the uniformity if their relief depth is distorted by small fabrication inaccuracies. In Refs. [2,3] uniformity errors $\sigma \approx 10\%$ were reported originating from a depth error of only 1%. A series of experiments on fan-out PMFEs, where the profile depth

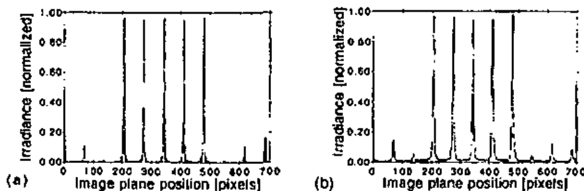

Fig. 5. Irradiance distribution scan through the central line in the image plane of a 5×1 fan-out with the configuration $(-3/-1/0/1/3)$ showing theoretical (a) and experimental (b) results.

Table 2
Measured uniformity error σ and efficiency η_t for a 5×1 fan-out element versus a variable depth scaling factor of the continuous surface relief profile

Depth scaling factor	0.80	0.90	1.00	1.10	1.20
Uniformity error σ	1.8%	1.7%	1.6%	1.4%	2.1%
Efficiency η_t	78.2%	82.1%	85.1%	80.7%	75.8%

was changed by constant depth scaling factors, showed a much superior performance with a uniformity error $\sigma<3\%$ over a depth scaling variation of up to 20%. The results are summarized in Table 2.

5. Conclusions

A novel approach for realizing planar focusing fan-out elements based on spatially interlaced lenses has been presented. These single planar optical elements can be described by a low number of parameters having a well-defined physical optics interpretation. It has been outlined how this a priori knowledge can be used for establishing concise and efficient mathematical algorithms for modelling the fan-out elements. In many cases of practical importance, making use of symmetry considerations, the absolute global optimum can be determined in a systematic search, which is not the case for approaches requiring more complicated optimization procedures such as simulated annealing. The description of these elements in terms of phase functions reveals their approximation to fan-out functions calculated by diffractive optics. The optimization of a 5×1 fan-out led to elements with a theoretically vanishing uniformity error and an efficiency of about 90%. Fan-out PMFEs fabricated by laser beam writing in photo resist showed a minimal experimental uniformity error of $\sigma=1.6\%$. The uniformity error remained below 3% when the surface relief depth was varied over a range of ±20% in order to simulate fabrication inaccuracies. This high fault tolerance *and* the availability of a variety of techniques, for example laser and e-beam writing, for the microfabrication demonstrate the suitability of such fan-out PMFEs for low-cost mass production by replication. These focusing fan-out elements also minimize the number of components, the cost and the size of microoptical systems.

Acknowledgements

The authors gratefully acknowledge Prof. Dr. R. Dändliker (IMT, Univ. Neuchâtel, Switzerland) for helpful discussions, M.T. Gale and H. Schütz for their support in the fabrication by laser beam writing, and J. Pedersen for performing the AFM measurements.

References

[1] D. Prongué, H.P. Herzig, R. Dändliker and M.T. Gale, Appl. Optics 31 (1992) 5706.
[2] M.T. Gale, M. Rossi, H. Schütz, P. Ehbets, H.P. Herzig and D. Prongué, Appl. Optics 32 (1993) 2526.
[3] J. Fagerholm, J. Turunen, A. Vasara and J. Westerholm, Proc. SPIE 1136 (1989) 253.
[4] R.E. Kunz and M. Rossi, Optics Comm. 97 (1993) 6.
[5] J.W. Goodman, Introduction to Fourier Optics (McGraw-Hill, San Francisco, 1968) Ch. 5.2.
[6] J.D. Gaskill, Linear Systems, Fourier Transforms and Optics (Wiley, New York, 1978) Ch. 10-6.
[7] M. Rossi and R.E. Kunz, Proc. IEE 379 (1993) 27.
[8] G. Hatakoshi and M. Nakamura, Appl. Optics 32 (1993) 3661.
[9] M.T. Gale, M. Rossi and H. Schütz, Proc. SPIE 2045 (1994).
[10] D. Wood, P. McKee and M. Dames, Proc. SPIE 1732 (1992) 307.